ROLE OF BRCA2 IN DNA REPAIR

CHANG JAW-SHIN

(B.SC. (HONS), NUS

A THESIS SUBMITTED

FOR THE DEGREE OF MASTER OF SCIENCE

DEPARTMENT OF PHYSIOLOGY

NATIONAL UNIVERSITY OF SINGAPORE

2009

Acknowledgement

I would like to thank my supervisor, Assistant Professor Srividya Swaminathan. I appreciate her continued patience and care in helping me with the completion of this thesis. I am grateful to my colleagues in the laboratory for their help in experiments, sharing of ideas and reagents. Special thanks to Deepa, Dianne, Cindy, Savitha, Gobi, Weiyi, Jia pei, Amelia, Saofiah and Joyce. I thank Dr. Ko Tun Kiat for giving me the COS7 cells and Ron for the help with confocal microscope. I thank CSI for the use of facilities and reagents. Finally, but most importantly, I would like to thank my family for being so understanding and supportive throughout these years.

TABLE OF CONTENTS

Abstract

BRCA2 is a tumour suppressor gene that maintains genomic stability by affecting proper DNA double-strand break repair via Rad51 mediated homologous recombination. Our recent investigations suggested the involvement of BRCA2 in O^6-alkylguanine DNA alkyltransferase (AGT) mediated DNA repair. Ubiquitously expressed AGT is believed to directly repair alkyl DNA lesions thus averting base transitions and strand breaks. This study assesses the importance of BRAC2 in this seemingly single step repair process. Interaction between BRCA2 and AGT is recognised. It is shown that cellular BRCA2 binds alkylated AGT preferentially. The Exon 11 region of BRCA2 specifically interacts with alkyl modified AGT and is capable of driving rapid cellular processing of this inactive enzyme. The ability of GFP tagged full length AGT to rescue sensitivity to alkylating drug is established in an AGT null cell line allowing for future AGT trafficking studies. We establish the requirement of multiple loading of AGT onto DNA to form nuclear repair foci. These loadings significantly hinder alkyl-AGT processing. AGT protein is held inactive by phosphorylation. Using the GFP tagged protein, alkyl-AGT modification seems principally driven in the cytoplasmic compartment. BRCA2 mediated recruitment of cytoplasmic factors driving AGT ubiquitination is indicated. The N-terminus of BRCA2 harbouring a transcription activation domain is capable of AGT expression regulation. These findings reveal that BRCA2 provides multiple levels of control over AGT biology such information is of tremendous value in the clinical management of tumours overexpressing AGT.

List of tables and figures

Abbreviations

231: MDA-MB-231

AB: Apoptotic bodies

AGT, MGMT: O^6-alkylguanine-DNA alkyltransferase

AGT-GFP: Full length AGT tagged with green fluorescent protein

ATCC: American Type Culture Collection

BAC: Bacterial artificial chromosome vector

BCNU: 3-bis-(2-chloroethyl)-1-nitrosurea, Carmustine

BER: Base excision repair

BRCA2, BR2: Breast Cancer susceptibility gene-2 and protein

BRCA1: Breast Cancer susceptibility gene-1 and protein

ChIP: Chromatin Immunoprecipitation

C-1: Capan-1

C-1pfl: Capan-1 transfected with full length BRCA2

CCNU: 1-(2-chloroethyl)-3-cyclohexyl-1-nitrosourea, Lomustine

CHX: Cycloheximide

CMV: Cytomegalovirus

COS7: African green monkey SV40-transfected kidney fibroblast cell line

CT: BRCA2 exons 12-27

DMEM: Dulbecco's modified eagle's medium

DSB: Double strand breaks

E11, exon11: BRCA2 exon11

E. coli*: Escherichia coli*

FP: Forward primer

GFP: Green fluorescent protein

IMDM: Iscove's Modified Dulbecco's Medium

HCT: HeLa cells transfected with BRCA2 exons 12-27

HE11: HeLa cells transfected with BRCA2 exon11

HNT: HeLa cells transfected with BRCA2 exons 2-10

HR: Homologous recombination

IF: Immunoflourescence microscopy

IP: Immunoprecipitation

KD: Knock down

LB: Luria-Bertani medium

MG132: Z-leu-leu-leu-CHO

MMC: Mitomycin C

MMR: Mismatch repair

MMS: Methyl methane sulfonate

MNU: 1-methyl-1-nitrosourea

MN: Micronucleus

NER: Nucleotide excision repair

NHEJ: Non-homologous end joining

NLS: Nuclear localisation signal

NT: BRCA2 exons 1-10

OB: Oligobinding domain

O^6G: O^6 position of guanine

O^6BG: O^6Benzylguanine

O^6-meG: O^6-methylguanine

O^6-ClethG: O^6-chloroethylguanine

PI: Protease inhibitors

pcinBRCA2: Derivative vector of pcDNA3 containing full length BRCA2

PCR: Polymerase Chain Reaction

RP: Reverse primer

RQPCR: Real-Time quantitative Polymerase Chain Reaction

ROS: Reactive oxygen species

TMZ: Temozolomide

1. Introduction

Deoxyribonucleic acid (DNA) contains the genetic instructions essential for the development and functioning of all known living organisms. This macromolecule will never be degraded in its entirety in a cell's lifetime. The unique role of DNA in long-term storage of information requires that it be passed down faithfully from parental cell to daughter cell. Errors in DNA coding can potentially disrupt cellular functions; therefore DNA repair is crucial for genomic stability and species longevity.

DNA can be damaged by mutagens which can alter DNA bases and thus the coding sequence. Both intrinsic and extrinsic mutagenic agents are capable of causing distinctive DNA damage. The intrinsic mutagenic agents include cellular metabolites, oxidants such as free radicals or reactive oxygen species (ROS) that can produce multiple forms of non-specific damages which include base modifications, particularly of guanosine and double strand breaks (Burney, 1999). The extrinsic mutagens cause specific damages for example; UV light causes thymine dimers that can cross-link pyrimidine bases (Gale, 1988) and gamma ray exposure or irradiation causes DNA double strand breaks.

Accumulation of multiple mutations that cause deleterious alterations of protein sequence and function can lead to tumorigenesis (Fischer, 1951). In order to maintain the fidelity of coding, cells have devised various means to repair lesions to DNA. These repair mechanisms include the base excision repair (BER) pathway,

nucleotide excision repair (NER) pathway, mismatch repair (MMR) pathway, homologous recombination (HR), non-homologous end joining (NHEJ) and O^6-alkylguanine alkyltransferase mediated repair.

The short patch base excision repair (BER) pathway, is the main repair modality, is initiated by a DNA glycosylase with the recognition of either a specific type of damaged DNA structure or an inappropriate base. Glycosylases flip the mutated base out of the DNA helix and cleaves it creating an abasic site on DNA. APE1 endonuclease recognises this site and nicks the damaged DNA on the 5' side of the abasic site creating a free 3'-OH. DNA polymerase β performs a one-nucleotide gap filling while replacing the baseless sugar. This repair is followed by sealing of the new DNA strand by DNA ligase. The less popular long patch pathway replaces between 2-10 bases utilising PCNA, DNA polymerase, FEN1 endonuclease and ligase for repair.

Nucleotide excision repair involves 9 major proteins, XPA, XPB, XPC, XPD, XPE, XPF, and XPG all derive from Xeroderma pigmentosum and CSA and CSB represent proteins linked to Cockayne syndrome. Additionally, the proteins ERCC1, RPA, Rad23, and others also participate in nucleotide excision repair. Nucleotide excision repair can be affected by two methods viz the global genome NER (GG-NER) and Transcription Coupled NER (TC-NER). Two different sets of proteins are involved in the distortion and recognition of the DNA damage in the two types of NER. In GG-NER, the XPC-Rad23B complex is responsible for distortion recognition (disrupted base pairing). In TC-NER, the ability of the lesion to stall RNA polymerase becomes critical. The stalled polymerase needs to be displaced to affect repair and the CS proteins (CSA and CSB) are thus required. The subsequent steps in GG-NER and

TC-NER are similar to each other. XPB and XPD, which are subunits of transcription factor TFIIH, have helicase activity and unwind the DNA (up to 30 bases) around the sites of damage. XPG protein has a structure-specific endonuclease activity, which makes an incision 3’ to the damaged DNA. Subsequently XPF protein, which is associated with ERCC1, makes the 5' on DNA. The dual-incision leads to the removal of a ssDNA thus creating a gap of 24-32 nucleotides. The resulting gap in DNA is filled by the cellular replication machinery.

Our current understanding of mammalian mismatch repair indicates the involvement of the MutS, MutH and MutL for repair. MutS heterodimer recognises the mismatched base on the daughter strand and binds the mutated DNA. MutH binds at hemimethylated sites along the daughter DNA, but its action is latent, being activated only upon contact by a MutL dimer which binds the MutS-DNA complex and acts as a mediator between MutS and MutH, activating the latter. The DNA is looped out to search for the nearest d(GATC) methylation site nearest the mismatch, which could be up to 1kb away. Upon activation by the MutS-DNA complex, MutH nicks the daughter strand near the hemimethylated site and recruits DNA Helicase II to separate the two strands with a specific 3' to 5' polarity. The entire MutSHL complex then slides along the DNA in the direction of the mismatch, liberating the strand to be excised as it goes. An exonuclease trails the complex and digests the ss-DNA tail. The exonuclease recruited is dependent on which side of the mismatch, MutH nicks the strand – 5’ or 3’. If the nick made by MutH is on the 5’ end of the mismatch, either RecJ or ExoVIII (both 5’ to 3’ exonuclease) is used. If however the nick is on the 3’ end of the mismatch, ExoI (a 3' to 5' enzyme) is used. The single-stranded gap created by the exonuclease can then be repaired by DNA

Polymerase III (assisted by single-strand binding protein), which uses the other strand as a template. The gap is finally sealed by DNA ligase. Dam methylase then rapidly methylates the daughter strand.

Homologous recombination pathway repairs DNA double-strand breaks when an intact copy of DNA is available. It is initiated by the exonuclease of the acivity of the Rad50/MRE11/NBS1 complex that cause a "resection" of the double-strand break, in which 5' end of the double-strand break is removed on each strand of the DNA duplex, leaving two 3' overhangs of single-stranded DNA. Next, in a process called strand invasion, one of these single-stranded overhangs forms a 'presynaptic filament' with Rad51 and its accessory proteins, which together then moves into a homologous strand. A displacement loop (D-loop) is formed during strand invasion between the invading 3' overhang strand and the homologous strand. After strand invasion, a DNA polymerase extends the invading 3' strand, changing the D-loop to more prominently cruciform structure known as a Holliday junction. Following this, DNA synthesis occurs on the invading strand, effectively restoring the strand on the homologous strand that was displaced during strand invasion.

In the absence of available DNA copies, cells recruit non-homologous end joining that simply links the broken DNA ends. The Ku heterodimer, consisting of Ku70 and Ku80, binds DNA ends and forms a complex with the DNA dependent protein kinase catalytic subunit (DNA-PKcs). The DNA Ligase IV complex, consisting of the catalytic subunit DNA Ligase IV and its cofactor XRCC4, performs the ligation step of repair. DNA-PKcs is thought to mediate end bridging. The Pol X family DNA polymerases Pol λ and Pol μ fill gaps during NHEJ and the nuclease Artemis is required for hairpin

opening and may also be involved in trimming damaged or non-homologous nucleotides.

These repair processes are cellular pathways that require the concerted activity of multiple proteins to repair often bulky destabilising lesions. However, the most frequent cause of point mutations in humans is the spontaneous addition of a methyl group to the highly reactive O^6 position of guanine (O^6G). O^6 position of guanine is frequently attacked by environmental agents, our own endogenous compounds, reactive oxygen species and chemotherapeutic agents. O^6G is highly reactive and O^6G alkyl lesions can cause G → A point mutation. Deleterious accumulation of point mutation can affect protein function. This specific damage is known to be solely repaired by O^6-Alkylguanine-DNA alkyltransferase (AGT), a unique DNA repair protein that is thought to carry out lesions repair without the help of any other co-factors.

1.1 O^6-alkylguanine DNA alkyltransferase

Alkyl lesion repair enzyme O^6-alkylguanine DNA alkyltransferase (AGT) was found in the late 1970's when the first homologue of O^6-alkylguanine DNA alkyltransferase called the Ada protein was first isolated from *Escherichia coli* (*E. coli*; Moore, 1994). It was shown to regulate the adaptive response to low levels of alkylating agents. By rescuing the Ada phenotype in *E. coli*, the human AGT cDNA was isolated from a cDNA library in the early 1990's (Brent, 1990; von Wronski, 1990; Major, 1990). To date O^6-Alkylguanine-DNA alkyltransferases are found to be constitutively expressed in prokaryotes, archea and many eukaryotes. The evolutionary conservation of AGT

suggests that it plays a fundamental role in maintaining genomic integrity. AGT knockout mice are more susceptible to toxicity and tumour induction by alkylating agents, whereas mice overexpressing AGT are considerably more resistant (reviewed in Margison and Santibanez-Koref, 2003). AGT clearly protects both normal cells and tumour cells against the toxic and mutagenic effects of O^6-alkylating agents and is therefore a crucial factor in mediating the resistance to the DNA alkylating class of chemotherapeutic agents.

1.2 AGT mediated repair

AGT is a small monomeric protein of 22KDa that can be divided into 2 major parts, viz the N terminal (aa 1~85) and C-terminal (aa 86~207) domains. The domains are inactive when separated but regain activity when in synergy. The N-terminal domain which exhibits a conserved α/β roll structure (Tubbs *et al.,* 2007) is essential for the proper folding of the C-terminus to its active configuration (Kanugula, 2003). The C-terminal domain contains the DNA binding site and the cysteine containing active site that binds to O^6-alkylguanine and acts as an acceptor of the lesion (Pegg AE., 2000).

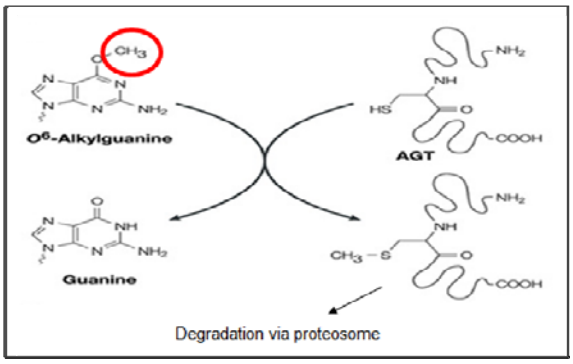

Figure 1, Mode of action of AGT in DNA repair. AGT transfers the alkyl lesions from

the DNA onto its active site in a single step reaction that leads to its cellular destruction (modified from Gerson, 2004)

AGT is a predominantly nuclear protein that directs alkyl lesions repair in DNA. It recognises alkyl lesion at the O^6 position of guanine in DNA and to a lesser extent at the O^4 position of thymine (Dolan, 1988). AGT uses its helix-turn-helix motif to bind substrate DNA via the minor groove. The alkylated guanine is then flipped out from the base stack into the Cys 145 active site for repair, by covalent transfer of the alkyl adducts (Fig, 1; Alkyl-AGT; Mitra, 1993; Pegg, 1995). The asparagine hinge (Asn137) couples the helix-turn-helix DNA binding and active site motifs while an arginine finger (Arg128) stabilises the extrahelical DNA conformation. Selectivity for guanine is provided by hydrogen bonds and steric interactions. It has been recently proposed that DNA lesions are detected by AGT by searching for weakened and/or distorted base pairs rather than the actual adduct (Tubbs *et al.*, 2007).

AGT repairs alkyl lesions at the 5' end of DNA roughly 3.3 times faster than at the 3' end in single stranded oligonucleotides with lesions near the ends (Daniels DS, 2004). Binding of AGT to DNA has been shown to be cooperative (Fried, 1996). It was noted that AGT-DNA complexes had greater than 1:1 stoichiometries. The human AGT: 16-mer DNA stoichiometry was found to be 4:1, a recognition that involves cooperative formation and movement of multi-protein (AGT) complexes (Rasimas, 2003). However, lesion repair involves one to one stoichiometries in that one AGT molecule can accept one alkyl lesion only.

The transfer of the alkyl group to AGT is thought to lead to a change in protein

conformation and the exposure of a specific motif (LXXLL). Alkyl-AGT is released from DNA and is rapidly degraded via the ubiquitin proteosomal pathway (Fig, 1; Srivenugopal, 1996; 2002). The signal and participants in the ubiquitination process are still unknown. It is possibly promoted by conformational change of alkyl-AGT, which results in steric clash between the S-alkylcysteine and Met134 (Daniels, 2000). Prior to alkylation, human AGT is a relatively long-lived protein with half-life of about 24 hour *in vivo* and in cell extracts (Liu and Pegg, 2002). The amount of AGT in cells at any given time is controlled by the rate of cellular degradation and re-synthesis (Marathi, 1993).

1.3 Importance of O^6-alkylguanine DNA alkyltransferase in chemotherapeutic resistance

Alkylating properties are also possessed by anticancer drugs used for cancer therapy. These alkylating agents include temozolomide (TMZ), streptozocin, procarbazine and dacarbazine, which methylate DNA, and carmustine (BCNU), lomustine (CCNU) and fotemustine, which chloroethylate DNA. *In vitro* and *in vivo* data suggest that, the principal mechanism of cell killing by these agents is by the formation O^6-alkylguanine in DNA. Although O^6-alkylguanine lesion is induced in small amounts (8% of total methylation products), it is detrimental to the cells if left unrepaired. AGT is the sole cellular repair protein involved in management of O^6G lesions.

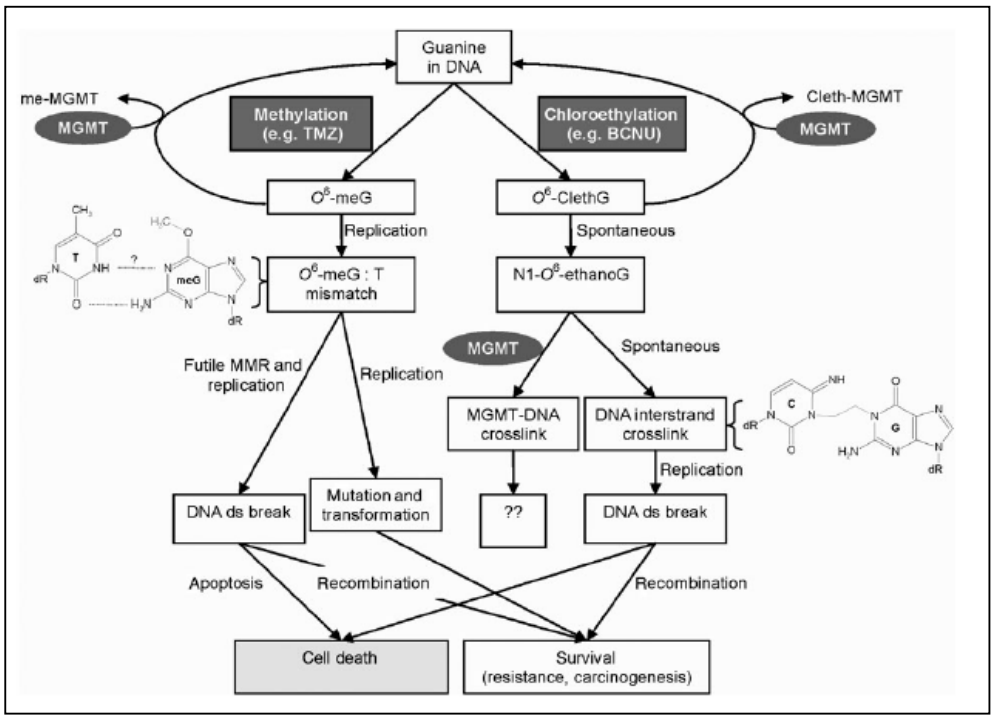

Figure 2, Mode of killing by methylating and chloroethylating drugs (Verbeek et al., 2008). Methylating drugs causes G to T mismatch; if the subsequent MMR is unable to repair the damage, DNA strand breaks (DSB) result and could lead to cell death. Chloroethylating drugs cause DNA interstrand crosslink that will lead to DNA DBS, if unrepaired, thus potentiating death. Coding alteration in cells escaping repair and death accumulate and lead to cellular transformation and carcinogenesis.

The cell killing mechanism of O^6-methylguanine (O^6-meG) and O^6-chloroethylguanine (O^6-ClethG) require DNA replication for induction of cell death (Fig, 2). Methylated O^6G is recognised as a thymine and thus mispaired with arginine during DNA replication. The next round of DNA replication would give rise to G:C and A:T transition mutations that constitute the molecular basis of the mutagenic and carcinogenic effects of these agents (Pauly, 1994). However, the resulting O^6-meG:T mispair can also be recognised by the post-replication mismatch repair (MMR)

system, which removes a section of the daughter strand along with the thymine, leaving the O^6-meG again to pair with thymine during the gap filling process. If replication of the gapped structure occurs, double strand breaks can form which, unless repaired by the recombinational repair pathways, result in cell death (Caporali, 2004). Since the toxicity of O^6-meG is replication-dependant and methylating agents are only marginally toxic to quiescent cells.

Chloroethylating drugs produce O^6-ClethG which is spontaneously converted into N^1-O^6-ethanoguanine by internal cyclization (Tong *et al.*, 1982). It will then react with cytosine on the complementary strand to form a covalent DNA interstrand cross-link. AGT recognises this lesion and repairs it. Replication of DNA containing such structures will result in stalled replication forks and is thus potentially lethal. The main difference in cell killing of methylating agents is that they require a functional MMR system, whereas chloroethylating agents do not (Verbeek *et al*., 2008).

Although AGT can direct alkyl lesions repair, it also promotes tumour resistance to alkylating agents that are commonly used in cancer therapy. Tumours overexpressing AGT are better able to cope with alkylating drug insults and exhibit resistance to therapy. Heightened AGT expression led resistance to therapy is the predominant cause of therapeutic failure. Regulatory approaches to reduce AGT levels have been suggested. These include the use of antisense oligos or ribozymes (Potter 1993) or promoter methylation silencing. However no viable clinical approach has resulted from blocking AGT synthesis thus far. High levels of AGT in tumours require higher drugs doses which lead to systemic toxicity. To cope with toxicity associated with the use of high doses of alkylating drugs, the use of inhibitors of AGT was suggested.

O^6-benzyl guanine (O^6BG) is the most well known inhibitor of AGT. It inhibits AGT by covalently transferring its benzyl group and forming a S-benzylcysteine residue in the AGT active site (Pegg, 1993). This leads to irreversible inactivation of the AGT protein (Pegg, 1995; 2000) and targets it for proteosomal degradation. However the use O^6BG is still questionable as ongoing phase II/III trials suggest that the dose of the alkylating agent that can be given without giving rise to bone marrow damage is limiting due to the lack of specificity of O^6BG towards the tumour. It is further soluble in organic solvents alone and research is focussed on generating water soluble inhibitors of AGT.

Ongoing studies in our laboratory strongly suggest that cells lacking Breast Cancer susceptibility Gene-2 (BRCA2) protein function exhibit extreme sensitivity to alkylating agents.

1.4 Breast Cancer susceptibility Gene-2

Germ line mutations of the *BRCA2* tumor suppressor gene with subsequent loss of the remaining wild-type *BRCA2* allele have been identified in up to 35% of familial breast cancer cases. A high frequency of allelic loss at the *BRCA2* gene locus has also been reported in a variety of sporadic epithelial tumors including oesophageal squamous cell carcinomas (SCC), and sporadic head and neck SCC (Gray, 2008). *BRCA*2 was discovered by genomic linkage search conducted in 15 high risk breast cancer families that were not linked to the BRCA1 locus. The gene is assigned to chromosome 13q12-q13 (Wooster *et al*., 1995) and does not show any mutational hotspots.

BRCA2 is a nuclear protein that is expressed in tissues in a cell cycle dependent manner (Bertwistle *et al*., 1997; Blackshear *et al*., 1998; Connor *et al*., 1997; Rajan *et al*., 1996; Sharan and Bradley, 1997). It is up regulated during S phase which correlates with the activation of homologous recombination during DNA replication (Vaughn, 1996).

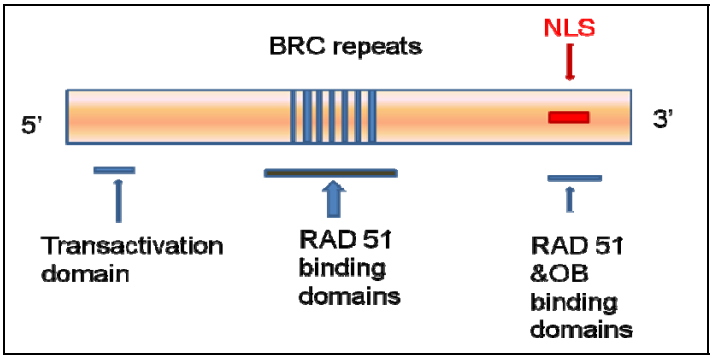

Figure 3, Diagram depicting the main functional domains of BRCA2. The N-terminus includes the transactivation domain; the exon 11 has 8 BRC repeats that bind to Rad51 and the C-terminus harbours 3 nuclear localisation signals, a Rad51 and an oligonucleotide binding domain.

BRCA2 translates to a very large protein made up of 3418 amino acids with a predicted size of 385KDa (Fig, 3; Chen *et al*., 1999). The region encoded by exon 3 has a 45-amino acid segment with weak similarity to the activation domain of the transcription factor c-jun. It is found to activate transcription in yeast when fused to the lexA DNA-binding domain (Milher, 1997). BRCA2 has a large exon 11 that encodes for eight, 30 to 40 residue motifs (Bork *et al*., 1996) called BRC repeats. These repeats are evolutionarily conserved across different species such as mouse, rats, dogs and chicken (Bignell *et al*., 1997; Warren *et al*., 2002). The BRC repeats have been shown

to bind to Rad51, a protein that is essential for DNA repair and genetic recombination, and promotes its oligomerisation (Fig, 4; Chen *et al*., 2004). BRCA2 controls the intracellular transport and function of RAD51. RAD51 oligomerisation is required for nucleofilament formation which is crucial for DNA recombination. Insight into the role of BRCA2 in RAD51 mediated recombinational repair was gained when the crystal structure of a carboxyl-terminal region of BRCA2 bound to DSS1 was revealed. The BRCA2–DSS1–oligo(dT)$_9$ complex revealed that BRCA2 contains a ssDNA binding motif. The BRCA2 carboxy-terminal domain stimulated the homologous pairing and strand-exchange activities of RAD51 *in vitro* (Yang, 2002). In BRCA2-deficient cells, RAD51 (which does not contain a consensus nuclear localisation signal) is inefficiently transported into the nucleus, suggesting that the one function of BRCA2 in cells is to move RAD51 from its site of synthesis to its site of activity (Davies *et al.*, 2001). In addition, BRCA2 also appears to control the enzymatic activity of RAD51.

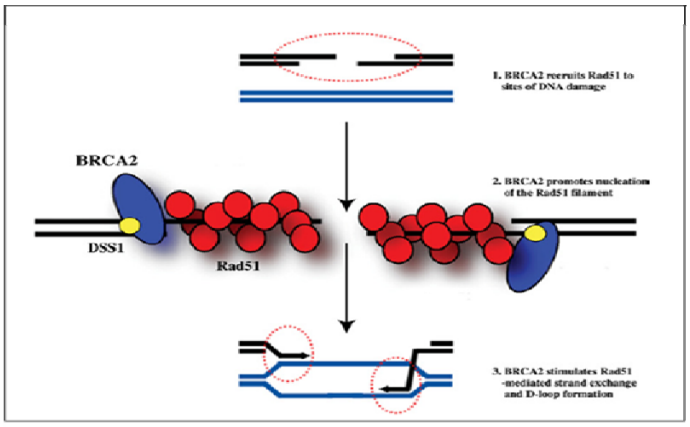

Figure 4, BRCA2 recruits Rad51 to sites of DNA damage and promotes nucleation of the Rad51 filament to sites of DNA double strand breaks. BRCA2 stimulates Rad51-mediated exchange and D-loop formation (taken from S.J. Boulton, 2006).

The C-terminus of BRCA2 has 3 nuclear localisation signal (NLS); of which 2 are

sufficient for the transportation of BRCA2 into the nucleus. This region also harbours many protein interacting domains such as the FANCD2 interacting region, oligobinding (OB) domain and a Rad51 binding domain.

Many proteins are known to interact with BRCA2. PALB2, which is a recently found "partner and localiser of BRCA2", co-localises at nuclear foci with BRCA2 and promotes its localisation and stability in key nuclear structures (eg. chromatin and nuclear matrix) and enables its recombinational repair and checkpoint functions (Bing, 2006). BRCA2 has also been found to form a complex with Smad3 through its MH1 and MH2 domains and synergise in regulation of transcription. Smad3 is an essential component in the intracellular signalling of transforming growth factor-β, which is a potent inhibitor of tumour cell proliferation (Olena, 2002). BRCA2 could be regulated by EMSY encoded protein product through *in vivo* interaction studies by its transcription activation domain. EMSY translocates, like BRCA2 and its bound partner Rad-51, to nuclear dot structures that appear after S-phase DNA damage. However, its precise role in repair and its relevance to the role of BRCA2 in HR repair processes still remains unclear (David, 2004).

BRCA2 is also known to bind and stabilise MAGE-D1, a member of the *MAGE* gene family of proteins. Expression of BRCA2 and MAGE-D1 synergistically suppresses cell proliferation independently of the p53 pathway (Xin, 2005).

1.5 Effects of BRCA2 loss

Studies have revealed that BRCA2 is essential for the maintenance of genomic stability in response to DNA damage especially in the repair of double strand breaks. Loss of heterozigosity of BRCA2 can lead to early onset familial breast or ovarian, cancers (Powell *et al*., 2003, Wooster *et al*., 1995; Collins *et al*., 1995; Cornelis *et al.,* 1995). Loss of BRCA2 is also observed in many sporadic cancers such as prostate and pancreatic cancers. Mutations in BRCA2 have also been implicated in a rare autosomal recessive disease, called Fanconi Anemia (Howlett, 2002).

BRCA2 knockout mice exhibit embryonic lethality by 7.5~8.5 days of gestation. This retarded embryonic growth indicates the imperative role of BRCA2 in normal embryonic development (Sharan *et al*., 1997). Brca2-deficient murine cells exhibit hypersensitivity to double stranded DNA break agents such as X-rays (Sharan *et al*., 1997). Sharan *et al*., 2004 studied the partial loss of BRCA2 by creating a Brca2 null mouse model transfected with the human BRCA2 transgene. This transgene was found to be poorly expressed in the gonads, and these mice were infertile, thus suggestive of the involvement of BRCA2 in mammalian gametogenesis.

1.6 Background to the proposed study

My previous research (Chang *et al*., 2006) involved generating an in-frame deletion of 105 bases in an evolutionarily conserved domain in exon 11 of BRCA2. This altered allele was created in a bacterial artificial chromosome vector (BAC) carrying full length human BRCA2 (BACBR2) utilizing an oligonucleotide aided homologous recombination approach called recombineering (Fig, 5; Swaminathan *et al*., 2001; 2004, Chang *et al*., 2006). The integrity of BAC was checked by restriction digestion and ruled out gross rearrangements. The nuclear expression of BRCA2 with 105bp deletion was confirmed by immunofluorescence staining. The study was an attempt to elucidate the importance of this conserved region in maintaining proper cellular functions supported by BRCA2.

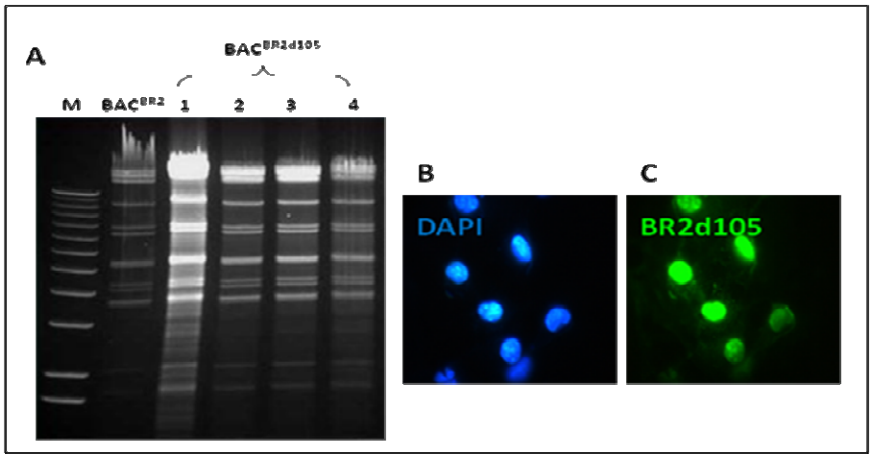

Figure 5A) BAC DNA integrity is intact after successful 105 bp deletion. Gel electrophoresis picture of BAC DNA samples of individual clones after EcoRV restriction enzyme digestion showed identical digestion patterns. B) DAPI nuclear staining of 3x flag tagged BR2d105 transfected COS7 cells. C) Flag antibody staining of 3XFLAG tagged BR2d105 expressing COS7 cells. The data demonstrates that the

transfected BR2d105 is mostly expressed in the nucleus.

COS7 was utilised as a model system to assess the involvements of this altered allele of BRCA2. Flag tagged BACBR2 bearing the conserved region deletion was transfected into COS7 cells. Our data (Fig, 6) indicates that presence of the altered allele bearing in-frame deletion of the exon 11 conserved region somehow renders the cells more sensitive towards alkylating damage. A recent collaborative study utilising a BAC tagged mouse model system also indicated similar sensitivities. Primary embryonic fibroblasts developed from a mouse expressing exon 11 altered mouse Brca2 protein, is sensitive to alkylating agents that create O^6–methyl guanine adducts (Philip *et al*., 2008). While AGT expression levels remain unaltered in these cells, the enzyme is dysfunctional. The study also indicates the involvement of Brca2 in mediating alkyl lesion repair affected by AGT.

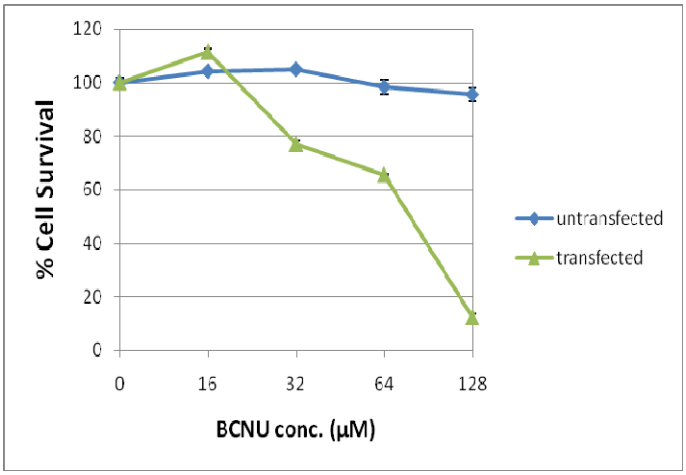

Figure 6, Drug sensitivity response of COS7 and BACBR2d105 transfected COS7 cells towards BCNU. COS7d105 cells are hypersensitive to BCNU when compared to COS7 cells.

Drug treatment on normal diploid cells with stable knock down of BRCA2 (80% knock down achieved) indicated that these cells are sensitive to alkylating drug treatment (Fig, 7) even though the AGT expression status is unchanged. IC_{50} is achieved at 24 µM of BCNU in the knock down cells, at which concentration the parental cells only showed 18% cell death.

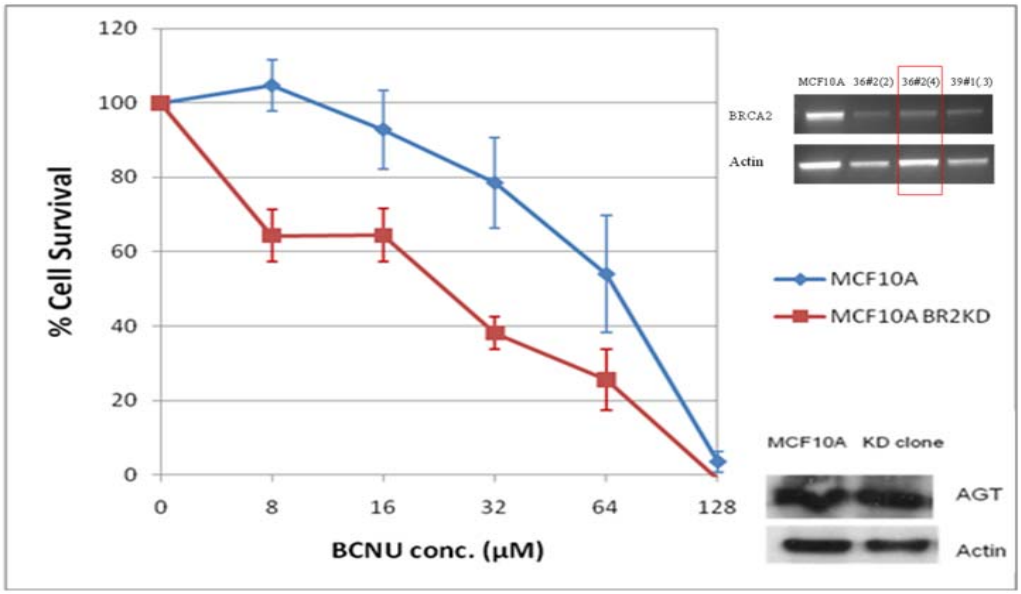

Figure 7, Drug sensitivity response of diploid mammalian cell line MCF10A and its BRCA2 knock down cells. Knock down cells are more sensitive to alkylating drug than normal MCF10A cells. Agarose analysis of BRCA2 mRNA expression in MCF10A and knock down clone is included at the top right hand corner. Western blot data on the AGT status in MCF10A and its knock down clone is included at the bottom right hand corner. AGT expression is not altered in the knock down cells, however the cells became more sensitive to alkylating drug.

Based on these observations, we hypothesise that BRCA2 is required in AGT mediated alkyl DNA lesion repair. This study discusses our assessment of the role(s) of BRCA2 and its domains essential for proper AGT function.

2. Materials and Methods

2.1 Materials

All cell culture media and reagents were obtained from Invitrogen. Cell lines were acquired from American Type Culture Collection (ATCC). All drugs were purchased from Sigma. Restriction enzymes and other reagents for DNA work were procured from New England Biolab (NEB). *Taq* Polymerases were purchased from Applied Biosystems and DNA kits from Qiagen.

2.2 Cell lines and cell cultures

MDA-MB-231 (human breast cancer), HeLa (human cervical adenocarcinoma), Capan-1 (human pancreatic adenocarcinoma), 293T (human embryonic kidney cells), HCC1937 (human breast cancer cell line), MCF7 (human breast cancer cell line), COS 7 (African green monkey cells), SKBR3 (human breast cancer carcinoma) and 468 (human breast adenocarcinoma) were obtained from American Type Culture Collection (ATCC) and sub-cultured according to ATCC protocols. All cells but for Capan-1 were maintained in Dulbecco's Modified Eagle's Medium (DMEM) supplemented with 10% heat-inactivated foetal bovine serum (Thermal Fisher Scientific Inc.) and maintained in a humidified 5% CO_2 incubator at 37°C. Capan-1 was maintained in IMDM supplemented with 20% serum (Hyclone).

2.3 Western blots

Cells were extracted in RIPA buffer (50 mM Tris-HCl, pH 8.0; 150 mM NaCl; 1 % sodium deoxycholate; 0.1 % SDS; 0.5% NP40) supplemented with protease inhibitors (Roche) and their concentration determined by BCA kit (Bicinchoninic acid protein assay, Pierce Biotechnology). The cell extracts were resolved on 6 % and 12 % denaturing SDS polyacrylamide gels according to the size of the protein under investigation. The proteins were transferred onto PVDF membranes (Bio-Rad). The blots were probed for the appropriate antibodies: Actin antibody (Pan-Actin Ab-5, Neomarkers), MGMT C-20 antibody (Santa Cruz), BRCA2 Ab1 and Ab2 antibodies (Neomarkers), BRCA2 I-17 antibody (Santa Cruz), anti-phospho ser/thr-pro MPM2 antibody (Upstate), anti-Flag M5, M2 antibody (Sigma), anti-phosphotyrosine HRP antibody (Millipore), GFP-HRP antibody (Santa Cruz), anti-cyclin B1 antibody (Santa Cruz), anti-cyclin D1 (Santa Cruz), anti-SUMO-1 antibody (Santa Cruz). This was followed by appropriate HRP conjugated secondary exposure and visualisation using enhanced chemiluminescence-plus detection system (Amersham Biobciences) or where indicated IRdye conjugated secondary secondary were used before direct scanning of blots (Odessey; Li-cor).

2.4 Drug sensitivity assays

Cells were plated at about 30% density on 96-well plates, one day prior to treatment. Drug treatment over a range of concentration was undertaken in serum-free/serum containing medium for 2 hr or longer. Medium with 2x serum was then added and

allowed for a recovery period of 72 hr. After recovery, metabolic activities in cells were assayed with MTS cell proliferation assay kit (Promega) as per instructions and survival response curves were plotted.

2.5 Immunoprecipitation

Cells were extracted using RIPA or TDEG (40mM Tris, pH 7.4; 0.5mM DTT; 1mM EDTA and 5% glycerol) buffers and supplemented with protease inhibitors tablet (Roche). 10μM of MG132 was added to stall proteosomal degradation of proteins. 1mg of whole-cell extracts were incubated with 10μg of antibody overnight with rolling at 4°C. The next morning, 40μl of PBS washed A/G sepharose beads (Millipore) was added to samples and rolled for 3 hours at 4°C. Centrifuged pellets were washed twice in 1ml RIPA /TDEG buffer. Proteins bound to the beads were then eluted by boiling at 95°C/10mins. The lysates were then resolved on SDS-PAGE and analysed by Western blot.

2.6 Immunoflurescent detection of protein

Cells were plated to 60~80% confluency on coverslips. The next day, untreated or those treated with 10 μunits of bleomycin for 1 hour and re-supplemented with serum for upto 6 hours. Cells were fixed using methanol at -20°C for 20 mins, permeabilised with Triton X-100, blocked using heat-inactivated goat serum and stained with anti-BRCA2 antibodies and anti-Rad51 antibodies. Proteins were visualised under Nikon fluorescent microscope using Alexa 488/568 IgG(H+L)

antibodies (Molecular Probes) and nuclei counterstained with DAPI. Staining for BRCA2 and AGT was undertaken in a similar protocol.

2.6.1 IF for chromatin bound proteins

Cells were plated on coverslips overnight and washed before treatment with detergent buffer to disrupt membrane and get rid of cytoplasmic content. Samples were fixed and blocked after which primary was applied overnight. After washing to remove unbound primary, samples were exposed to appropriate secondary at room temperature for 1 hour. Washed samples were counterstained with DAPI and mounted on slides for fluorescence imaging.

2.7 Cloning

2.7.1 Cloning of 3XFlag Constructs

Three different constructs of different BRCA2 regions were engineered: p3xFLAG-CMV-10-exon2-10; p3xFLAGCMV-10-exon11; p3xFLAG-CMV-10-exon12-27. The vector p3xFLAG-CMV-10 (Sigma) harbours the ampicillin resistance gene for cloning selection, neomycin resistance gene for selection of stable mammalian cell lines, cytomegalovirus immediate-early (CMV) promoter for high-level expression in a wide range of mammalian cells and 3xFlag epitope-tag for identification. All the three constructs were engineered by cloning the respective BRCA2 segments into the NotI/ HindIII cloning sites of p3xFLAG-CMV-10.

2.7.2 Preparation of insert

Each of the three different segments of BRCA2 were amplified by Polymerase Chain Reaction (PCR) from the template pcinBRCA2 (a pcDNA3 derivative vector containing full length BRCA2), linearised by digestion at its unique NheI site. For cloning into the vector, the inserts were engineered with a NotI restriction site at 5' end and HindIII restriction site at 3' end. Primers were designed as shown in Table 1 and used in amplification of the respective inserts.

Insert	**Forward Primer (FP)**	**Reverse Primer (RP)**
Exon 2-10 (NT)	5' gAT CAT gCg gCC gC CCT ATT ggA TCC AAA gAg Agg CCA AC 3'	5' gAT CAT AgA TCT CCA AAA gAg CTA gTT AAg gAC AAA gTT gg 3'
Exon 11(E11)	5' gAT CAT gCg gCC gC gCT TTT gAA gCA CCA CTT ACA TTT g 3'	5' gAT CAT AgA TCT TCT ggA gTg CTT TTT gAA gCC TT 3'
Exon12-27 (CT)	5' gAT CAT gCg gCC gCT CAT gCC ACA CAT TCT CTT TTT ACA Tg 3'	5' gAT CAT AgA TCT gAT ATA TTT TTT AgT TgT AAT TgT gTC CTg CT 3'
Description	FP, non-seq extending bases, Not I RE site, hu BRCA2 for cloning into p3xFLAG-CMV-10 as NotI/HindIII segment	RP, non-seq extending bases, HindIII RE site, hu BRCA2 for cloning into p3xFLAG-CMV-10 as NotI/HindIII segment

Table 1, Primers designed for the amplification of the respective BRCA2 segments.

The PCR conditions were as followed: Initial denaturation at 94°C was followed by 35 cycles of denaturation at 94°C for 30s, annealing at 60°C for 30s and extension at

72°C for 1min/kb, followed by a final extension at 72°C. The amplified products were visualised on a 0.8% agarose gel after PCR. The PCR products were generated using GeneAmp high-fidelity PCR system (Applied Biosystems). Taq DNA polymerase system (Qiagen) was employed for other confirmatory PCRs. Samples amplified were subsequently purified using PCR Purification Kit (Qiagen) followed by restriction enzyme digestion of NotI and HindIII at 37°C water bath for 2 hrs and run on a 0.8% agarose gel. The bands of interest were excised and purified using QIAquick Gel Extraction Kit (Qiagen). The obtained insert DNA were finally resuspended in 1XTE (10mM Tris-HCl, pH 8.0; 1mM EDTA) and quantitated by Nanodrop.

2.7.3 Preparation of vector

Cell pellets from 3 ml overnight culture of p3xFLAG-CMV-10 carrying *E. coli* cells were processed for DNA extraction by alkaline lysis method. DNA pellet obtained by centrifugation was washed two times with 70% ethanol, air dried and reconstituted in 1XTE, pH 8.0. Large scale DNA preps were performed using Qiagen Maxi Kits (Qiagen) as per kit instructions. Similar to preparation of insert, RE digestion was firstly performed on p3xFLAG-CMV-10 with NotI and HindIII enzymes, at 37°C water bath for 2 hrs and ran on 0.8% agarose gel. The band of interest was excised and purified using Gel Extraction Kit (Qiagen) followed by nanodrop quantification. Vectors and inserts were ligated as described under section 2.8.

2.7.4 Cloning of AGT-GFP fusion protein

Full length AGT was cloned into pEGFP-N1 vector (Biosciences Clontech) via available KpnI/HindIII cloning sites of the vector.

2.7.5 Preparation of insert

Full length AGT was amplified by Polymerase Chain Reaction (PCR) from the template pCMV-SPORT AGT linearised by digestion at its unique ClaI restriction site. AGT was amplified using forward primer 5' gAT CAT AAg CTT gCC ACC ATg gAC AAg gAT TgT gAA ATg AAA CgC ACC AC 3' with reverse primer 5' ATg ATC ggT ACC AAg TTT Cgg CCA gCA ggC ggg gA 3' in a PCR with denaturation at 94°C and followed by 35 cycles of denaturation at 94°C for 1min, annealing at 50°C for 1min and extension at 72°C for 2 mins, followed by a final extension at 72°C. The PCR product was generated using *AmpliTaq* PCR system (Applied Biosystems). Amplified fragment was purified using PCR Purification Kit (Qiagen) followed by restriction enzyme digestion with HindIII and KpnI, digested fragments were purified using QiaexII Kit.

2.7.6 Preparation of vector

Cell pellets from overnight culture of pEGFP-N1 carrying *E. coli* cells were processed for DNA extraction by Qiagen Maxi Kits (Qiagen) as per kit instructions. Similar to preparation of insert, RE digestion was firstly performed on pEGFP-N1 with HindIII and KpnI, at 37°C water bath for 2 hrs and digests run on an 0.8% agarose-TAE gel. The band of interest was excised and purified using QIAEXII gel extraction kit

(Qiagen).

2.8 Ligation and Transformation

The purified inserts were ligated with the digested vectors at 3:1 molar ratio using Ligation High kit (TOYOBO) as per instructions, at 16°C for 30 min. 2.5µl of the ligated samples were mixed with chemically competent DH5α *E. coli* cells (Invitrogen; 50µl). After incubation on ice for 30 min, samples were subjected to heat shock at 42°C for 90s and replaced on ice for 2 mins. The cells were rescued in SOC medium and recovered at 37°C for one and a half hour with shaking. Recovered cells were then plated on LB plates containing 25µg/ml Kanamycin (Sigma) for selection at 37°C for pEGFP-N1 vector while for p3XFLAG-CMV-10 vector 50 µg/ml ampicillin was used for selection.

2.9 Screening of Recombinants

Preliminary verifications were performed directly on clones picked from agar plate and were analysed for positive transformants which were then resuspended in Luria Bertani medium (LB). Concomitantly, a master plate was prepared for the selected clones. Upon positive result from PCR, clones were picked from master plates and inoculated into 3 ml of LB containing 25µg/ml kanamycin or 50µg/ml of ampicillin. The cultures were allowed to grow to mid-log phase (OD600 = 0.5-0.7) and the plasmid DNA were extracted via alkaline lysis (*Plasmid Mini* kit; Qiagen). Further verification was performed on digestion with different restriction enzymes. After

affirmative verification, large scale DNA preparations (*Maxi* prep) were performed. Sequencing was then undertaken to confirm site specific and in-frame cloning (ABI Big Dye sequence terminator kit).

2.10 Mammalian transfection and cell sorting

The p3XFLAG-CMV-10 with NT, E11, and CT inserts were transfected into 293T cells and HeLa cells; and the AGT-GFP construct was transfected into HeLa and 231 cells according to an optimized *Lipofectamine* protocol (6 well format; Invitrogen). Briefly, $4x10^5$cells were plated in 2 ml medium without antibiotics one day prior to transfection. 1µg of maxiprep DNA was complexed with 5µl of Lipofectamine at room temperature for 45 minutes in dark. Cells plated overnight were washed once with Opti-MEM and incubated with the complex for 6 hrs, then supplemented with an equal volume of growth medium containing 2X serum and incubated overnight. Twenty-four hours post-transfection, fresh medium was replenished. Cells were cultured in growth media containing Geneticin (Invitrogen) which was replaced daily (800 µg/ml for HeLa and 1mg/ml for MDA-MB-231) for 10~15 days and followed by 3 days of recovery. The AGT-GFP transfectants were sorted using fluorescence-activated cell sorting (FACSAria; BD Biosciences). All constructs were verified for expression by RT-PCR, Western Blot and immunofluorescence.

2.11 Long term colony formation

Cells were plated in a 96 well plate at 2000 cells/well one day prior to treatment. Cells treated with Bleomycin, Streptozocin, MNU or BCNU did not contain serum treatment. Serum was replenished at the end of the 2 hr treatment. Other drugs were added directly with serum. The next day, cells were trypsinised and plated at a density of 500 cells/well in 6 well plates in triplicate. The plates were left to recover for 10 days, after which cells were fixed and colonies stained with crystal violet. Crystal violet was solubilised with 1% of SDS and absorbance read at 570nm wavelength using an ELISA plate reader (Bio-Rad). Percentage cell survival was plotted using untreated as a readout control.

2.12 Real time tracking of AGT-GFP

Sorted HeLa and 231 cells transfected with AGT-GFP were plated on round coverslips to a confluency of 80%. The cells were treated with a high dose of BCNU (200μM) for 2 hours without serum and then supplemented with 10% foetal bovine serum. Time lapse tracking for GFP was carried out on cells using Nikkon confocal microscope at 100X magnification over a period of 24 hours with hourly imaging.

2.13 Micronuclei count

Sorted HeLa and 231 cells transfected with AGT-GFP were treated with BCNU (10, 20 and 40 μM) or bleomycin (10, 20 and 40 μunits) or streptozocin (10, 20 and 40 μM) in

serum free medium for 2 hours and supplemented with serum at the end of the treatment. Cells were allowed to recover overnight before counting micronuclei in 500 cells.

2.14 *In vitro* AGT degradation assay

Total cell lysates in TDEG buffer were supplemented with 5 mM $MgCl_2$, 2mM ATP, and 100µM O^6-Benzylguanine. The mixture was incubated at 37°C and the rate of AGT degradation was measured using aliquots (30µg) taken at different time intervals. Each aliquot was mixed with 5X protein dye, 3% of β-mercaptoethanol and boiled for 5 mins prior to being resolved by 12% SDS–PAGE. Western immunoblot for AGT was undertaken and actin was detected on stripping. The rates of AGT protein degradation were determined by quantifying the 22 KDa band in comparison to untreated controls. Data was normalised using Actin.

2.15 *In vivo* AGT degradation assay

Cells plated on 6-well plates were either treated with (10µM cycloheximide (CHX), 80µM O^6-benzylguanine and 25µM MG132) or with (200µM BCNU, 10µM MG132 and 10µM Lactacystein) for indicated times. Cells were harvested using ice cold buffer (50mM Tris-Cl, pH7.8; 0.1mM EDTA; 5mM DTT and complete protease inhibitors) and 25µg of lysates were run on a 12% SDS-PAGE for AGT detection and quantification.

2.16 ChIP Assay

Cell were cross-linked and lysed in buffer. Sonication sets of 10X with 10 seconds on and 30 seconds off intervals were carried out on the cell lysates. ChIP was performed as per instruction (Chromatin Immunoprecipitation (ChIP) Assay Kit,Upstate) and IP for BRCA2 was carried out. After reverse cross-linking, DNA purification using sodium acetate and absolute ethanol were performed and DNA obtained were bisulfite treated. Post-bisulfite treatment was carried out by adding 5.56µl of 3M NaOH, 37°C/15mins. 27.78µl of 9M NH_4OAc (pH7.0) to a final concentration of 3M was then mixed followed by addition of 50µl of 3M NaOAc (pH5.2) to correct the pH to <7.0. 1ml of QX1 was added and rotated for 10 min/RT, DNA was finally purified according to the QiaexII protocol. 30ng of DNA was used for AGT promoter PCR amplification. A nested PCR of 25 µl was firstly completed with FP 5' ggA TAT gTT ggg ATA gTT 3' and RP 5' CCA AAA ACC CCA AAC CC 3' at 50°C annealing, followed by equally dividing the PCR volume into half and amplified with unmethylated promoter specific primers (FP 5' TTT gTg TTT TgA TgT TTg TAg gTT TTT gT 3' and RP 5' AAC TCC ACA CTC TTC CAA AAA CAA AAC A 3') and methylated promoter specific primers (FP 5' TTT CgA CgT TCg TAg gTT TTC gC 3' and RP 5' gCA CTC TTC CgA AAA CgA AAC g 3') using 55°C annealing. Amplicons were visualised on agarose gels.

2.17 Real-Time PCR

Transfected cells were trypsinised and washed with 1X PBS before total RNA extraction using TRIZOLR Reagent (Invitrogen) as per manufacturer’s instructions.

Prior to RT-PCR, total RNA extracted were subjected to 1 unit of RNase free DNaseI treatment (Qiagen) at 37°C for 10 minutes to remove residual DNA contamination. The DNaseI enzyme was inactivated at 65 °C for 10 minutes. Transfectants were assayed for its AGT gene expression by quantifying mRNA levels using Applied Biosystems TaqMan. RQ-PCR was performed using MGMT and GAPDH probes in 25µl volume on the ABI PRISM 7700 Sequence detection system. Each analysis used 100ng of starting cDNA material. GAPDH was used as an endogenous control to normalise the expression data. Probes within exon 5 for AGT and exon 3 for GAPDH were used in the study.

2.18 Nuclear-Cytoplasmic Extractions

The nuclear and cytoplasmic cell extracts were obtained by using CelLytic Nuclear Extraction Kit as per instructions (Sigma). The resulting preparations were used directly in SDS PAGE and immunoblot for BRCA2 and its fragments, AGT or AGT-GFP detection.

3. Results & Discussion

Previous studies based on a COS7 model indicated the involvement of BRCA2 in AGT regulated repair. To test out our hypothesis that full length BRCA2 is required for AGT mediated alkyl lesions repair, drug toxicity assays were performed on various cell line carrying functional or dysfunctional BRCA2 using various genotoxins. Our choice of drugs was based on lesions generated and position on base targeted such as N^7, O^6, or N^3 positions on DNA bases.

3.1 BRCA2 compromised cells are sensitive to alkylating drugs targeting O^6 position of guanine

Alkylating chemotherapeutics are highly favoured in clinic because they target a pathway that is solely governed by a single enzyme. O^6 position of guanine (O^6G) is frequently attacked because it is highly reactive. If left unrepaired G to A transition mutation results (Rinne *et al*., 2005). Alkylating agents of the S_N1 type (e.g. MNU and BCNU) affect both oxygens and nitrogens in DNA bases whereas S_N2 type agents (e.g. MMS and MMC) alkylate only the nitrogens.

BCNU induced O^6G lesions can undergo molecular rearrangements to create a DNA interstrand crosslinking between N^1 of guanine and N^3 of cytosine of the opposite strand. It is a monofunctional alkylating agent that has some selectivity for chloroethylating guanine at the O^6 position (Beranek, 1990).

Capan-1 cells (a human pancreatic adenocarcinoma cell line, C-1) were chosen in this study as a BRCA2 null cell line because it lacks one allele of *BRCA2* and carries the other allele with a 6174delT alteration (Abbot *et al.*, 1998). This alteration results in a $BRCA2^{tr}$ without its C-terminal nuclear localisation signal. This causes $BRCA2^{tr}$ to mislocalise in the cytoplasm. Of the many cell lines tested for BRCA2 (Fig, 8), HeLa expresses high levels of BRCA2 and MDA-MB 231 cells were chosen as an AGT null cell line that express BRCA2 (Fig, 9).

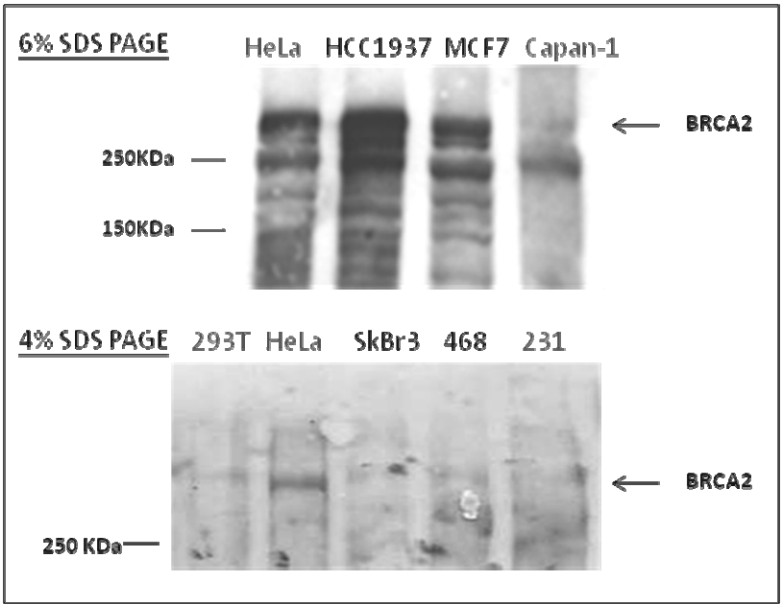

Figure 8, Western blot analysis of BRCA2 expression in various human cancer cell lines. Detection was undertaken using an anti-full length BRCA2 antibody. Capan-1 cells do not express full length BRCA2.

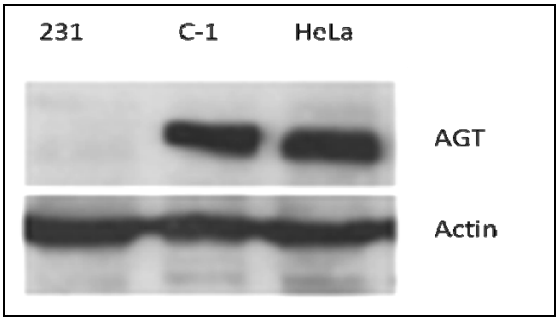

Figure 9, Western blot analysis of AGT and actin expression. AGT expression in Capan-1 and HeLa are similar, while MDA-MB 231 does not express AGT.

Cell lines were exposed to varying doses of BCNU, allowed recovering for 3 days, and drug toxicity/cell survival was assessed. HeLa cells showed dose dependent sensitivity to BCNU with an IC_{50} of 128µM (Fig, 10A). Capan-1 cells (C-1) however were hypersensitive with an IC_{50} of 45µM of BCNU. Sensitivity exhibited by Capan-1 cells was similar to drug sensitivity of an AGT null cell line MDA-MB 231 (mammary adenocarcinoma; referred to as 231).

In order to investigate whether this sensitivity was only specific to O^6 alkylguanine lesion, other drugs that cause alkyl damages at different positions in bases were investigated. Sensitivity of cells towards 4-acetoaminofluorene (AAF) was investigated. This drug causes mainly N^7G lesions. HeLa and 231 cells exhibited minimal sensitivity towards this drug. Capan-1 cells were resistant to this drug (Fig, 10B).

A.

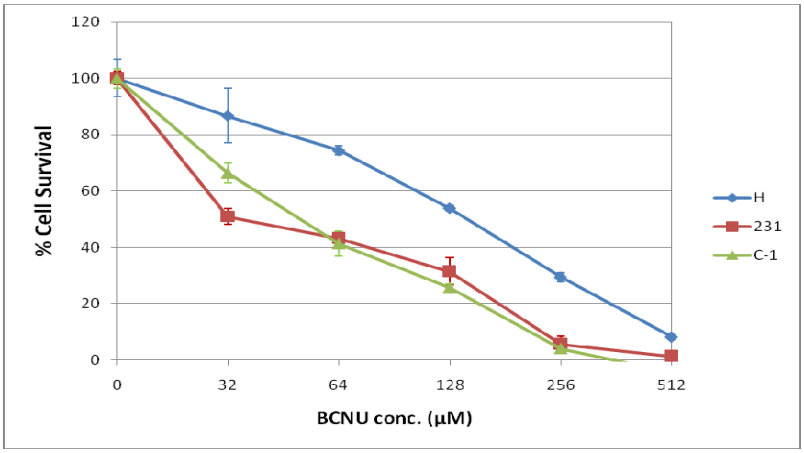

B.

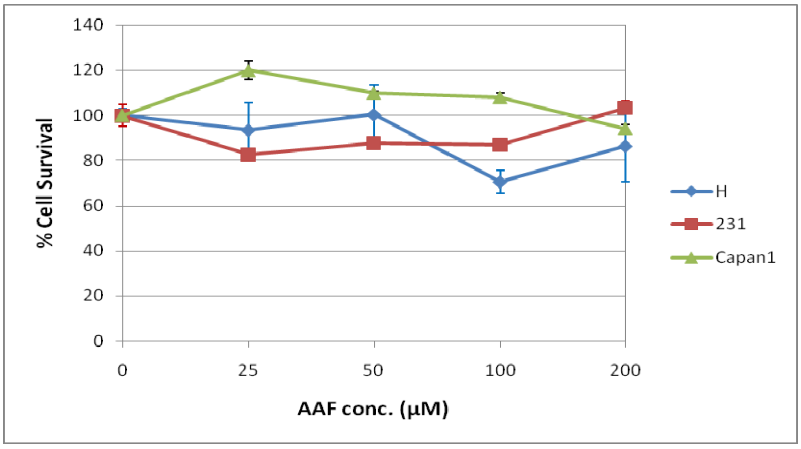

Figure 10, Drug sensitivity responses to BCNU and AAF. A) Capan-1 exhibits similar drug sensitivity pattern to 231. B) Capan-1 and 231 are not sensitive to AAF. Data presented represent mean values and standard deviations of three independent assessments.

MNU is a SN_1 type alkylating agent that generates ethylation damage at N^7G, and N^3G, N^3A positions of DNA (Rinne *et al*., 2005). HeLa and Capan-1 cells were marginally sensitive to MNU (Fig, 11A). 231 cells were more sensitive to MNU at all doses and exhibited about 30% cell death at 512µM of MNU.

We also undertook assessment of Methyl Methane Sulfonate (MMS) which mainly causes N^7 alkyl lesions and generates 3-methyl purine that is repaired by BER. HeLa exhibited minimal toxicity at lower drug concentration but exhibited heightened toxicity at 128µM of MMS with about 70% cell death. Capan-1 cells showed resistance at 128µM with 70% cell survival (Fig, 11B). However the errors bars at this point were high. Compared to HeLa cells, 231 cells showed only 10% cell survival at 128µM which was not significantly different from HeLa cells based on the errors bars.

A.

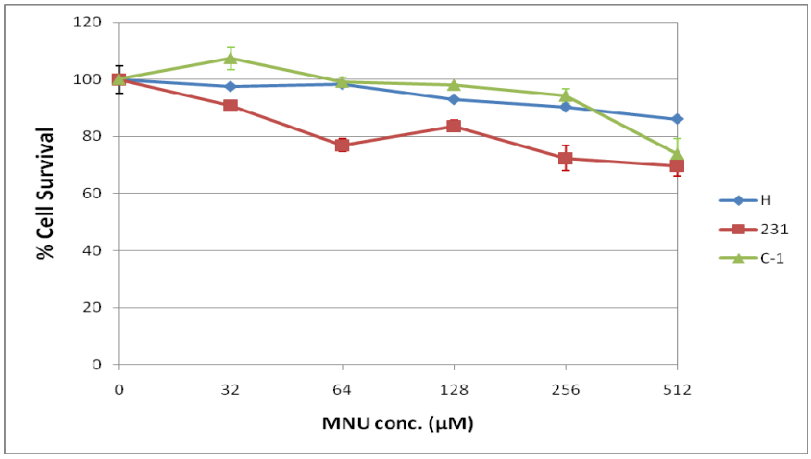

At 64µM, HeLa and 231 p-value=0.0165

At 256µM, HeLa and 231 p-value=0.0052

B.

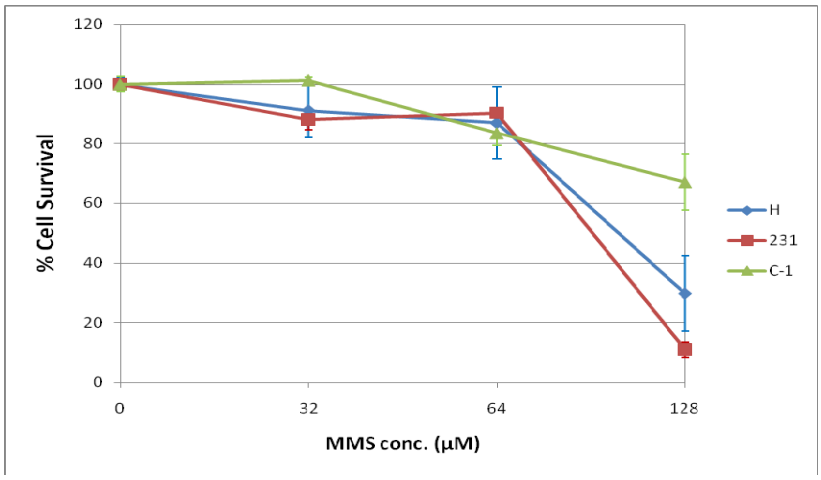

At 128µM, Capan-1 and HeLa p-value=0.683

Figure 11, Drug sensitivity responses of HeLa, Capan-1 and 231 cells. A) HeLa and Capan-1 cells are marginally sensitive to MN while 231 is slightly more sensitivity to MNU. B) All cell lines exhibit similar responses to MMS. Data presented represent mean values and standard deviations of three independent assessments.

Taken together the sensitivity of Capan-1 cells to BCNU is significantly surprising because AGT expression in these cells is similar to HeLa cells. Our previous data from the knock down of BRCA2 in MCF10A cells indicates them to be about 1.5 times more sensitive to BCNU drug treatment than normal MCF10A cells suggesting that BRCA2 is important for AGT mediated repair. We undertook to explore a possible interaction between AGT & BRCA2. Thus co-immunoprecipitation analysis for AGT and BRCA2 was undertaken.

3.2 Interaction between BRCA2 & AGT is strengthened after alkyl modification of AGT

Co-Immunoprecipitation (co-IP) of BRCA2 and AGT was carried out in cells solubilised in RIPA buffer. High salt was used to extract these nuclear proteins. Since salt can interfere with AGT mediated activity; the buffer was then diluted to 150 mM NaCl before pull downs were undertaken.

Initial immunoprecipitation of AGT using BRCA2 antibodies was classified as unsuccessful as there was no pull down of AGT in untreated HeLa lysate. However after generation of alkyl-AGT by exposure to O^6BG, significant pull down was observed (Fig, 12). The specificity of IP was confirmed using normal IgG as control. We checked for serine/threonine and tyrosine phosphorylation of AGT using their specific antibodies in the BRCA2 pull down and were unable to detect phosphorylated forms of AGT.

Reciprocal IP was able to pull down AGT, but detection of BRCA2 was a problem. This is because cleaving proteins from beads is routinely performed at 95°C. BRCA2 is a heat labile protein that is known to be degraded under such conditions. This data suggested a possible interaction between alkyl-AGT and BRCA2 and did not necessitate a phosphorylation modification of alkyl-AGT.

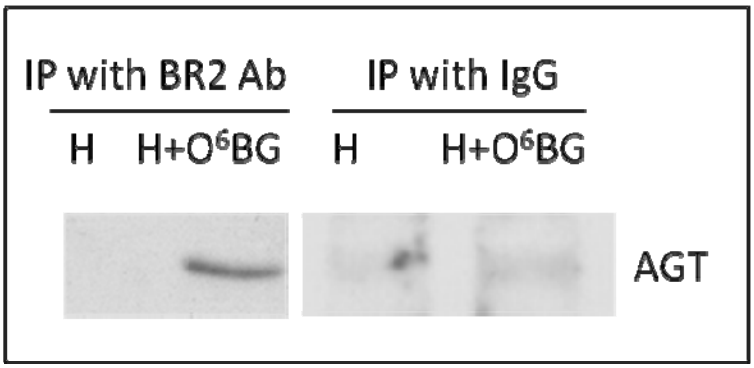

Figure 12, Western Blot detection of AGT in IP of O^6 BG treated and untreated lysates using anti-BRCA2 antibodies. AGT is pulled down only in O^6BG treated lysate.

3.3 E11 region of BRCA2 is possibly important for AGT mediated repair

A 105 bp deletion in the evolutionarily conserved region of exon 1 was generated previously in a BAC (bacterial artificial chromosome) carrying full length BRCA2 (Chang *et al*., 2006). We assessed the effect of this deletion in COS7 cells.

The BCNU insensitive COS7 cells were only marginally sensitive to BCNU after exposure to O^6BG (Fig, 13). However, transfecting BACBR2d105 into COS7 cells heightened their sensitivity towards BCNU with IC_{50} at 80µM. On depleting AGT with O^6BG the IC_{50} further shifted to 42µM indicating the compromised function of AGT in this background.

This suggests that the 105bp region by itself is important for AGT function or it may be part of a larger region that might be important for AGT biology. $BRCA2^{tr}$ expressed in Capan-1 cells has this conserved region of exon 11. From our data on the

sensitivity of COS7d105 and that of Capan-1 cells towards BCNU, we were prompted to study the exon 11 region and the C-terminus region of BRCA2 for their role in AGT regulation. We thus cloned the exon 11 and the C-terminus region of BRCA2 (Fig, 14) into p3XFLAG-CMV-10 plasmid (Materials & Methods 2.7) and transfected the same into HeLa cells.

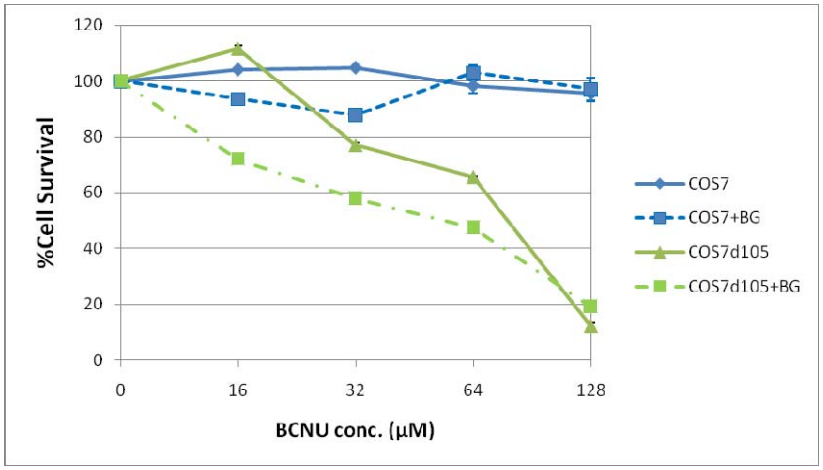

Figure 13, Drug sensitivity response of COS7 and COS7d105 cells to BCNU. The COS7d105 cells exhibit hypersensitivity towards BCNU and O^6BG exposure enhances this sensitivity. Data presented represent mean values and standard deviations of three independent assessments.

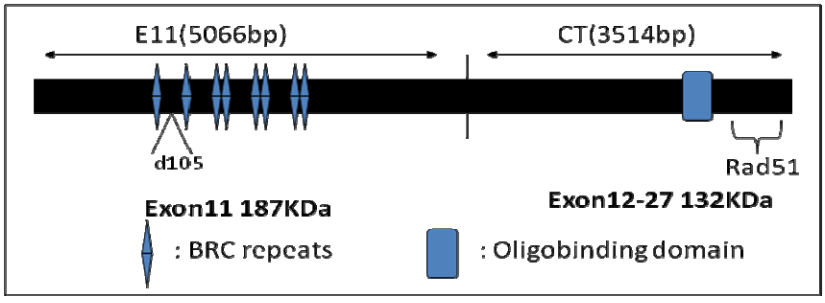

Figure 14, Schematic representation depicting the size and regions of BRCA2 segments that were cloned into p3XFLAG-CMV-10 plasmid.

3.4 Stable expression of Exon11 and CT BRCA2 in 293T cells

The Exon 11(E11) fragment of BRCA2 harbours 8 BRC repeats, 6 of which are important for Rad51 binding and transport into the nucleus to affect homologous recombination repair. The C terminus (CT) of BRCA2 has a Rad51 binding domain and an oligonucleotide binding domain. The different sections were cloned into a p3xFLAG-CMV-10 vector for transfection into 293T cells. 293T is a human embryonic kidney cell line transfected with SV40 Large T-antigen. We undertook transfection of AGT into 293T cells as it lacks endogenous AGT expression (Fig, 15). We assessed AGT localisation after further transfection with the BRCA2 fragments.

AGT localisation in the cell was predominantly nuclear after transfection of the segments of BRCA2 (Fig, 15). AGT remains a nuclear protein. We also analysed stable expression of the various BRCA2 segments. Western blot showed positive protein expression for CT and E11 of 132kDa and 187kDa respectively (Fig, 16; Lee *et al.*, 2007).

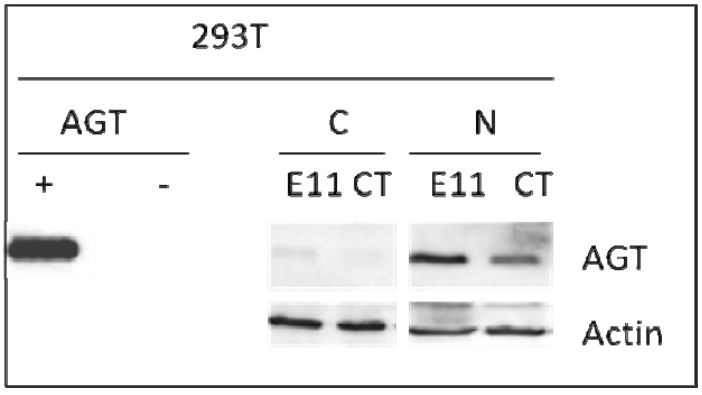

Figure 15, Western blot detection of AGT expression in 293T transfected with full length AGT (293T-AGT; Left). Right, AGT expression analysis in nuclear and

cytoplasmic fractions of 293T-AGT cells transfected with different segments of BRCA2.

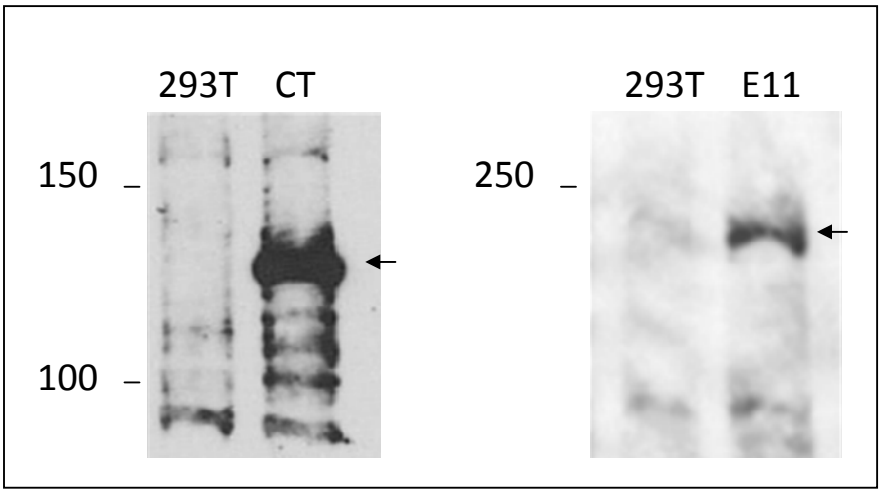

Figure 16, Western blot detection of various BRCA2 segments. E11 expresses an 187KDa protein and CT expresses a 132KDa protein. Blots were probed with anti-Flag antibodies (Lee *et al.*, 2007*).*

3.4.1 E11 expression render AGT transfected 293T cells sensitive to BCNU

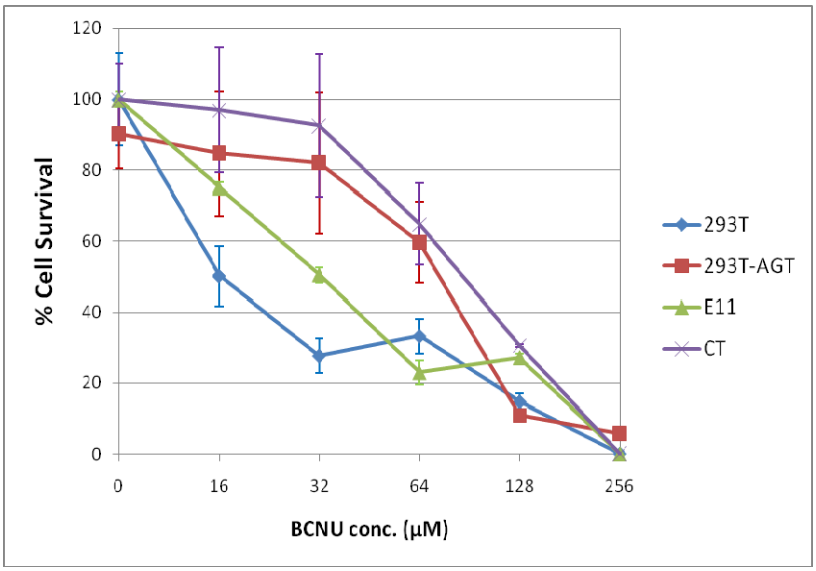

Figure 17, BCNU sensitivity of 293T cells transfected with different BRCA2 segments. E11 cells exhibit similar sensitivity profile to 293T cells even though they express functional AGT. Data presented represent mean values and standard deviations of three independent assessments.

293T cells were extremely sensitive to BCNU with an IC_{50} of 16µM BCNU. After transfecting with full length AGT the 293T-AGT cells became less sensitive to BCNU with an IC_{50} of about 75µM. This suggested that the exogenous AGT was functional in these cells. Interestingly, when BRCA2 E11 segment was transfected into 293T-AGT cells, the cells exhibited increased sensitivity with an IC_{50} of 32µM (Fig, 17). This suggests that this region of BRCA2 is affecting the cell in a way that the transfected AGT becomes unable to support the repair of alkyl lesions. On the other hand, CT region does not alter the sensitivity of 293T-AGT cells to BCNU. However this is an artificial system, where exogenous AGT was transfected. The 293T cells itself may

lack other components that are crucial for AGT biology. Thus we went on to utilise a system that supported both AGT and BRCA2 functions.

3.5 Stable expression of Exon11 and CT BRCA2 in HeLa cells

HeLa, a cervical carcinoma cell line, expresses endogenous full length BRCA2 and AGT. In this cell line AGT function can be neutralised with O^6BG (Fig, 42). Exposure to 100µM of BCNU caused about 45% cell death and 50µM of O^6BG caused about 40% cell death. Co-addition of 100µM BCNU and 50µM O^6BG enhanced the cell death to 60%. O^6BG is thus able to neutralise and inhibit the function of AGT in this cell line and enhances sensitivity of cells to BCNU. HeLa cells were transfected with E11 or CT BRCA2 constructs (cloned into p3XFLAG-CMV-10 plasmid) and stable clones selected. Western blot showed positive protein expression for E11 and CT of 187kDa and 132kDa respectively (Fig, 18).

Full length BRCA2 was mainly found in the nucleus in HeLa cells (Fig, 55A). One fifth of the cytoplasmic fraction and half of the nuclear fraction were analysed (Fig 18). The nuclear fraction of HE11 exhibited a smaller fragment and we cannot rule out the possibility of other protein. From our western blot data in Fig, 18A, given the unequal load it was unclear whether E11 was expressed in the cytoplasm and/or nucleus. We thus performed Immunofluoresence (IF) staining, and clarified that E11 was mainly expressed in the cytoplasm (Fig, 18B). The CT fragment was mainly expressed in the nucleus of HeLa cells (Fig, 18A). The presence of NLS in this cloned segment possibly supported translocation of this fragment into the nucleus.

A)

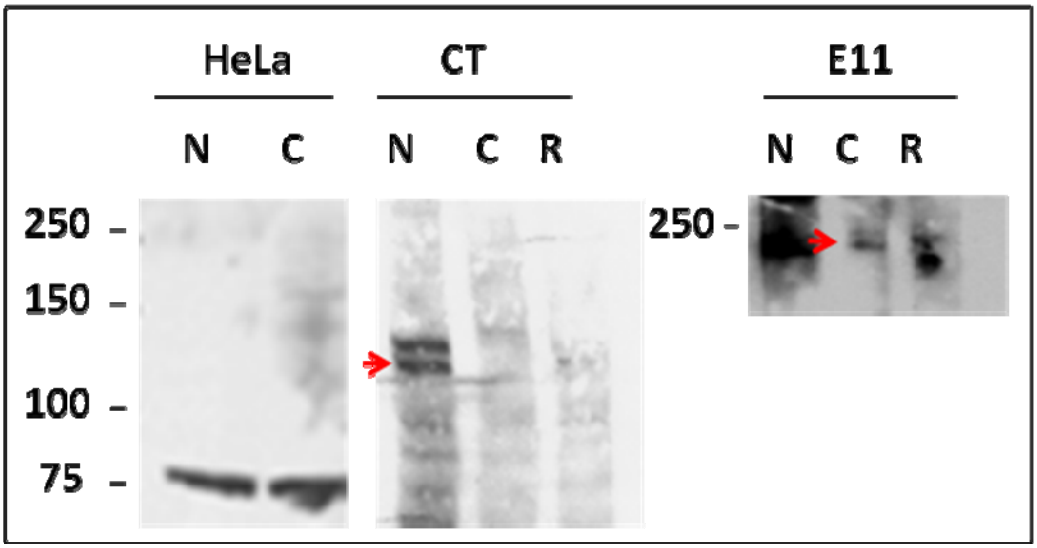

B)

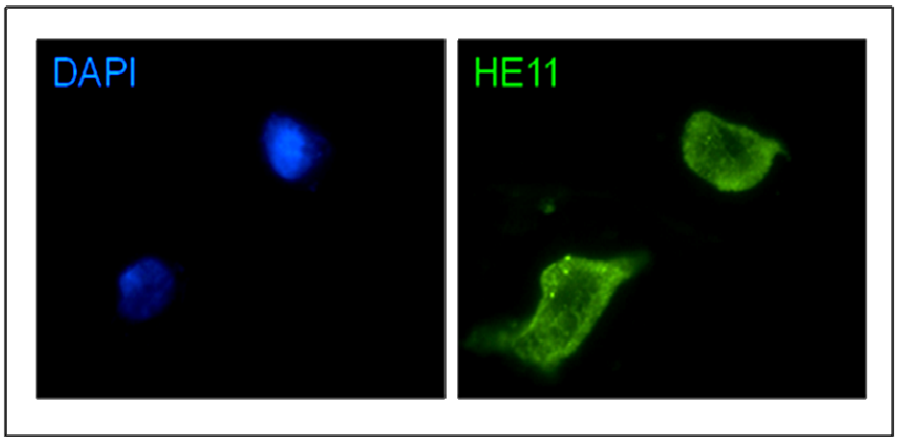

Figure 18, A) Detection of BRCA2 CT and E11. N represents the nucleoplasmic extract; C represents the cytoplasmic extract; R is the insoluble residue. B) IF detection of E11 fragment of BRCA2. E11 is found to be localised mainly in the cytoplasm in HeLa cells.

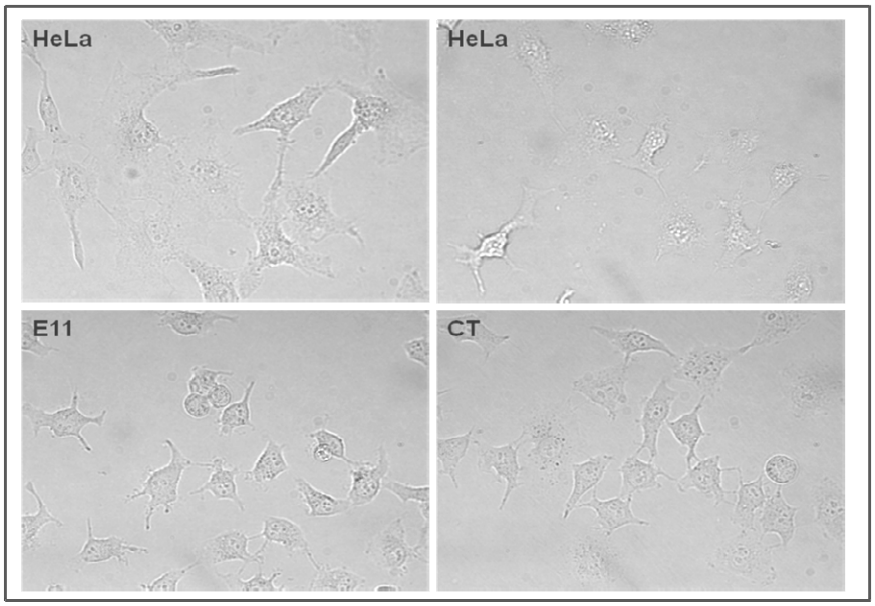

Figure 19, Phase contrast microscope images of untransfected and transfected HeLa cells at similar plating densities. There were no gross morphological changes after transfection. Images were taken under 40X magnification.

We noted that the transfected cells were less spreading in comparison to untransfected HeLa cells (Fig, 19). However, the gross morphology and growth rates of HeLa cells were unchanged after transfection with the different BRCA2 segments. Preliminary expression analysis indicates that E11 and CT cells express reduced levels of many extracellular matrix binding and focal adhesion molecules. Our microarray data showed that multiple genes involved in cell adhesion and extracellular matrix are downregulated over 2 folds in both E11 and CT cells in comparison to untransfected HeLa cells (Appendix 6.5).

3.6 Exon11 BRCA2 renders transfected cells more sensitive to specific DNA lesions

To investigate whether the cause of sensitivity of COS7BR2d105 cells and Capan-1 cells to BCNU was a specific or non specific effect. We undertook assessment of drugs sensitivity of BRCA2 transfected cells to an array of relevant genotoxins.

3.6.1. Analysis of DNA double strand break repair

Bleomycin creates double strand breaks in DNA, so repair of this damage is expected to require functional BRCA2 (Fig, 4). Sensitivity to DBS in DNA could not be observed within a few generations, thus a clonogenic assay for survival was undertaken. HeLa cells were sensitive to bleomycin with about 35 to 38% surviving after treatment with 20 to 40µunits drug. E11 was much compromised upon bleomycin treatment. It exhibited 19 to 23% cell survival after bleomycin exposure (Fig, 20). The CT terminus was also sensitive in comparison to HeLa but not as sensitive as E11. About 28% cell survival was evident at 40 µunits of bleomycin. Its sensitivity was in between that of HeLa and E11 with between 28 to 31% cell surviving between 20 and 40µunits.

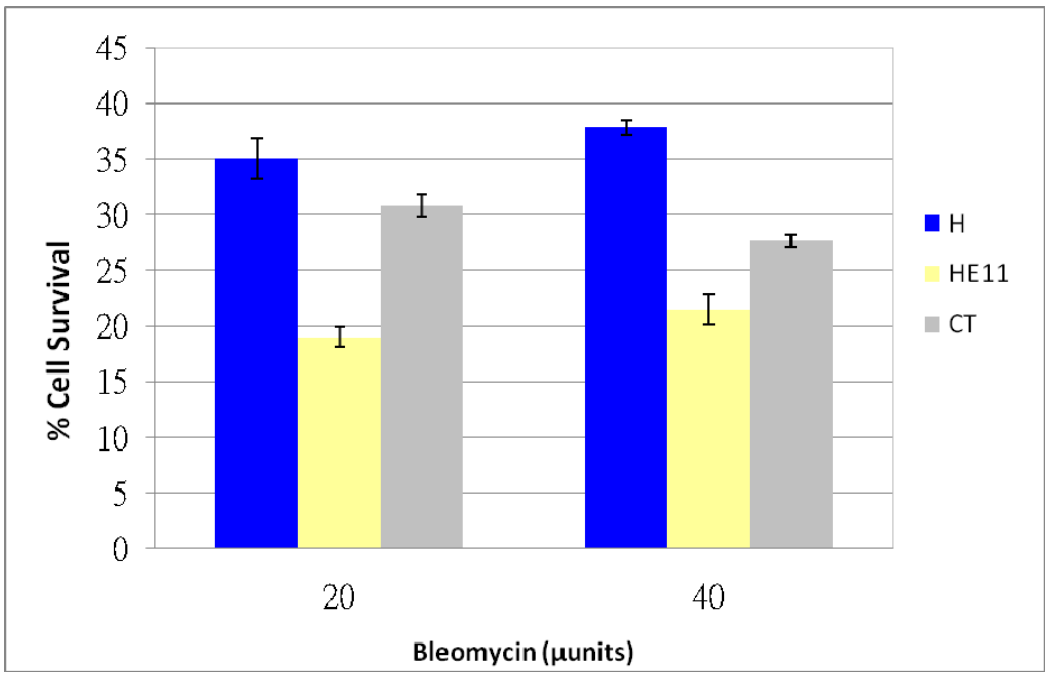

Figure 20, Long term survival responses of HeLa; E11 and CT expressing HeLa cells after bleomycin treatment. HE11 exhibited significantly enhanced sensitivity to bleomycin in comparison to HeLa cells. Data presented represent mean values and standard deviations of three independent assessments.

To assess the cause for heightened sensitivity, immunoflurescence staining was undertaken on HeLa and HeLa E11 cells on exposure to bleomycin. Cells were then fixed using methanol and stained for BRCA2 and Rad51 using their specific antibodies. Untreated HeLa cells showed poor diffuse, cellular staining for Rad51 with considerable protein in the cytoplasm (Fig, 21). After 6 hours of bleomycin treatment, Rad51 staining increased in both cellular compartments while the cytoplasmic staining was diffuse, nuclear Rad51 was punctate. There were between 20 to 30 foci observed per cell (Fig, 21). Rad51 staining increased dramatically on treatment and some nuclear membrane staining was also observed possibly relating to protein under transport.

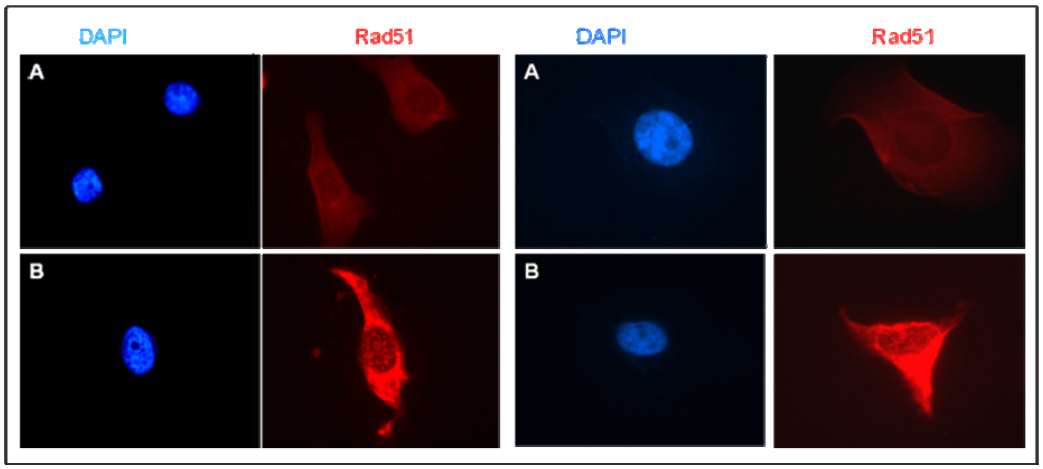

Figure 21, IF images of HeLa cells stained with Rad51 antibodies. A) In untreated HeLa, Rad51 was mainly localised in the cytoplasm. B) On treatment with bleomycin, nuclear Rad51 foci were observed.

We utilised an anti-BRCA2 antibody that specifically stained the E11 fragment and did not recognised endogenous BRCA2 (Fig, 22). The staining of BRCA2 E11 remained unchanged before and after treatment and it was mainly localised in the cytoplasm (Fig, 22). After bleomycin treatment, majority of Rad51 remained in the cytoplasm and foci formation was extremely poor. There were between 5 to 15 foci observed per cell. It must be noted that those transfected HeLa cells possess full length endogenous BRCA2. The diminished foci formation and cytoplasmic localisation of Rad51 in these transfectants suggests that the exon 11 fragment could bind Rad51 and possibly hinder its transport. This explains the higher sensitivity of the HeLa E11 cells to bleomycin treatment.

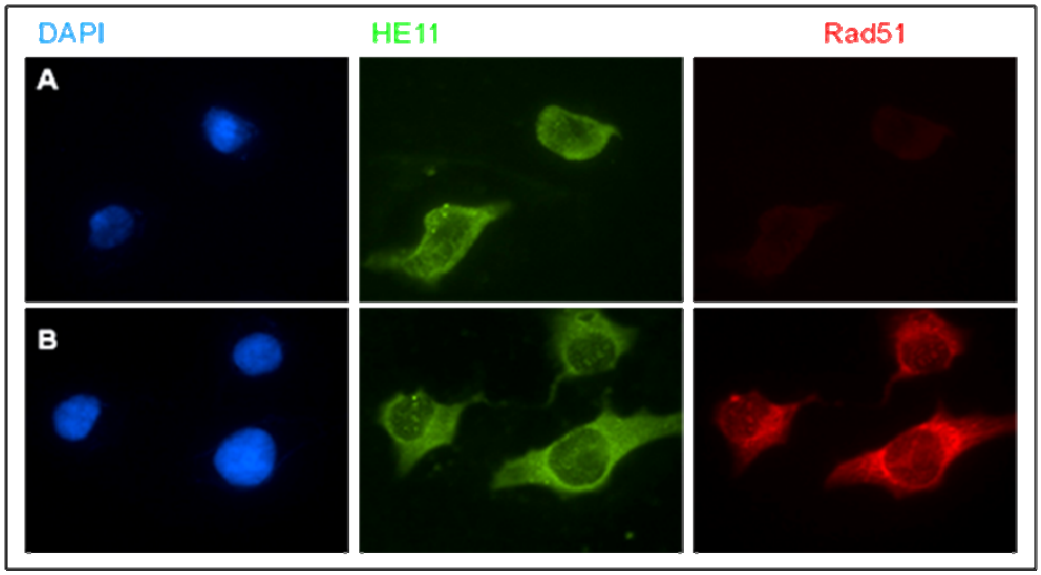

Figure 22, HeLa cells stained with BRCA2 E11 specific and Rad51 antibodies. A) In untreated HeLa E11 cells, Rad51 was mainly localised in the cytoplasm. B) In HeLa E11 cells treated with bleomycin for 6 hours, Rad51 foci formation was moderately to severely reduced.

The increased in sensitivity of CT cells to bleomycin could therefore be due to the competitive binding of Rad51 by the CT fragment (CT harbours the terminal Rad 51 binding domain).

3.6.2. Analysis of DNA repair capabilities

Analysis of the repair capabilities of E11 and CT by exposure to Methyl Methane Sulfonate (MMS) lesions were undertaken (Fig, 23). MMS reacts predominantly by an S_N2 alkylating mechanism and has the capacity to form single-strand breaks which are repaired by DBS (double-strand break) repair. All the cells tested exhibit similar sensitivity profiles. All cells tested showed dramatic sensitivity between 64 and 128 µM MMS. Massive sensitivity resulted in 70% cell death in HeLa cells, 80% cell death in HE11 cells and 95% in CT cells. Guanine modifications at the N^7 position is the predominant DNA lesion generated on MMS exposure. This drug can also cause 3-methyl purines that are routinely repaired by the BER pathway. Our data suggests that the transfected cells may be slightly more sensitive to MMS due to their double strand repair hindering abilities discussed in the previous section. However, we do not consider these differences to be of significance.

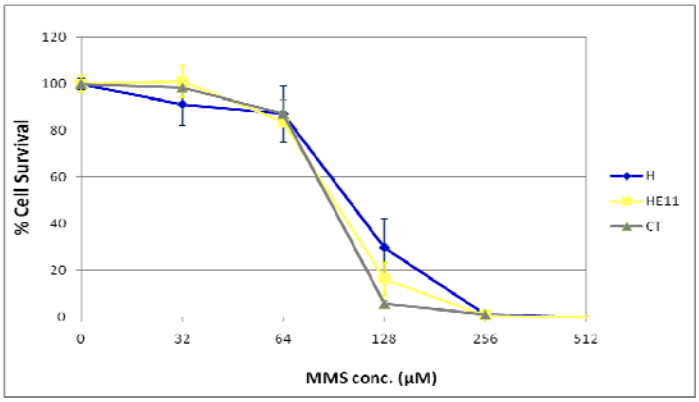

Figure 23, MMS sensitivity of HeLa and transfected cells. HeLa and the tranfescted cells demonstrate similar sensitivities towards MMS. Data presented represent mean values and standard deviations of three independent assessments.

MNU, an S_N1 type alkylating agent generates N^3 lesions on guanines, N^1 and N^3 lesions on adenine, N^3 lesions on cytosine and O^4 lesions on thymine. While all other lesions are managed by the BER pathway, the O^4 thymine lesions can be repaired by AGT. All our cell lines exhibited similar drug response profiles to MNU indicating unchanged capabilities (Fig, 24). It is likely that our choice of assay (short term sensitivity) was limiting our analysis of cellular responses and thus we additionally pursued long term survival responses in these cells (Fig, 26).

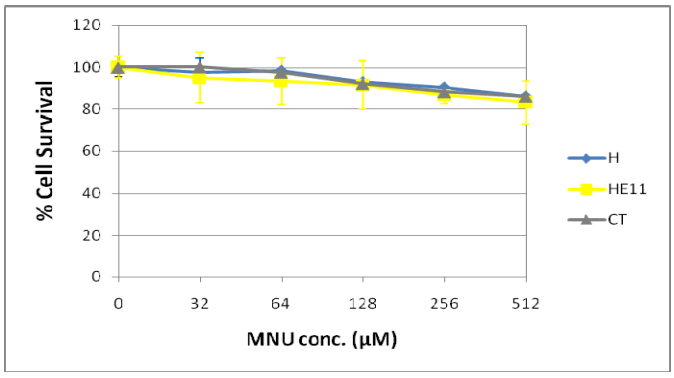

Figure 24, Short term toxicity responses to MNU. All cells tested exhibited mild

sensitivity to MNU. Data presented represent mean values and standard deviations of three independent assessments.

When short term BCNU drug responses were analysed, HeLa cells showed a dose dependent profile with an IC_{50} of about 128µM of BCNU (Fig, 25). E11 was more sensitive to BCNU at all concentrations compared to Hela with an IC_{50} of 64µM of BCNU exposure. CT responded similar to HeLa cells with IC_{50} of 128µM of BCNU. As discussed earlier, BCNU lesions are predominantly repaired by AGT. The transfection of E11 fragment into HeLa cells thus rendered the cells more sensitive towards this class of alkylating DNA damage despite unchanged levels of AGT.

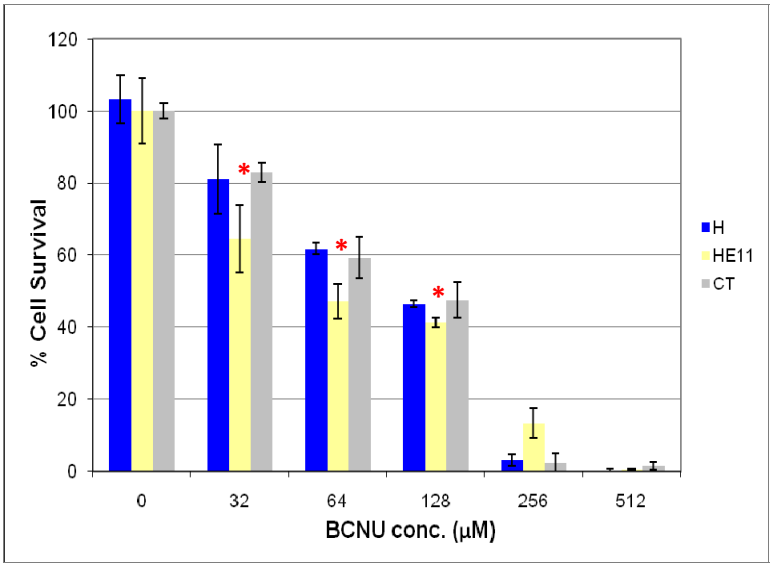

Figure 25, Short term drug survival responses of HeLa and HeLa transfected with different BRCA2 fragments exposed to BCNU. HE11 cells were the most sensitive across different concentrations of BCNU. Data presented represent mean values and standard deviations of three independent assessments.

To confirm these effects we tested the cells in clonogenic survival assays. In the long

term assays for BCNU sensitivity, HeLa cells showed 40% cell survival with an initial 10μM BCNU exposure. However, only 20% E11 cells survived at the same dose. The CT cells exhibited about 45% cell survival (Fig, 26A). E11 also appeared to form bigger colonies than HeLa and CT cells after drug treatment (Fig, 26B). Even though E11 could form bigger colonies, there was no apparent difference in growth rate between HeLa, HeLa E11 and HeLa CT cells. While unexplained, this phenomenon was repeatedly observed in all clonogenic survival assays. We hope that future detailing of the expression proteome in these cells using tiling arrays will clarify details of this unique observation.

A)

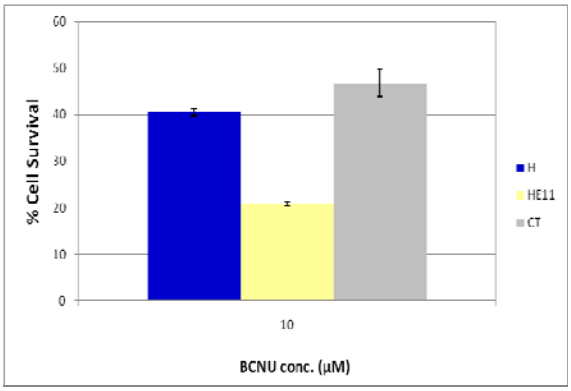

B)

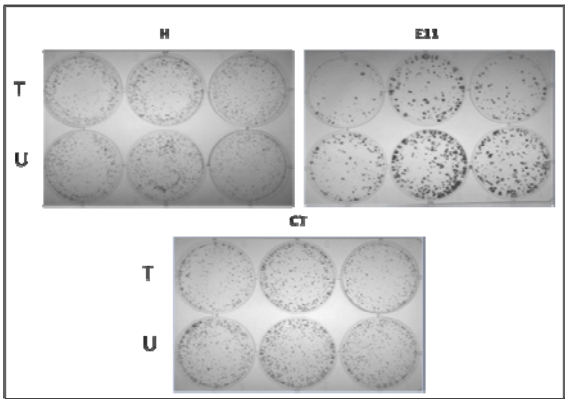

Figure 26, Long term BCNU sensitivities of HeLa and its transfectants. A) Percentage

cell survival quantitated and expressed as histogram. Data presented represent mean values and standard deviations of three independent assessments. B) Images of long term colony formation after 10µM BCNU treatment, the top row of wells (T; triplicates) represent the treated cells, while the bottom row (U; triplicates) are the untreated cells.

Streptozocin is a synthetic antineoplastic agent, consisting of a nitrosourea moiety interposed between a methyl group and a glucosamine. Streptozocin induced intrastrand crosslinks by DNA alkylation are principally repaired by AGT. If left unrepaired, they may inhibit DNA replication and these lesions may generate DNA strand breaks that would require homologous recombinational repair. All cells tested were insensitive to streptozocin in short term assay conditions. Based on our understanding of the lesion generated and its repair, we undertook clonogenic survival assessments to establish the long term toxicity of this class of DNA damaging agent. While HeLa cells were able to tolerate the drug, E11 cells exhibited hypersensitive to streptozocin on long term culture. Between 10 to 15 % HE11 cells survived exposure to 10 to 40µM streptozocin (Fig, 27A). This was not surprising, as we showed earlier that E11 cells are also compromised in their Rad51 mediated repair activity (HR; Fig, 20). We were thus able to obtain increased cytotoxicity by targeting 2 pathways crucial for the maintenance of genomic fidelity. Further analysis of the CT clones was not undertaken as they did not show enhanced sensitivities to BCNU in comparison to HeLa cells in our short term and long term assays.

A)

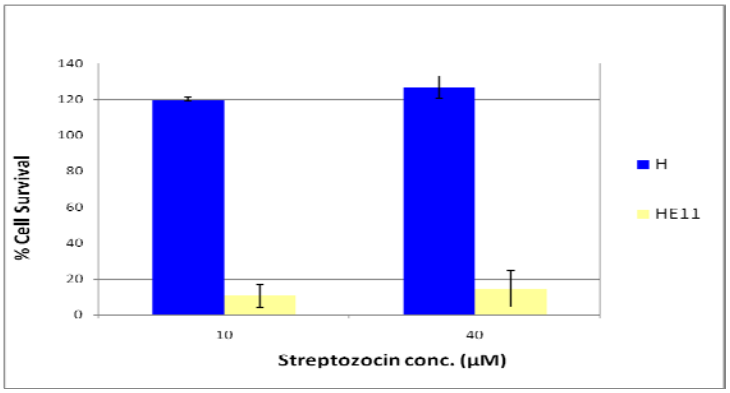

B)

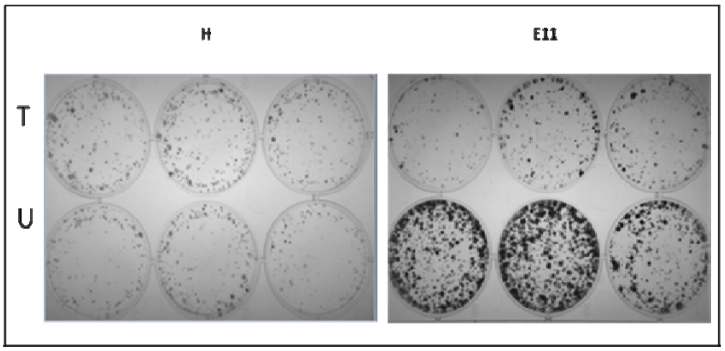

Figure 27, A) Long term survival response of cells to streptozocin. E11 is extremely sensitive to streptozocin in comparison to HeLa. Data presented represent mean values and standard deviations of three independent assessments. B) Images of the long term colonies of HeLa and HE11 after 10µM of Streptozocin treatment, the top row of wells (triplicates) represent the treated cells, while the bottom row (triplicates) are the untreated cells.

We questioned why Exon11 rendered the cells to be highly sensitive to alkyl DNA damaging agents, despite the presence of high levels of endogenous AGT. Could there be an interaction between the E11 fragment and AGT? Hence, we undertook immunoprecipitation analysis.

3.7 E11 and CT region of BRCA2 support AGT interaction

We performed pull downs to assess for protein-protein interaction. AGT was pulled down from 1 mg of total cellular protein. Reciprocally, Flag specific antibodies were used to pull down the E11/CT BRCA2 fragments. IP was performed on cells treated either with (A) 100 µM of O^6-Benzylguanine (O^6BG) for 6hrs, in presence of proteosomal inhibitor, MG132 or (B) 200 µM of BCNU treated cells followed by a 16 hours recovery. O^6BG modifies AGT by direct alkylation while BCNU causes indirect AGT modification by creating an alkyl-DNA lesion first. Presence of MG132 blocks proteosomal processing of the alkyl-AGT.

We first assessed the BRCA2-AGT interaction in 293T cells expressing AGT under the control of a CMV promoter. Using BRCA2 specific antibody to pull down from HeLa lysates, weak interaction with AGT was noted. Interaction between BRCA2 and AGT was heightened in O^6BG exposed HeLa lysates presumably due to alkyl-AGT generation. Using flag specific antibodies for pull down studies on the 293T transfected cells; we observed AGT pull down only from O^6BG treated lysates (Fig, 28). IgG controls were run, and there was no pull down. The untreated samples did not have AGT pull down using flag and BRCA2 specific antibodies. Both E11 and CT fragments seemed able to bind alkyl-AGT. While multiple sites of interation between proteins is possible, we noted that the CT expressing cells were not sensitive to BCNU while the E11 cells were (Fig, 17). Since the 293T model is a doubly transfected model, we decided to shift our analysis to a system supporting endogenous AGT and BRCA2 (using HeLa cells).

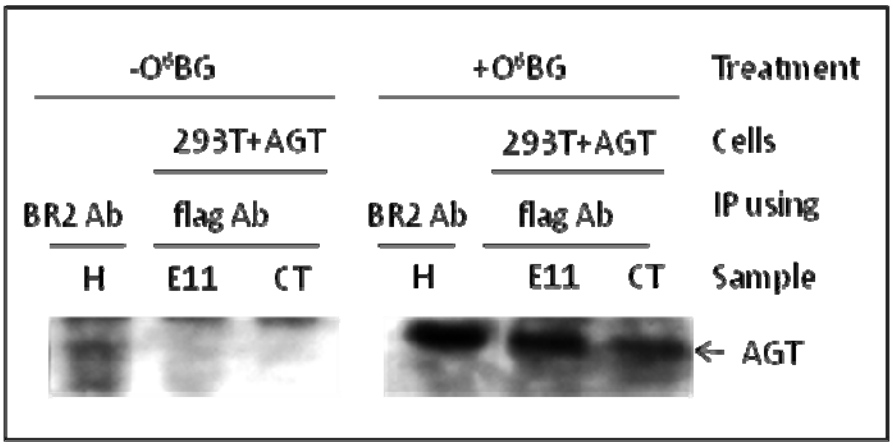

Figure 28, HeLa and 293T clones IPed with BRCA2 and flag specific antibodies respectively. Lysates were either untreated or treated with O^6BG. There was preferential pull down of AGT after O^6BG treatment.

In HeLa cells, AGT pulled down was achieved only after exposure to O^6BG (Fig, 29). This indicated that full length BRCA2 interacts with alkyl-AGT preferentially. In the HeLa transfected cells, E11 and CT were also able to pull down AGT after O^6BG exposure but to a lesser individual extent when compared to HeLa. The binding of the E11 and CT fragments to alkyl-AGT could cumulatively account for the pull down observed in the total HeLa lysates on O^6BG treatment. Normal mouse IgG was used to establish the specificity of the pull downs.

To test the relevance of these interactions with alkyl-AGT, we undertook pull downs on lysates from BCNU treated cells. We were able to observe AGT interaction with the E11 fragment of BRCA2 on BCNU exposure (Fig, 29). Our cloning strategy did not include NLS for BRCA2 exon11 and visualisation by IF showed that exon11 was indeed localised in the cytoplasm (Fig, 18). Our data suggests the possibility of exon11 region of BRCA2 interacting with alkyl-AGT in the cytoplasm of cells. Interestingly, the

CT region did not interact with AGT in lysates from BCNU exposed cells (Fig, 29). This suggested that the BRCA2 CT-alkyl-AGT interaction was not supported on generation of a DNA lesion but only possible on O^6BG exposure.

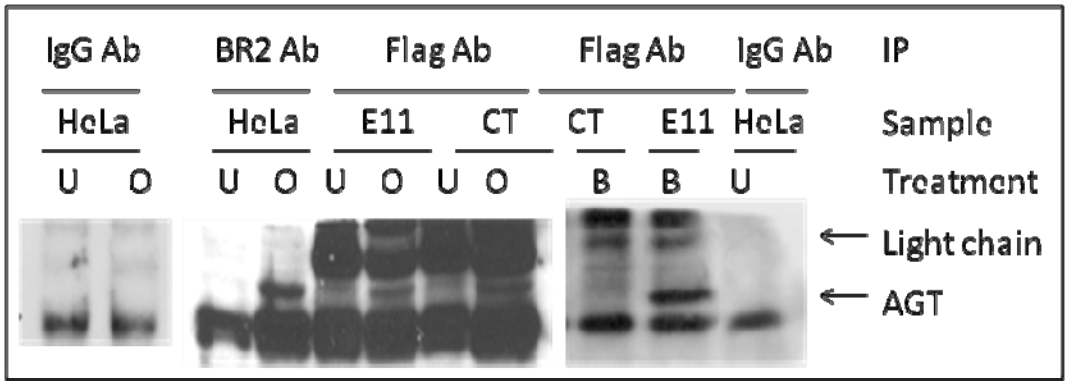

Figure 29, HeLa clones IPed with flag specific antibodies. Untreated cells (U), O^6BG treated cells (O) and BCNU treated cells (B) were used for lysate preparations. BRCA2 segments preferentially pull down AGT after either BCNU or O^6BG exposure (in collaboration with Nurul).

Reciprocal IP was performed using anti-AGT antibodies but BRCA2 detection was difficult possibly, in part, due to less efficient pull down of BRCA2 using anti-AGT antibodies. If multiple AGT molecules interact with one BRCA2 then the efficiency of pull down using anti-BRCA2 antibody would be far greater than the reverse IP. Further, BRCA2 protein has been reported to be heat labile if incubated at temperatures more than 55°C (F Chen, 2004). However it was not possible to cleave the protein off the beads at the recommended temperature, and we had to resort to boiling at 95°C. This possibly added to the poor detection of BRCA2 in our reciprocal IPs.

To date, AGT is thought to act alone in the alkyl lesions repair. After repairing the lesions, it is believed that alkyl-AGT is inactivated, ubiquitinated and targeted for proteosomal destruction (Srivenugopal, 1996). 1:1 stoichiometry of lesion repair is recognised. To repair further lesions, fresh synthesis of AGT is required. Little is known about the transport of AGT and it has been hinted that there may exist a molecule that assists and mobilises AGT, protein that lacks its own NLS. After establishing the interaction between BRCA2 and AGT, we decided to assess AGT processing in the cells in an attempt to gain further insights into BRCA2's possible role in proper AGT function.

Previous reported efforts to tag AGT at the N terminus have generated functional dead proteins. We thus cloned full length AGT gene into a green fluorescent protein plasmid that tagged the GFP protein onto the C-terminus region of AGT. This fusion protein has an estimated size of 48KDa, due to the combined size of green fluorescent protein (26KDa) and AGT (22KDa).

3.8 AGT localisation and transport in cells

3.8.1 AGT-GFP expression models

In an attempt to traffic AGT in live cells we created a GFP tagged AGT. Full length AGT was cloned into pEGFP-N1 vector such that the fusion protein expressed GFP at the CT of AGT. GFP vector and insert (AGT) were ligated on directional cloning and resulting AGT-GFP plasmid was transformed into DH5α cells. Three positive colonies were picked for restriction digestion analysis and PCR analysis (Fig, 30). We confirmed that clones #2 and #3 were successfully transformed with AGT-GFP plasmid (Fig, 30). PCR using specific primers for pEGFP-N1 plasmid sequences should provide the following. For successful transformants a 1093bp is expected. pEGFP-N1 plamisd alone would produce a 312 fragment amplicon, and AGT in its parent pSPORT plasmid would not amplify anything using these primers. We confirmed that clone #2 and #3 represented AGT cloned into pEGFP-N1. We digested miniprep DNA samples with SacI and XhoI. On successful cloning a 647bp release is anticipated (Fig, 30). Maxiprep was performed on #2 and #3 to obtain pure plasmid for sequence analysis. We confirmed that #2 and #3 maintained frame for AGT-GFP expression (Fig, 31; Appendix 6.2 & 6.3). pAGT-GFP #2 was then transfected into HeLa and 231 cells. Two rounds of Geneticin selection, each lasting 2 weeks, was performed on HeLa and 231 cells after which the cells were sorted by FACS (Appendix, 6.4) based on their GFP expression levels. For all further studies, sorted cells expressing high levels of GFP were utilised.

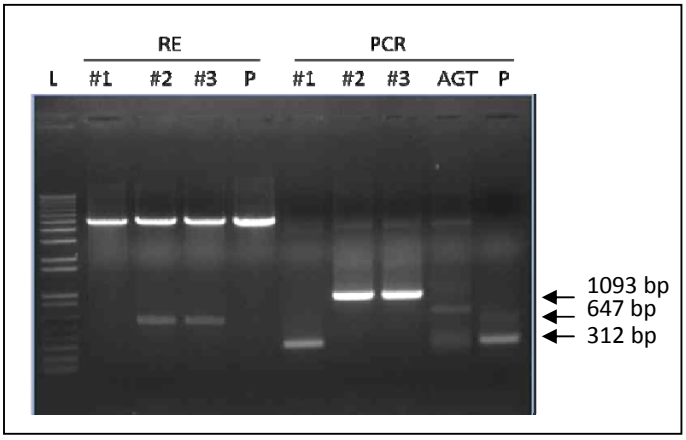

Figure 30, Agarose gel analysis of digested fragments of picked colonies after transformation. PCR showed that clones #2 & #3 carry AGT-GFP, P represents parent plasmid; AGT represents parental plasmid pSPORT with AGT cloned in it. L is the 1Kb+ DNA ladder.

A)

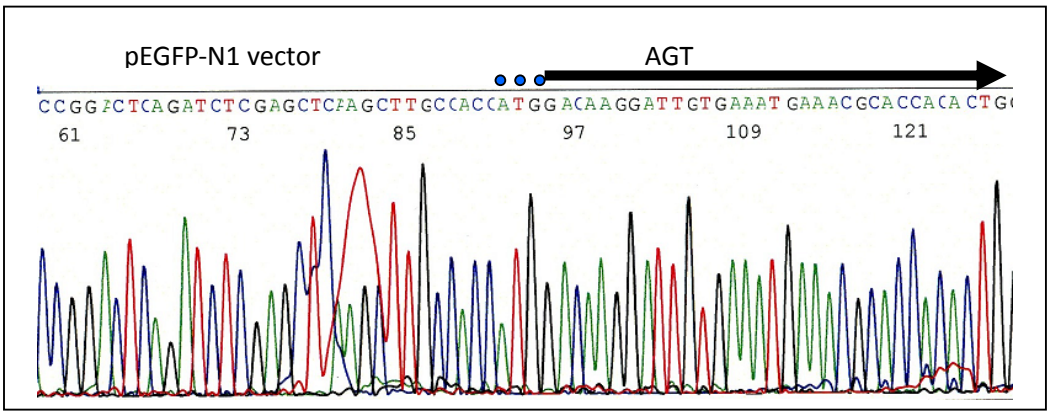

B)

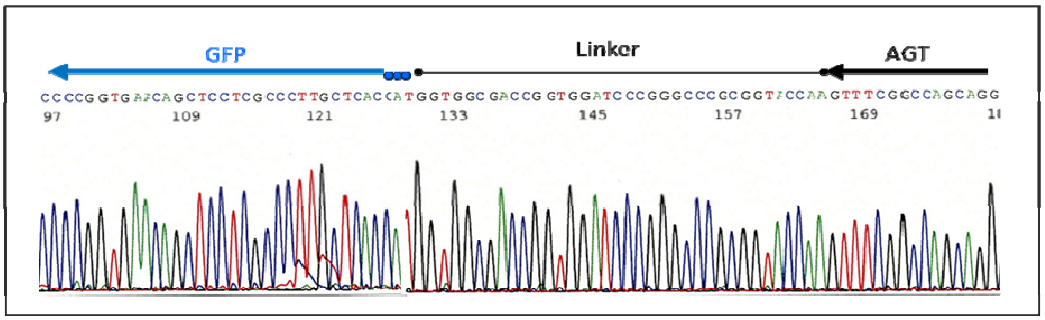

Figure 31, A) Sequence of AGT-GFP with forward primer. B) Sequence of AGT-GFP with

reverse primer. AGT was successfully cloned into pEGFP-N1 vector and frame was maintained for expression of the fusion protein.

AGT-GFP plasmid transfection into 231 and HeLa cells produced a 48 KDa fusion protein of AGT-GFP that was detectable by either AGT (Fig, 32) or GFP specific antibodies. AGT-GFP was observed to be mostly nuclear by fluorescent microscopy (Fig, 33). AGT-GFP retained the fluorescence properties of GFP together with the nuclear localisation characteristic of endogenous AGT. *In vivo* AGT-GFP trafficking study were carried out after successful selection and sorting.

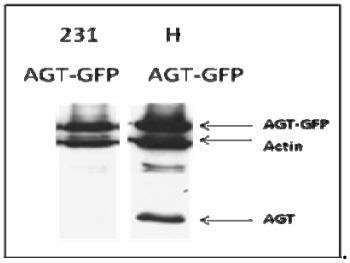

Figure 32, SDS-PAGE western immunoblot analysis of AGT-GFP expression in 231 and HeLa cells transfected with AGT-GFP plasmid. Actin was used as a loading control. Both 231 and HeLa cells expressed high levels of the fusion protein, while only HeLa cells expressed the endogenous AGT protein.

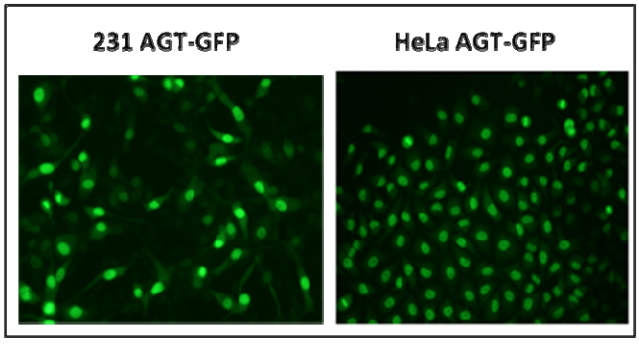

Figure 33, AGT-GFP expression in sorted cells (for high expression) under 5X magnification. AGT-GFP was predominantly nuclear in both transfected cell lines.

3.8.2 AGT-GFP trafficking in cells

We sorted HeLa and 231 transfected cells into 3 populations expressing different levels of AGT-GFP (negative, low and high). The high expressors were used in our analysis. To study the biology of AGT-GFP in cells after alkyl insult, the sorted HeLa and 231 cells transfected with AGT-GFP were treated with 200 μM of BCNU. After 2 hours treatment samples were supplemented with serum and visualised under a Nikon C1 Plus Confocal Microscope System. A CO_2 and temperature regulated chamber was utilised to study live cells plated on coverslips. Images were captured hourly.

In transfected HeLa cells, we observed strong nuclear punctate signal for AGT-GFP at the end of 2 hours of BCNU treatment (T1) and this strong signal lasted up to T4 (Fig, 34). The foci sites were maintained throughout 21 hours; however the signal intensity went down by 5 hours after the initial 2 hour BCNU treatment (T5). By T6 there was high signal reduction of AGT-GFP and by T8 hour some AGT-GFP signal regeneration was observed. The cells were monitored until T20 but no significant alterations were observed from those presented at T12 (Fig, 34). The foci formation perceived in the nucleus of the cells suggested that AGT-GFP localised to sites of DNA damage after BCNU insult. From T6 to T8, AGT-GFP staining was less intense, and was still visible in cytoplasm; yet complete loss was not visualised in the cells. This suggested that some AGT-GFP was being processed after BCNU insult. Complete loss was not visualisable possibly due to constant re-synthesis of AGT-GFP over time (protein was under the conrtol of the CMV promoter).

Time lapse study of AGT-GFP trafficking in HeLa cells (U~T6) GFP

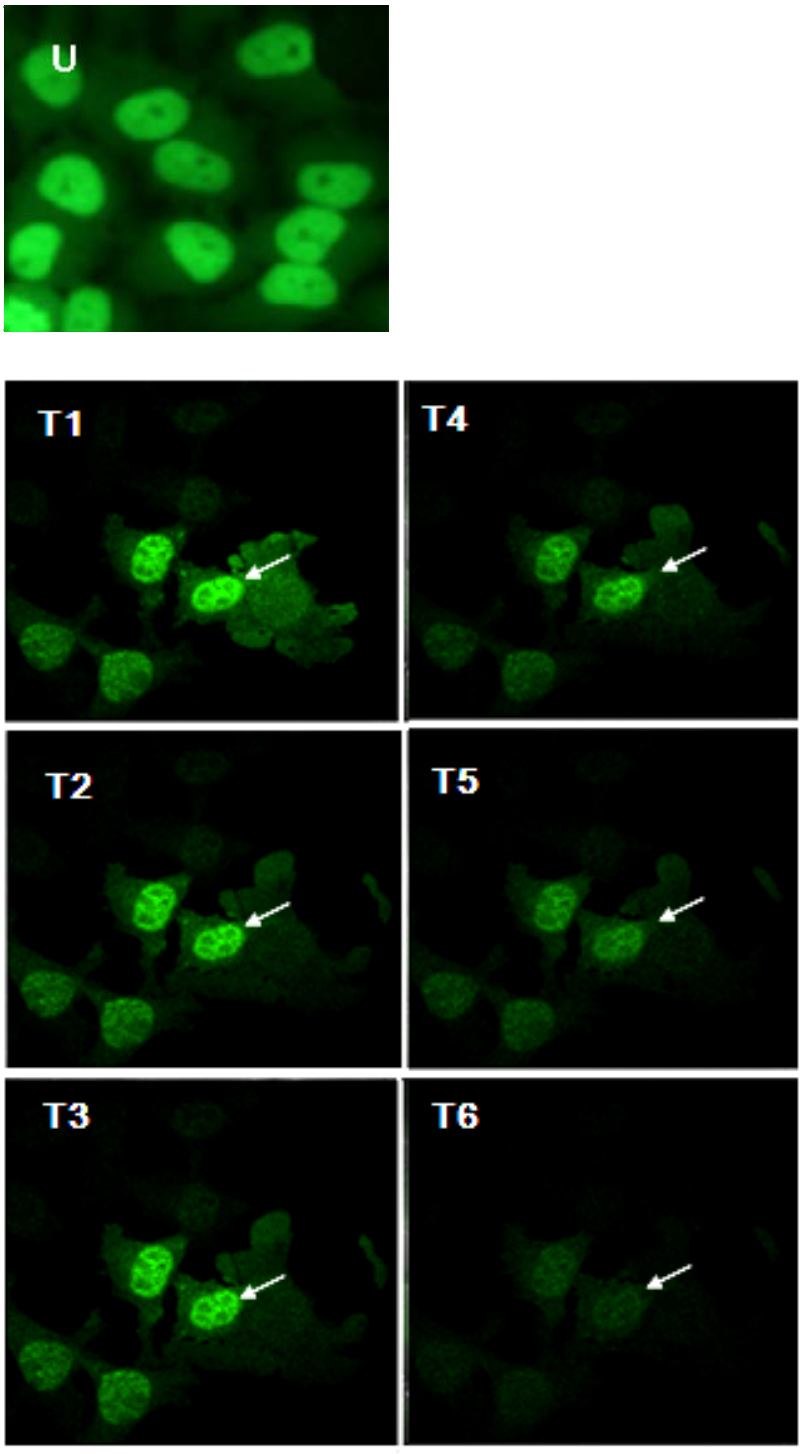

Time lapse study of AGT-GFP trafficking in HeLa cells (T7~T12) GFP

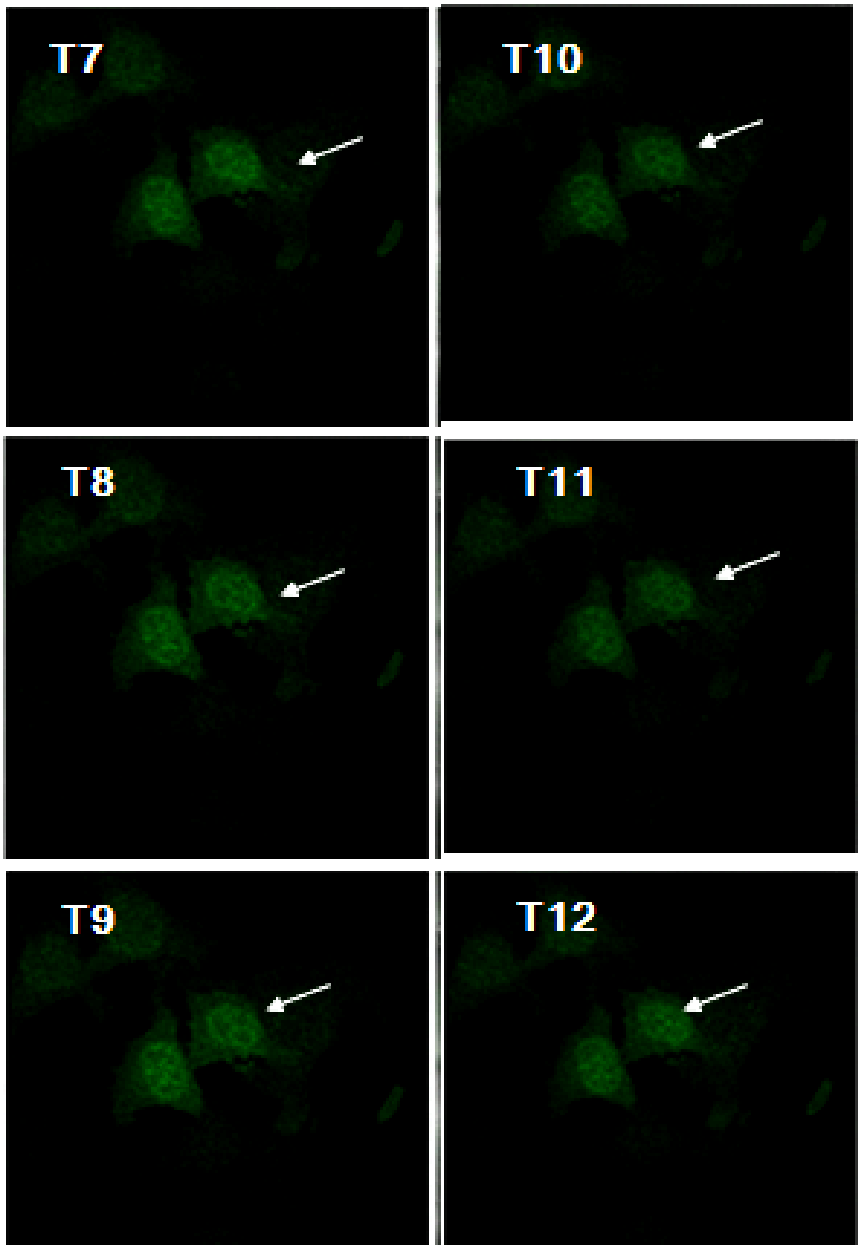

Figure 34, Time lapse imaging of AGT-GFP in HeLa cells. A two hour treatment with 200 µM BCNU was undertaken and images acquired at the end of the treatment were designated T1. Images were acquired hourly under oil immersion 100X magnification. Representative images over 12 hours are included here. Arrows indicated the cells that were tracked. AGT-GFP became puntacte after BCNU treatment.

Increased mobility of 231 AGT-GFP cells were observed in our study. This is not surprising as 231 is a highly transformed cell line. In contrast to HeLa AGT-GFP cells, no punctate signal was observed in transfected 231 cells after BCNU treatment (Fig, 35). Nevertheless, AGT-GFP signal gradually reduced from T1 to T6 as observed in the cell indicated by the colour coded arrows. Like HeLa cells transfected with AGT-GFP, AGT-GFP signal in 231 cells was also reduced after exposure to BCNU suggesting that AGT-GFP processing was also supported in 231 cells. Complete loss of AGT-GFP signal was also not perceived in 231 cells for reasons of constant re-synthesis.

AGT-GFP localisation in the 231 cells (U-T6) GFP

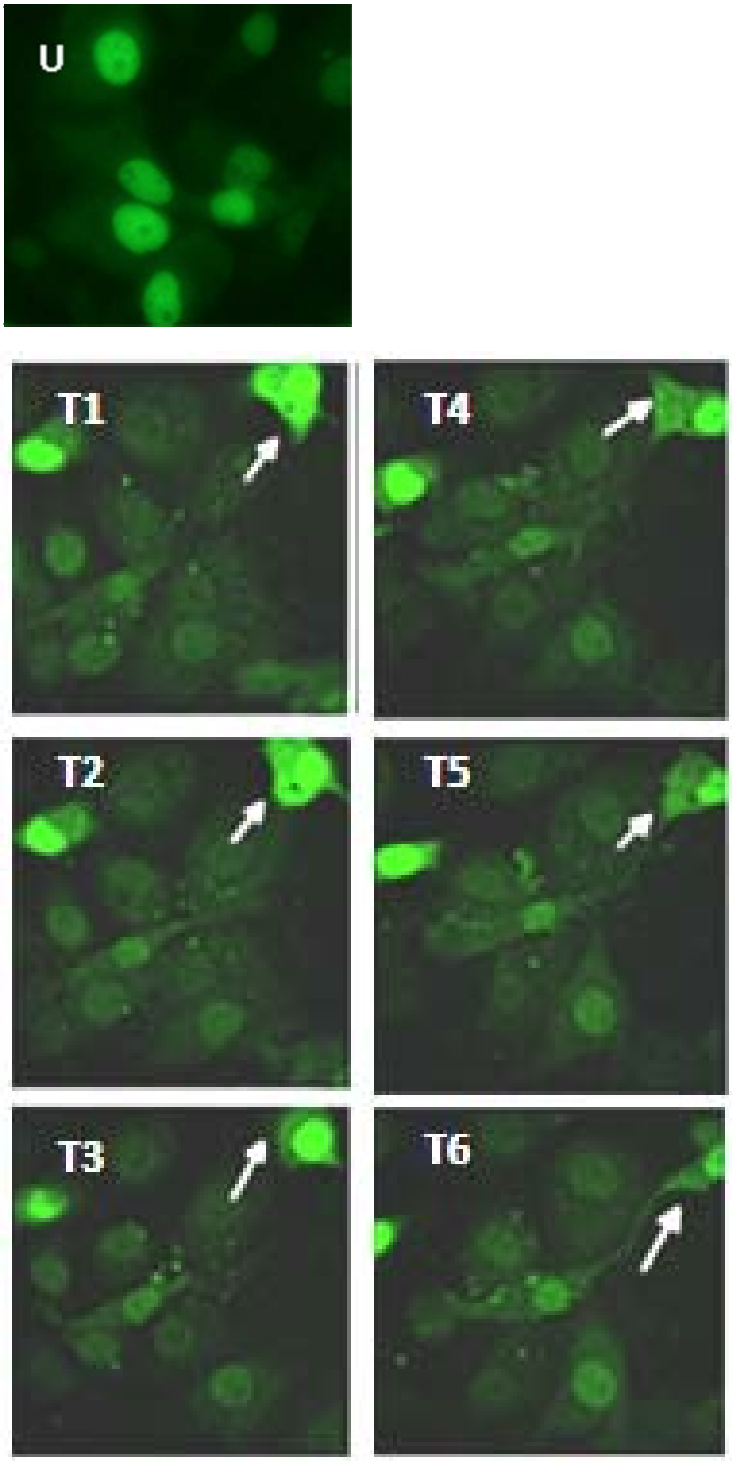

AGT-GFP localisation in the 231 cells (T7-T12) GFP

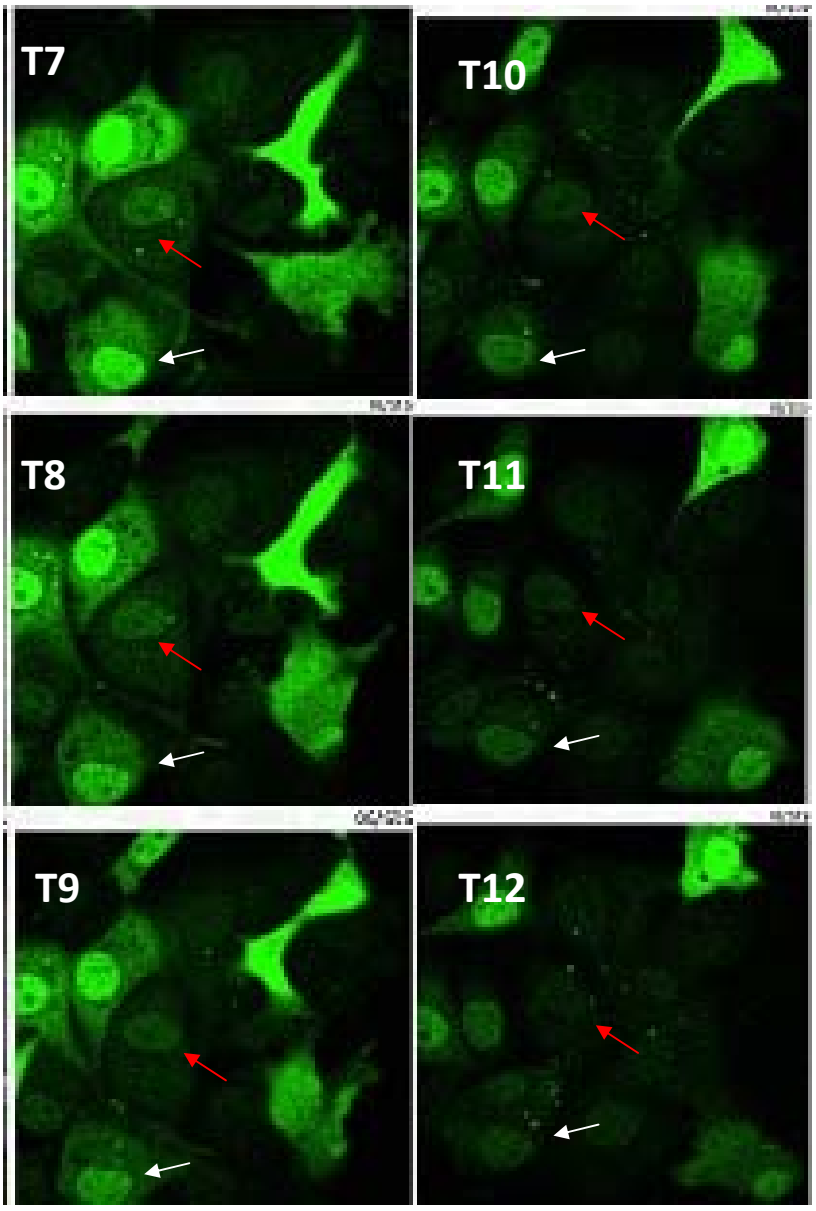

Figure 35, AGT-GFP localisation in transfected 231 cells from T1 to T12 after BCNU treatment. AGT-GFP signal was diffuse nuclear but reduced after exposure to BCNU. Arrows indicate the cells that were tracked; pictures were taken under oil immersion 100X magnification.

It is reported that AGT binds to DNA in a co-operative manner with four AGT molecules binding to one 16 mer of lesion carrying DNA (Joseph J. Rasimas, 2004). However, the same has not been established on genomic DNA. It is further interesting that lesion repair stoichiometries are 1:1 in that one AGT molecule repairs only one DNA lesion. Based on our findings we postulate that AGT-GFP in HeLa cells utilises endogenous AGT binding to sites of DNA damage as an anchorage point for AGT-GFP loading thus allowing for visualisation of foci. Since 231 cells do not have endogenous AGT, foci formation is not supported. The processing of AGT-GFP in both cells seemed retarded in that we were not able to visualise complete loss of signal at any given time. This could also be due to limiting lesions generation (short term BCNU exposure) or due to constant synthesis of the fusion protein. We observed speckled nuclear AGT in BCNU treated HeLa cells. This leads us to propose that AGT loading onto sites of damage may be concerted and cooperative in cells. The foci formation response could be a mode to regulate protein turnover in cells. We proposed to study the ability of the AGT-GFP to support essential interactions in an attempt to clarify their lesion processing abilities.

3.8.2 AGT-GFP possibly interacts with BRCA2

We then undertook IP of AGT-GFP with BRCA2 to assess whether exogenous AGT-GFP hinders AGT interaction with BRCA2. 1 mg of total cellular protein from HeLa AGT-GFP cells was used in the reciprocal pull down of AGT and/or BRCA2. BRCA2 specific antibodies were used to pull down AGT, while AGT specific antibody was used to pull down BRCA2. Western blot was probed with a GFP-HRP antibody, and the specificity of GFP antibody was confirmed using HeLa lysate as control or with BRCA2 specific antibodies.

BRCA2 antibodies were able to pull down AGT-GFP from the HeLa AGT-GFP lysate (Lane 1; Fig, 36). AGT antibody was also able to pull down AGT-GFP and BRCA2 (Lane 2). AGT antibody was able to pull down more AGT-GFP when compared to AGT-GFP co-IPed with anti-BRCA2 antibody. The GFP-HRP antibody specifically identified the tagged proteins in lysates (Lane 3-4). The interaction between BRCA2 and AGT-GFP was clarified from the observation of reciprocal IP. Very little pull down of BRCA2 by AGT antibody suggested that multiple bindings of AGT exist in BRCA2. BRCA2 non-detection in the lysates was due to our unability to load sufficient amounts of lysate (minimally 100μg of total protein is required for detection of BRCA2). For the purpose of BRCA2 detection we attempted to cleave the pulled down proteins off the beads under denaturing conditions at a lower temperature of 65°C for 10 minutes. Using this method, we were able to detect BRCA2 in the loading wells in our IPed samples.

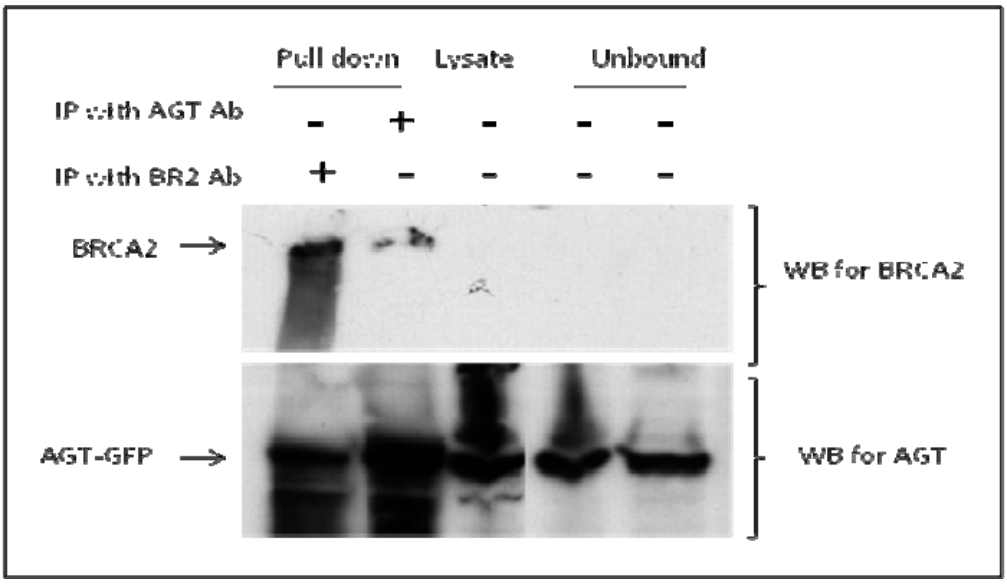

Figure 36, Reciprocal IP utilising full length BRCA2 antibodies and AGT specific antibodies. AGT-GFP could interact with BRCA2.

3.8.3 AGT-GFP is processed differently than endogenous AGT

On nuclear and cytoplasmic extraction of HeLa cells transfected with AGT-GFP, we observed differences in the sizes of endogenous AGT in different compartments. On SDS-PAGE analysis, the mobility of cytoplasmic AGT was slightly retarded in comparison to nuclear AGT. Such mild differences were not clarified with exogenous AGT-GFP. We suspected the differential mobility might be due to varying post-translational protein modifications such as phosphorylation. Thus we reprobed the blot with anti-phosphorylation antibodies and anti-acetylated lysine antibody. We could not detect AGT phosphorylation on reprobing with anti-phosphorylated serine/threonine/tyrosin antibodies possibly due to the harsh stripping conditions employed in multiple reprobings. However we believe that AGT is a phosphorylated protein when in the cytoplasm (discussed in 3.10.1; Fig, 51).

We also observed a ~29KDa band that was present in both untreated nuclear and cytoplasmic fractions when probed with anti-AGT antibody. This band was the predominant form of AGT in the cytoplasm. We questioned if this band was due to post-translational protein modifications such as ubiquitination or sumoylation, as they can cause significant increase in protein size. These modifications are involved in a diversity of processes and are some of the largest known post-translational modifications. Polyubiquitination specifically targets proteins for degradation by the 26S proteasome. Monoubiquitination serves as a sorting signal that directs membrane proteins for degradation within the lysosomal compartment (Haglund, 2003). SUMO appears to be involved in a larger variety of cellular processes, including nuclear transport, maintenance of genome integrity, transcriptional regulation and signal transduction (Hay, 2005). We assessed for possible ubiquitinated or sumoylated forms of AGT. The blot was reprobed with anti-ubiquitin antibody (data not shown) and anti-SUMO antibody. The ~29KDa form did not correspond to a ubiquitinated protein. The ~29KDa band on AGT western blot corresponded to a sumoylated protein. Computer based sumoylation prediction software showed a predicted sumoylation site at 364aa in GFP protein. After 16 hours of 200 μM BCNU treatment, the sumoylated GFP fragment was less apparent in both the nuclear and cytoplasmic compartments. This suggested that sumoylation of AGT-GFP could have a protective hold on the protein and desumoylation could be important for the fusion protein's activity.

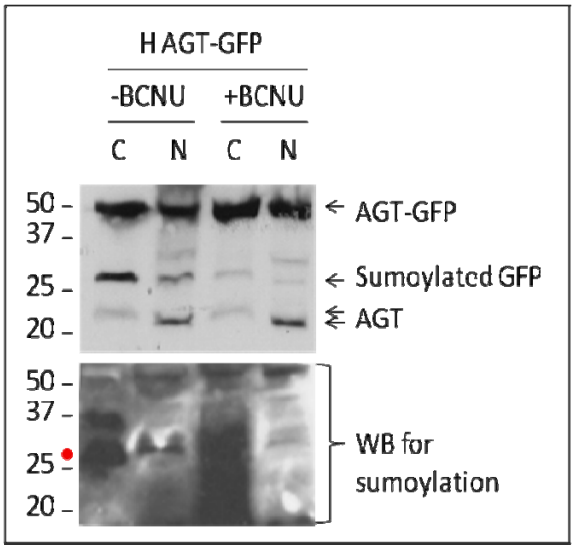

Figure 37, Western blot analysis of AGT in BCNU treated HeLa cell transfected with AGT-GFP. The blot was reprobed with anti-SUMO antibodies.

To study AGT processing, degradation of the protein was tracked by exposing lysates with O^6BG at indicated time points over a period of 18 hours (Fig, 38). Whole cell lysates of Hela and 231 cells transfected with AGT-GFP were treated with O^6BG, ATP and $MgCl_2$ to study the *in vitro* AGT processing. ATP was added as the energy source for ATP dependent proteosomal degradation. Western blots were probed with antibodies against AGT, GFP and Actin; infrared secondary antibodies (800nm and 680 nm; Li-cor) were utilised for convenience of detection.

It was observed that the signal for endogenous AGT and AGT-GFP did not visibly disappear or alter over time. We observed other fragments of sizes between 25 to 37KDa (in green) being enriched after treatment in HeLa AGT-GFP cells, we could however not rule out that they could be modified versions of the endogenous protein (Fig, 38A). The ~29KDa GFP fragment was observed across the blot (red arrow). HeLa AGT-GFP cells showed higher molecular weight green staining greater

than 50KDa after 18 hour treat, indicating that AGT-GFP was possibly getting modified and thus functional.

In 231 AGT-GFP cells, those small molecular bands observed below 50KDa came from processed AGT-GFP (Fig, 38B). 231 AGT-GFP cells also showed higher molecular weight green staining greater than 50KDa after 18 hour treatment, indicating that AGT-GFP was possibly getting modified. The absence of reduction of AGT-GFP in the cells could be due to slower *in vitro* processing of AGT-GFP. Poor processing of endogenous AGT could be due to high amount of competitive AGT-GFP in the lysate. Thus we went on to study *in vivo* processing of AGT and AGT-GFP.

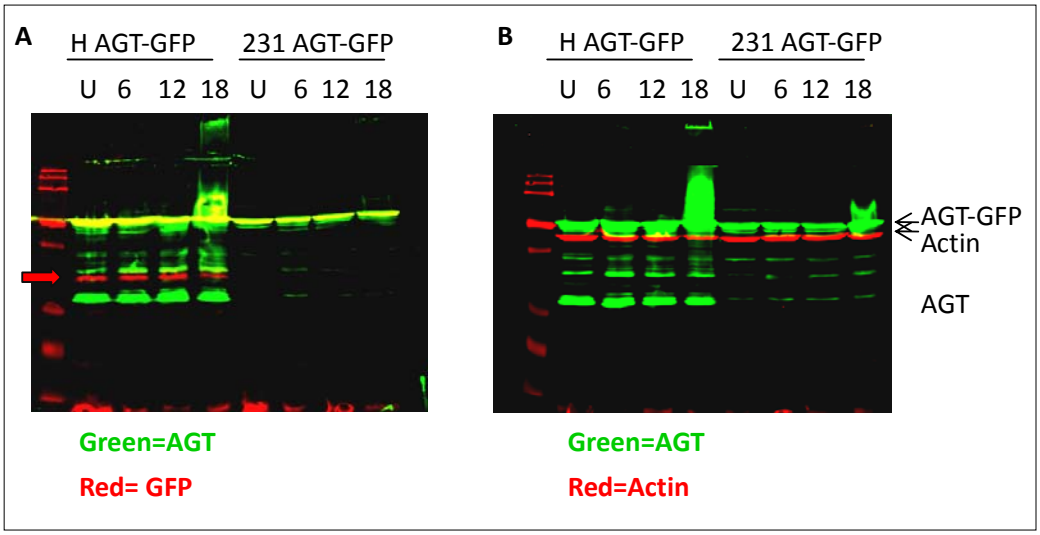

Figure 38, In vitro degradation of AGT and AGT-GFP on 200 µM of O^6BG treatment. Red arrow indicates the sumoylated fragment.

For *in vivo* analysis, Cells were treated with 200 µM of O^6BG; nuclear and cytoplasmic extracts were prepared at indicated time points and resolved on a 12% SDS PAGE (Fig, 39). Blots were probed with antibodies against AGT and Actin. Blot for nuclear

extracts was stripped and reprobed for cyclin B1. However, poor signals ensued owing to harsh stripping requirements to remove the AGT primary signals. Data for the same is thus not included here and actin was used instead in comparisons. We were able to detect significantly lower levels of AGT in the nuclear compartment at 10 hours and none was detected at 16 hours (Fig, 39). We observed a few higher molecular weight fragments between 25 to 37 KDa representing modified AGT in this compartment. This could indicate that alkyl-AGT could be modified and processed in the nuclear compartment or that alkyl-AGT was transported to the cytoplasm for processing.

In the cytoplasm compartment, we were able to see significant AGT reduction on exposure to O^6BG. We also observed significant modified forms of AGT in this compartment at 8-10 hours. This suggested that endogenous protein is rapidly processed and modified in the cytoplasm on O^6BG exposure. The rate of AGT-GFP processing by O^6BG was severely retarded or synthesis matched processing and thus we were unable to visualise AGT-GFP losses within the time tested.

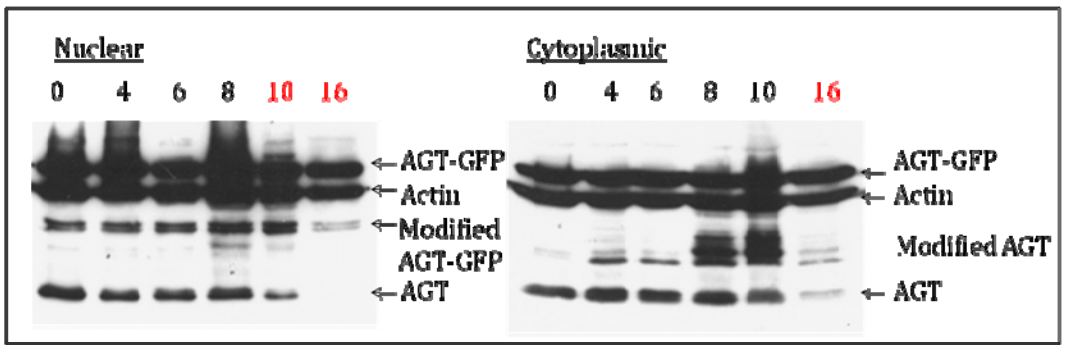

Figure 39, Western blot analysis of AGT in the nucleus and cytoplasm after 200 µM of O^6BG treatment. Modified AGT were observed on treatment in the cytoplasmic compartment.

On alkylation, AGT is believed to be processed by the proteosomal pathway hence we used proteosomal inhibitors to analyse poteosomal processing of AGT. *In vivo* AGT-GFP processing was performed by addition of 200 µM of BCNU alone or with co-administration of proteosomal inhibitors (10µM of MG132 or 10µM of Lactacystein). Treated cells were lysed in RIPA buffer at indicated time points (Fig, 40). 50µg of total cell lysate was analysed by SDS PAGE. The blots were probed with GFP-HRP antibody to visualise the processing of the fusion protein.

On BCNU treatment, smaller AGT-GFP degradation products (less than 50KDa) were observed (Fig, 40). Similarly sized products were observed even with co-addition of MG132 or Lactacystein. However, we observed larger size bands after 6 hours BCNU treatment in Lactacystein stabilised cells. This suggested that GFP processing via proteosome was severely retarded and cellular processing by non-proteosomal pathway (proteases) is likely (Petr *et al*., 2009). Taken together our IF and *in vivo* degradation data suggest persistent AGT-GFP foci after treatment. This could be due to poor processing of the fusion protein. It is possible that non-proteosomal degradation did not require protein modification before degradation. Given the ability of AGT-GFP to be modified by O^6BG, form foci and interact with BRCA2, we studied the protective ability of AGT-GFP in transfected cells.

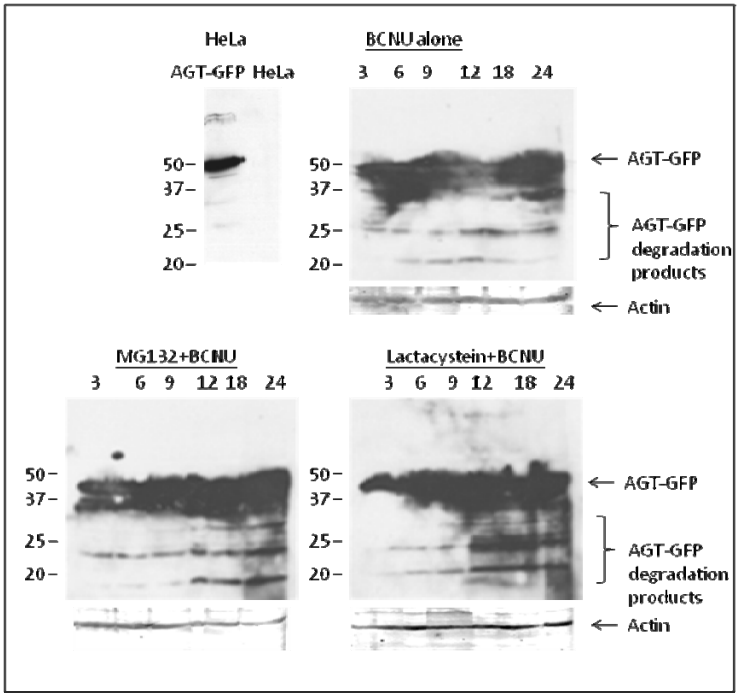

Figure 40, Western blot analysis using anti-GFP antibody. In vivo AGT-GFP status in HeLa cells after 200μM BCNU treatment with or without MG132 or Lactacystein.

3.8.4 AGT-GFP induces BCNU tolerance in 231 cells but not in HeLa cells

Alkylation damage on HeLa and 231 cells transfected with AGT-GFP was undertaken to study whether AGT-GFP could confer protection in these cells. HeLa cells showed dose dependent susceptibility to BCNU across varying concentrations (Fig, 41). Introduction of AGT-GFP did not improve the resistance of these cells to BCNU attack. IC_{50} of HeLa cells and those of transfected HeLa cells remained at 128μM of BCNU (Fig, 41). 231 cells that do not have endogenous AGT are hypersensitivity towards BCNU with an IC_{50} of 32 μM. After transfection of AGT-GFP into 231 cells, they were better able to cope with BCNU lesions with an IC_{50} of about 175μM. They were able to tolerate BCNU exposure better than untransfected HeLa cells. This indicated that AGT-GFP was protective in 231 cell lines but not in the HeLa background.

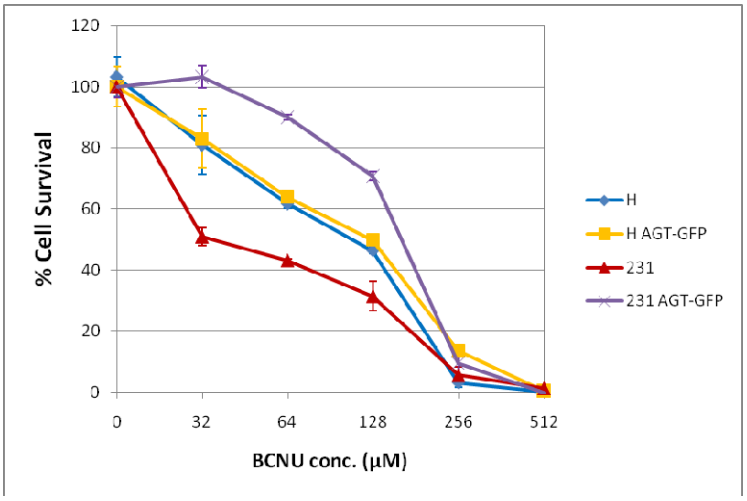

Figure 41, BCNU sensitivities of untransfected and AGT-GFP transfected HeLa and 231 cells. 231 AGT-GFP showed protection against alkylating treatment in comparison with 231 cells, while AGT-GFP did not enhance protection against alkylating agent in HeLa cells. Data presented represent mean values and standard deviations of three independent assessments.

It is known that AGT inhibition by O^6BG can enhance the cytotoxicity of (2-chloroethyl) nitrosoureas both *in vitro* and *in vivo* (Dolan *et al*., 1990, 1991, 1993a,b; Friedman *et al*., 1992; Mitchell *et al.*, 1992; Gerson *et al.,* 1993, 1994). To study whether AGT-GFP was functional in transfected HeLa and 231 cells, short term drug sensitivity test with O^6BG mediated AGT neutralisation was also undertaken.

a)

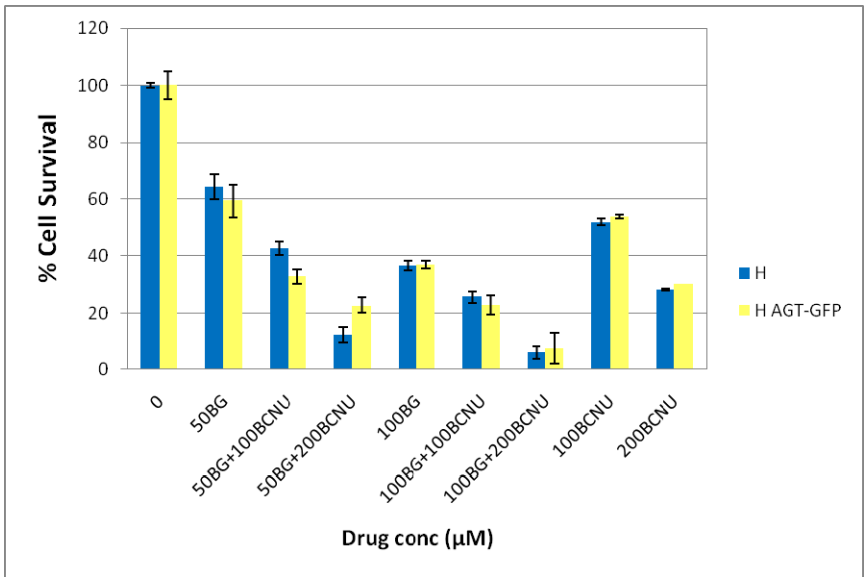

b)

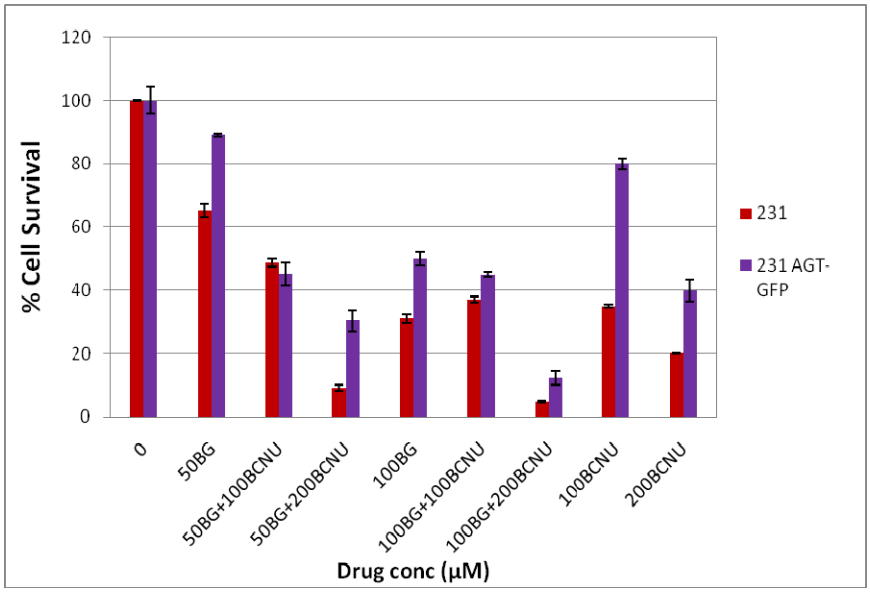

Figure 42, a&b) BCNU sensitivity with and without O^6BG depletion in HeLa and 231 cells transfected with AGT-GFP. Data presented represent mean values and standard deviations of three independent assessments.

In HeLa cells, 50 to 100 µM of O^6BG alone could cause 40% to 60% cell death (Fig, 42a). 100 to 200µM of BCNU alone could cause 48% to 75% cell death. Combination

of the two (O^6BG and BCNU) resulted in greater cell death of 60% to 90%. HeLa AGT-GFP cells exhibited similar sensitivities at the same doses suggesting the inability of AGT-GFP to affect proper lesion repair.

In 231 cells, 50 to 100 µM of O^6BG alone could cause 40% to 70% cell death (Fig, 42b). 100 to 200µM of BCNU alone could cause 65% to 80% cell death. 231 cells were generally more sensitive to BCNU than HeLa cells as they lack endogenous AGT. Combination of the two drugs (O^6BG and BCNU) resulted in greater cell death of 50% to 95%. On AGT-GFP transfection, the sensitivity of 231 cells to O^6BG was reduced, from 40% to 10% at 50 µM O^6BG and 70% to 50% cell death at 100µM O^6BG. Presence of AGT-GFP improved cell survival responses to BCNU. About 80 % survived at 100µM and 40% suvivred at 200µM BCNU. O^6BG was able to neutralise AGT-GFP and rendered transfected 231 cells sensitive to BCNU. While 80% survived in 100µM of BCNU alone, co-administration with 100µM O^6BG brought down survival to 43%. 40% survived at 200µM BCNU but was severely reduced to 10% on co-administration of 100µM O^6BG. Thus AGT-GFP was able to confer protection in 231 cells even in the absence of foci formation on BCNU exposure. This suggested foci formation was not essential for repair function, and possibly inhibited processing of lesions altered alkyl-AGT.

To understand the reason for AGT-GFP dysfunction in HeLa background, we further assessed transfected cells for their growth characteristics.

3.8.5 AGT-GFP transfected HeLa cells exhibited retarded growth due to increased genomic instability

A standard 3T3 assay was performed over 18 days to study growth characteristics of the HeLa and 231 transfected cells in comparison to controls. In our hands, HeLa cells and 231 cells exhibited similar growth rates initially (Fig, 43). AGT-GFP transfected 231 cells exhibited slower growth initially but the rate picked up by day 15 to levels comparable to 231 cells. AGT-GFP transfected HeLa cells showed poor growth rate among all cell lines tested. The cultures grew 50% slower than HeLa cells at any given time. We believe that the slower growth rate masked the cell survival figures in our test conditions of short term BCNU exposure (Fig, 43). To test this hypothesis we did long term clononogenic survival assays in HeLa and 231 cells transfected with AGT-GFP.

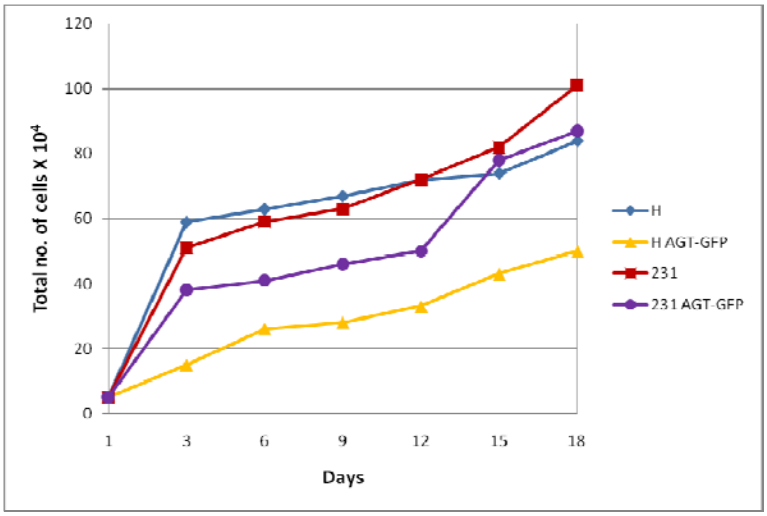

Figure 43, Standard 3T3 assay to assess growth rates of HeLa and 231 clones expressing AGT-GFP. HeLa AGT-GFP clone exhibited slower growth rate compared to the parental cell line.

Transfected cells were treated with 40 µM of BCNU and allowed to recover for 10 days before fixing with methanol and staining with crystal violet. 231 cells were highly sensitive to 40µM of BCNU with no colonies obtained after treatment (Fig, 44A). On transfection with AGT-GFP, 231 cells were better colonising and tolerating of BCNU. About 43% 231 AGT-GFP cells survived 40µM BCNU in long term clonogenic survival assay. In contrast, Hela cells transfected with AGT-GFP continued to be sensitive to BCNU at comparable levels to HeLa cells (Fig, 44B). However, we noted that HeLa cells transfected with AGT-GFP could generally form bigger colonies compared to HeLa cells.

A)

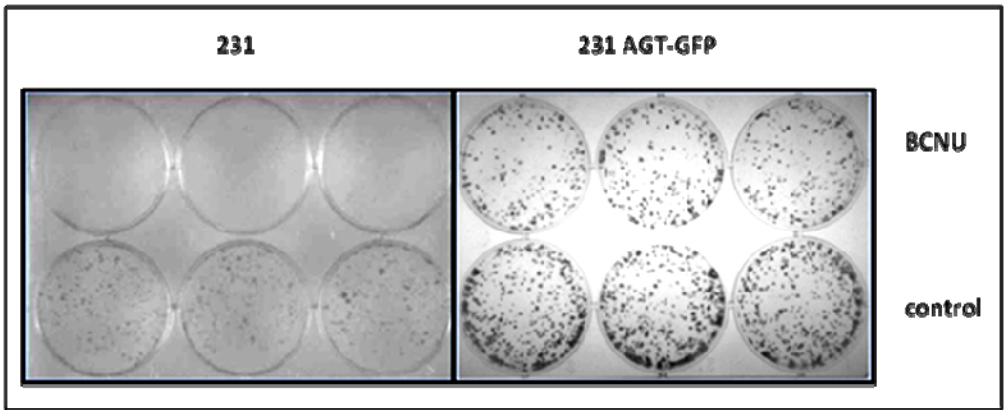

B)

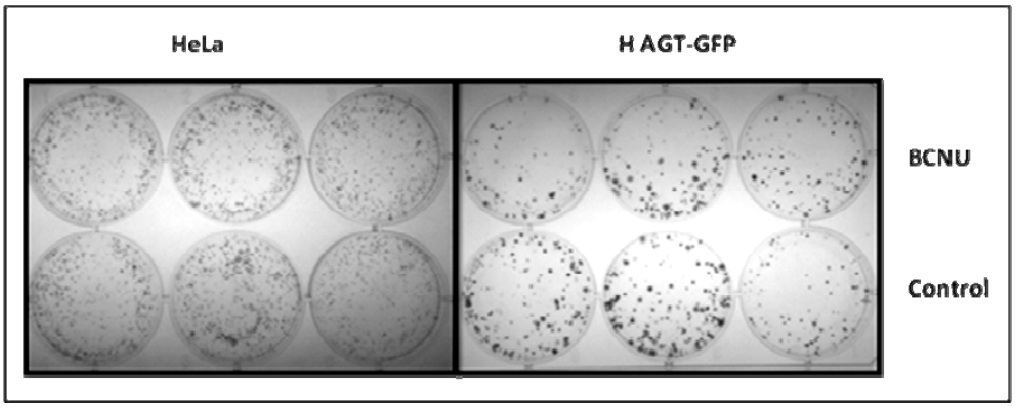

Figure 44, Images of long term colony formation of 231 and 231 AGT-GFP cells, HeLa

and HeLa AGT-GFP cells treated with 40μM of BCNU. Control represents untreated cells.

HeLa cells transfected with AGT-GFP were capable of foci formation after BCNU treatment (Fig, 34). But foci formation does not signify protection against damage. To understand why AGT-GFP transfected HeLa cells had retarded cell growth, and if AGT-GFP was supporting repair in HeLa transfected cells, we tested for genomic instability in the transfected cells. Based on our observations this far, we argue that on exposure to drugs the genomic instability in HeLa transfected cells should be higher than in 231 transfected cells if the AGT-GFP was not protective in this background. We were specifically interested in instability created by alkyl lesions. If AGT-GFP was functional and protective, fewer lesions would result. We thus used instability generated in cells after alkylating treatment to check for the function of AGT-GFP.

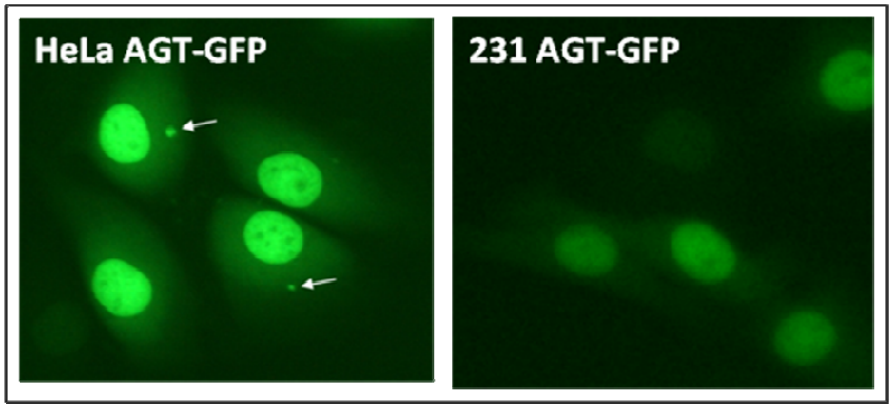

Figure 45, Hela AGT-GFP cells exhibiting single micronucleus.

The number of micronuclei (MN) were assessed in exponentially growing cultures. Tables 2 and 3 indicate the number of MN scored per 500 cells. MN were readily observable in transfected HeLa cells and poorly in 231 cultures (Fig, 45). Untreated HeLa transfected cells had a combination of 2.6% MN (genomic instability) while 231 transfected cells only had 0.8% MN.

	Untreated	**BCNU/µM**			**Streptozocin/µM**			**Bleomycin/µunits**		
		10	**20**	**40**	**10**	**20**	**40**	**10**	**20**	**40**
MN	9 (1.8)	29 (5.8)	18 (3.6)	20 (4)	48 (9.6)	45 (9)	36 (7.2)	70 (14)	54 (10.8)	18 (3.6)
Multi MN	4 (0.8)	2 (0.4)	2 (0.4)	20 (4)	33 (6.6)	50 (10)	18 (3.6)	84 (16.8)	164 (32.8)	258 (51.6)
AB	4 (0.8)	0	0	0	15 (3)	0	9 (1.8)	18 (3.6)	50 (10)	87 (17.4)

Table 2, Test for genomic instability before and after genotoxins exposure in HeLa transfected cells. Micronuclei and apoptotic bodies were scored. Data is presented as number per 500 of HeLa transfected cells. Percent instability is expressed in parenthesis. MN represents micronucleus, MN represents multiple micronuclei and AB represents apoptotic bodies.

	Untreated	**BCNU/µM**			**Streptozocin/µM**			**Bleomycin/µunits**		
		10	**20**	**40**	**10**	**20**	**40**	**10**	**20**	**40**
MN	4 (0.8)	2 (0.4)	10 (2)	5 (1)	29 (5.8)	20 (4)	30 (6)	50 (10)	42 (8.2)	51 (10.2)
Multi MN	0	0	0	4 (0.8)	7 (1.4)	3 (0.6)	5 (1)	108 (21.6)	116 (23.2)	231 (46.2)
AB	3 (0.6)	0	0	0	32 (6.4)	25 (5)	29 (5.8)	4 (0.8)	36 (7.2)	75 (15)

Table 3, Test for genomic instability before and after genotoxins exposure in 231 transfected cells. Micronuclei and apoptotic bodies were scored. Data is presented as

number per 500 of 231 transfected cells. Percent instability is expressed in parenthesis. MN represents micronucleus, MN represents multiple micronuclei and AB represents apoptotic bodies.

The cultures were then exposed to BCNU, streptozocin and bleomycin. Bleomycin forms complexes with iron that reduce molecular oxygen to superoxide and hydroxyl radicals which cause single and double strand breaks in DNA. Data in tables 2 and 3 show that both transfected cultures were equally and highly sensitive to bleomycin exhibiting many single MN, multiple MN (multi-MN) per cell and apoptotic bodies (AB). On 40 μunits of bleomycin treatment, transfected HeLa cells had 3.6% MN, 51.6% multi-MN and 17.4% AB; while 231 transfected cells had 10.2% MN, 46.2% multi-MN and 15% AB. We further tested effects of BCNU and streptozocin treatments.

BCNU induced O^6G lesions can undergo molecular rearrangements to create a DNA interstrand crosslinking between N^1 of guanine and N^3 of cytosine of the opposite strand. BCNU is able to generate more lesions in transfected HeLa cells than 231 cells (Tables 2 and 3). Increase in number of MN, multi-MN was dose dependent reflecting that AGT-GFP was not protective in the HeLa background. Tranfected HeLa cells had significant instability at higher BCNU concentration with 4% MN and 4% multi-MN but not so much in transfected 231 cells which had 1% MN and 0.8% multi-MN.

Streptozocin is a glucose analog and is easily taken up by cancer cells. It is a potent alkylating agent that directly methylates DNA and also causes DNA strand breaks, DNA adducts, chromo aberrations and micronuclei led cell death (Alejandro, 2002).

Thus streptozocin worked better than BCNU and led to higher genomic instability in treated cells. Transfected HeLa cells showed 7.2% MN, 3.6% multi-MN and 1.8% AB at 40µM Streptozocin. Tranfected 231 cells exhibited 6% MN, 1% multi-MN and 5.8% AB at the same dose.

The micronuclei and apoptotic body count demonstrated that HeLa cells transfected with AGT-GFP were more sensitive to drugs than 231 transfected cells (Tables 2 and 3). The inability of AGT-GFP to protect led to higher intrinsic instability in the HeLa background that was heightened on drug exposures (Table 2).

Our data suggested that AGT-GFP localisation and formation of foci complexes after damage is dependent on endogenous AGT. Such complexes are poorly proteosomal processed (Fig, 34) and possibly lead to replication fork stalling and thus poor growth characteristics. Transfected 231 cells did not form foci but AGT-GFP could confer protection (Fig, 35; Fig, 41; Fig, 42). Based on these observations we suggest that transfected HeLa cells would be a good model to study AGT recruitment and loading to sites of damage (as endogenous AGT also form foci), while transfected 231 cells would be a good model to study AGT processing.

After studying AGT-GFP trafficking in the cells, interaction of BRCA2 and AGT, we wished to analyse AGT stability.

3.9 BRCA2 in AGT stabilisation

3.9.1 Sensitivity of AGT to proteosomal degradation

Alkylated AGT loses further repair ability and is processed by ubiquitin modification and proteosomal degradation. We thus proposed to study the involvement of BRCA2 in AGT processing after alkyl insult. *In vitro* AGT degradation was performed in cell lysates with the addition of 100μM of O^6BG, $MgCl_2$ and ATP.

Significant amount of AGT was observed in all untreated lysates (HeLa, HE11 and HCT) and AGT remained stable in the absence of alkylation exposure (Fig, 46). On O^6BG exposure, we were able to drive AGT degradation using O^6BG. However the rate of AGT degradation in all cell lines was different. By 12 hours we observed 12% AGT loss in HeLa cells, 40% loss in E11 cells and 15% loss in CT cells. Further visualisation of AGT depletion was not noted in all 3 cell lines, by increasing time, possibly due to ATP hydrolysis. To clarify the observed hastened AGT processing in HE11 cells, we decided to study AGT processing *in vivo*.

A) HeLa cells

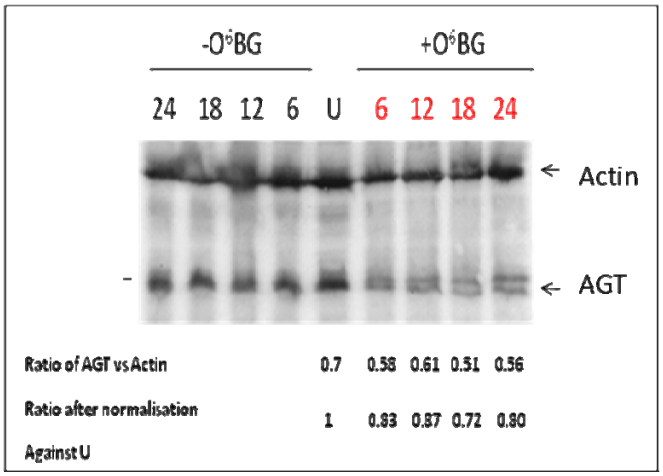

B) HeLa E11 cells

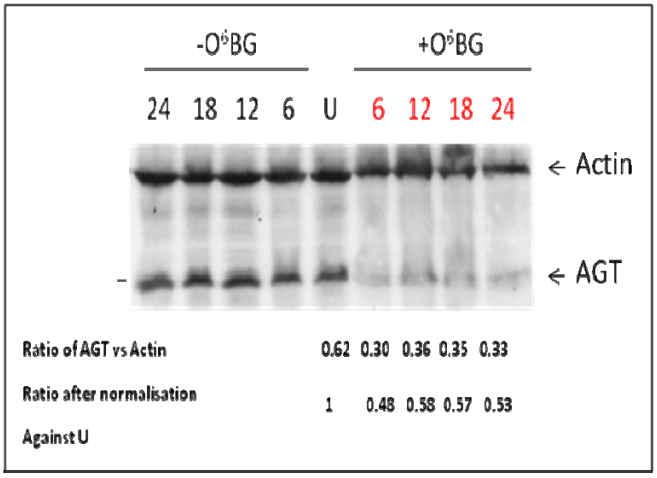

C) HeLa CT cells

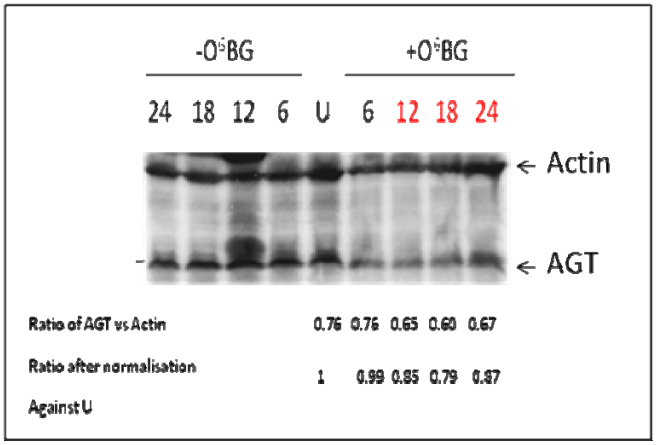

Figure 46, Analysis of in vitro AGT degradation in HeLa, HE11 and HCT cells.

AGT *in vivo* degradation was carried out in the presence of 10 μM cycloheximide (CHX) to prevent further synthesis of proteins *in vivo*. Cycloheximide exerts its effect by interfering with the translocation step in protein synthesis thus blocking translational elongation. 80 μM of O^6BG was added to drive degradation of AGT *in vivo*.

CHX was not toxic to cells at the dosage used. Even on CHX treatment, significant levels AGT were observed indicating that large AGT protein pools were maintained in HeLa cells. We observed AGT depletion after O^6BG exposure in all cell lines. The rate of degradation in all cell lines was very different. Significant AGT reduction by 18 hours was observed in HeLa cells with about 64% AGT depletion (Fig, 47A). HE11 had dramatic AGT reduction by 6 hours with 80% loss (Fig, 47B). HCT had about 27% loss by 6 hours (Fig, 47C). By 10 hours, HeLa cells had about 87% AGT left, E11 had 36% AGT left and CT had 62% AGT left. HE11 cells thus seemed capable of driving faster AGT degradation *in vitro* and *in vivo* than HeLa and HeLa CT cells.

A) HeLa cells

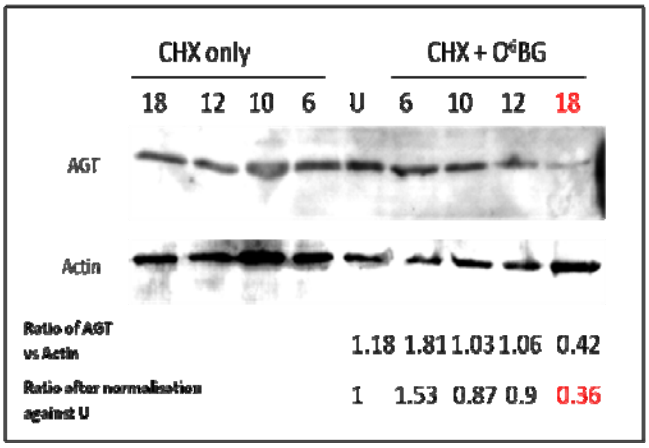

B) HeLa E11 cells

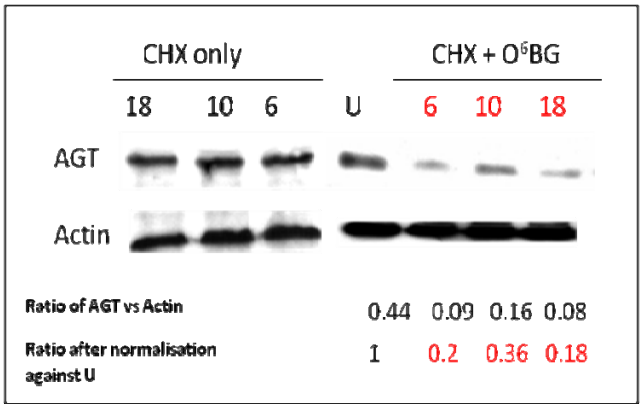

D) HeLa CT cells

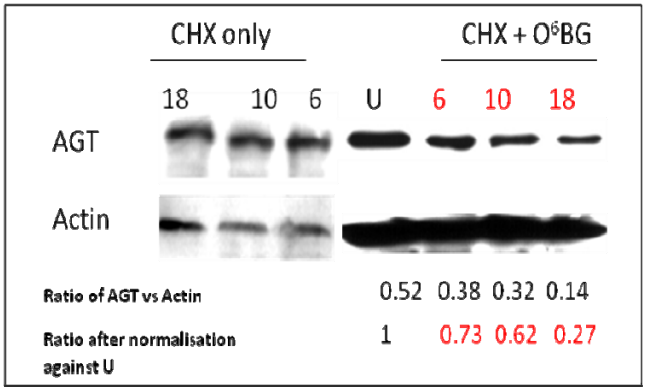

Figure 47, In vivo AGT processing in HeLa and HeLa transfected cells.

To test the importance of E11 region, we assessed our COS7BR2d105 tranfected cells for AGT *in vivo* degradation. 10 µM of cycloheximide and 80 µM of O^6BG were added to live cells and lysates were made at indicated time points, resolved by SDS PAGE and probed for AGT.

AGT reduction was evident by 6 hours in COS7 cells with about 58% reduction (Fig, 48). Massive loss of AGT was observed by 10 hours in COS7 cells. In contrast, AGT reduction of about 87% was observed in COS7d105 cells by 6 hours and we were unable to detect the protein at subsequent time points (Fig, 48). We propose that the loss of 105 bp in exon 11 BRCA2 destabilises the structure of the BRCA2 protein in a way that the altered BR2d105 protein binds to alkyl-AGT better thus allowing improved processing.

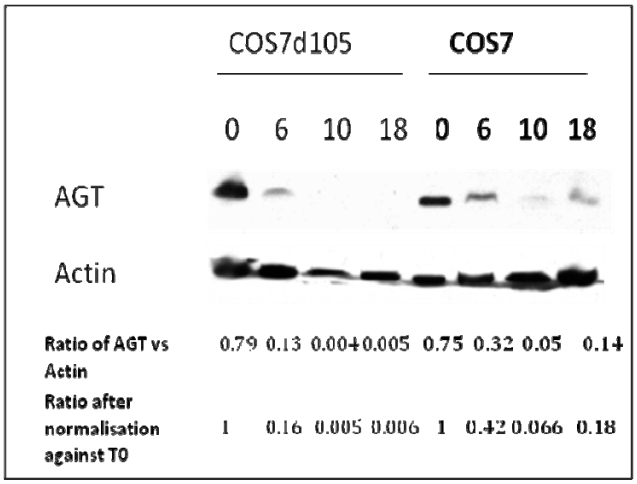

Figure 48, AGT degradation in vivo in COS7 and COS7 cells transfected with BRCA2d105. AGT degradation was dramatic in the COS7d105 cells.

Thus far, our data had shown that HeLa E11 cells displayed higher sensitivity to agents that could cause alkyl damage to DNA when compared to HeLa and HeLa CT cells. They also could bind alkylated AGT preferentially. Rapid loss of cellular alkyl-AGT and unaltered rate of AGT synthesis could explain the sensitivity of HeLa E11 cells to BCNU (Fig, 25).

To assess where modified AGT degradation occurs, we treated HeLa Exon 11 cells with 200µM of BCNU for 2 hours and allowed recovery for 24 and 30 hours. One set of treated cells were supplemented with MG132 to block proteosomal degradation. At indicated time points, cells were lysed and nuclear/cytoplasmic fractions extracted. Protein samples were applied on 4 to 12% gradient gels and probed with anti-AGT and anti-BRCA2 antibodies. Actin was used as a cytoplasmic loading control and Cyclin-D1 as a nuclear loading control.

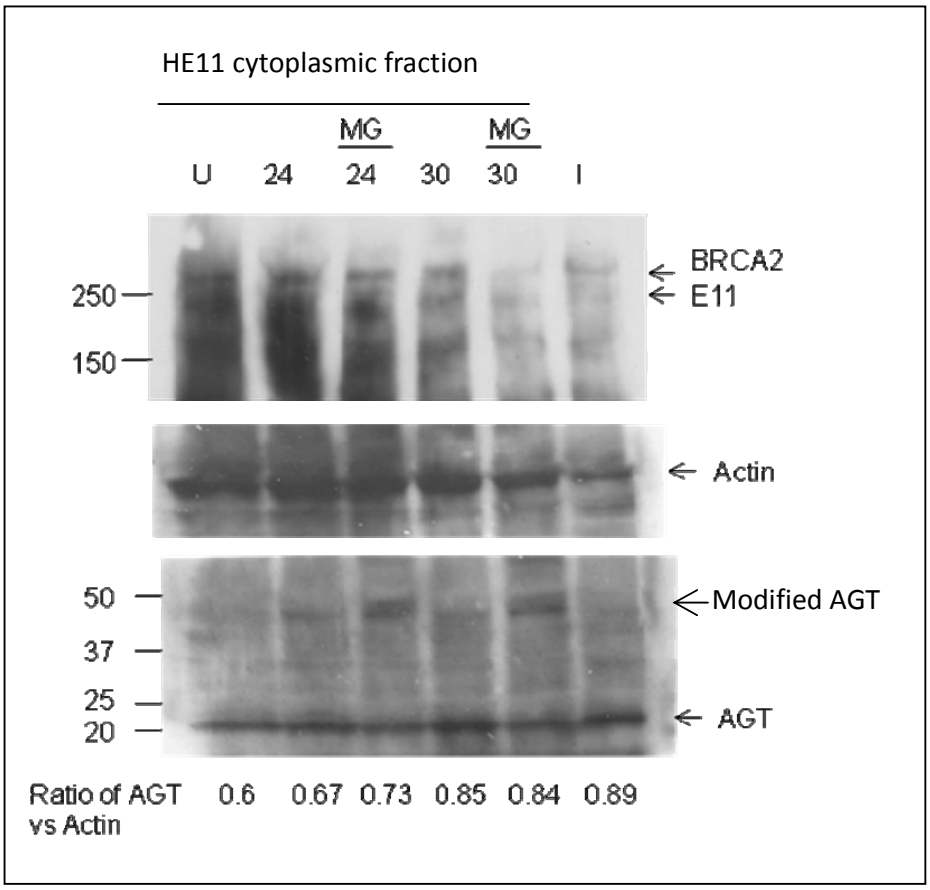

Figure 49, Western blot analysis of cytoplasmic fractions of HeLa E11 cells untreated/treated with BCNU. MG represents MG132 inclusion, U represents cytoplasmic fractions of untreated cells, and I represents total cell lysate/input.

AGT was detected in the cytoplasmic fraction at all time points (Fig, 49). The amount of AGT after 24 hours of BCNU treatment was similar to that of untreated nuclear cell lysate. After 30 hours of drug treatment, there was slight increase of AGT about 4% in the cytoplasmic compartment. We could not rule out constant AGT re-synthesis as we did not block protein synthesis using CHX in this assay. However we observed a higher molecular weight band (between 37 to 50KDa) on BCNU treatment that was enriched on MG132 addition. This suggested that modified forms of AGT were generated upon BCNU treatment in the cytosol. We could not compare the amount

of AGT in MG132 stabilised lysates with lysates that were not treated with MG132 as we did not include MG132 stabilised untreated HeLa E11 nuclear lysate as a control. Full length BRCA2 was detected in all lanes in the cytoplasmic fractions. E11 fragment of BRCA2 was also detected in all lanes indicating its cytoplasmic presence at all times.

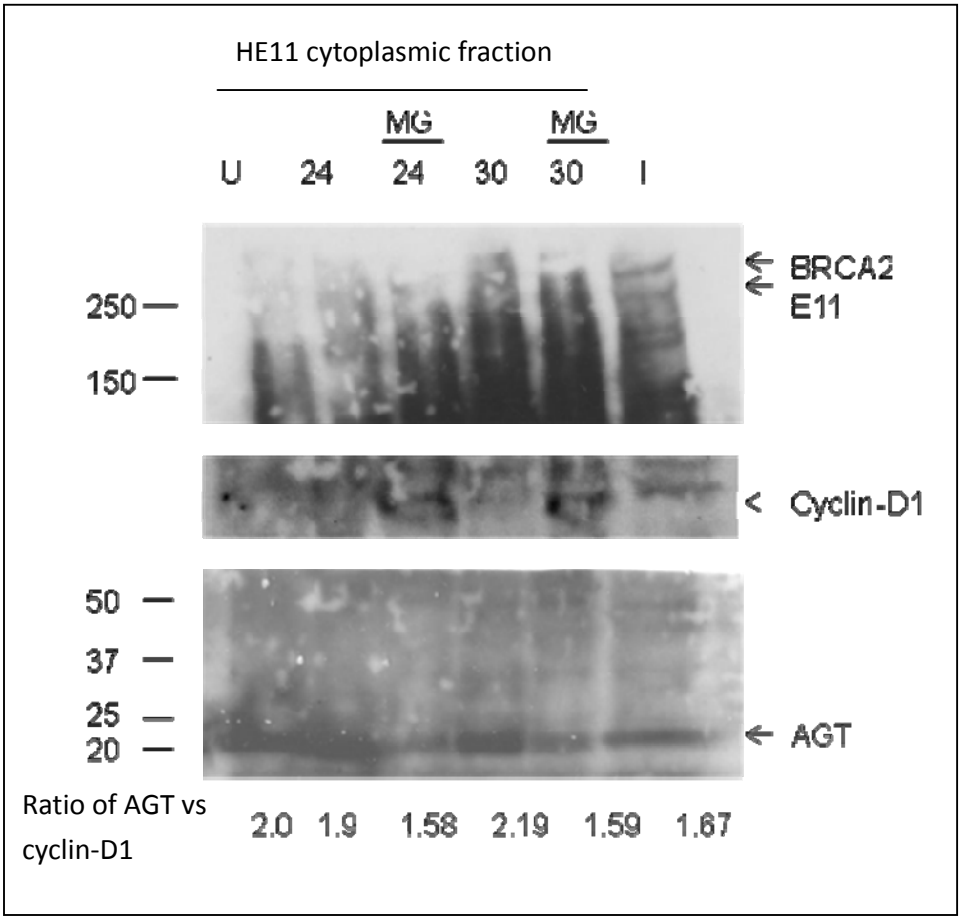

Figure 50, Western blot analysis of nuclear fractions of HeLa E11 cells untreated/treated with BCNU. MG represents MG132, U represents nuclear untreated cells, and I represents total cell lysate/input.

In the nucleus, AGT was detected at all time points and possibly at higher levels than the cytoplasmic fractions (Fig, 50). The amount of AGT detected after 24 hours of BCNU treatment was similar to levels before treatment. After 30 hours of BCNU treatment, there was a slight AGT increase of about 10%. We cannot rule out constant transport of cytoplasmic AGT into the nucleus and believe that such localisation may account for such increases. We did not observe any higher molecular bands in the nuclear compartment after BCNU treatment. Even with MG132 stabilisation, MG132 mediated proteosomal block was discerned on cyclin D-1 staining where cyclin-D1 was stabilised by MG132. Full length BRCA2 was detected weakly in all lanes but the E11 fragment of BRCA2 was not detected in the nuclear fractions. From these observations we speculated that modified alkyl-AGT generated in the nucleus is transported into the cytoplasm, where it is modified for proteosomal processing. The availability of the cytosolic E11 of BRCA2 in HE11 cells allows for rapid recruitment of factors essential for AGT processing.

3.10 Regulation of AGT in cells

3.10.1 Role of phosphorylation in maintaining AGT stability

Protein phosphorylation is the most common mechanism by which protein function is reversibly regulated in cells. As many as one-third of all cellular proteins are covalently modified by phosphorylation at some point in time. Most proteins are found to be phosphorylated at serine threonine or at available tyrosine residues. These residues can also be modified by other reactive groups such as acetylation. Signalling via such side chain modifications allow for diversity of functions in proteins.

Srivenugopal *et al.,* 2000 used computer-assisted motif analysis to reveal multiple phosphorylation sites in AGT. A single tyrosine phosphorylation motif was predicted and multiple, even overlapping serine/threonine phosphorylation sites were found. Sites for serine/theronine kinases such as protein kinase A (PKA), casein kinase II (CKII), protein tyrosine kinase (PTK) and glycogen synthase kinase 3 (GSK3) were identified. They also showed that AGT could exist as a phosphoprotein in cells. The value of such modification is however unclear.

There are conflicting reports regarding the role of AGT phosphorylation in cells. It is unclear whether phosphorylation protects AGT and prevents its repair function, or if it is a modification subsequent to repair and drives alkyl-AGT degradation. (Mullapudi SR, 2000; Srivenugopal KS, 2000; Lim IK, 2000). Therefore, we investigated the involvement of phosphorylation in AGT processing. Lysates assessed for *in vitro*

degradation were primarily probed for AGT and then reprobed with anti-phosphoserine/threonine/tyrosine antibodies to detect modified forms of AGT. Actin was used as a loading control.

AGT was observed to be phosphorylated in the untreated samples (U) of HeLa and HeLa cells transfected with E11 or CT of BRCA2 (Fig, 51). This suggested that exogenous BRCA2 segments do not interfere with phosphorylation modification of AGT in cells. On O^6BG treatment phosphorylation on AGT disappeared in all cell lines tested. This implied that endogenous AGT exist in a phosphorylated form and becomes dephosphorylated upon treatment. However it was still unclear whether dephosphorylation occurs before alkyl lesion transfer or subsequently.

A) HeLa cells

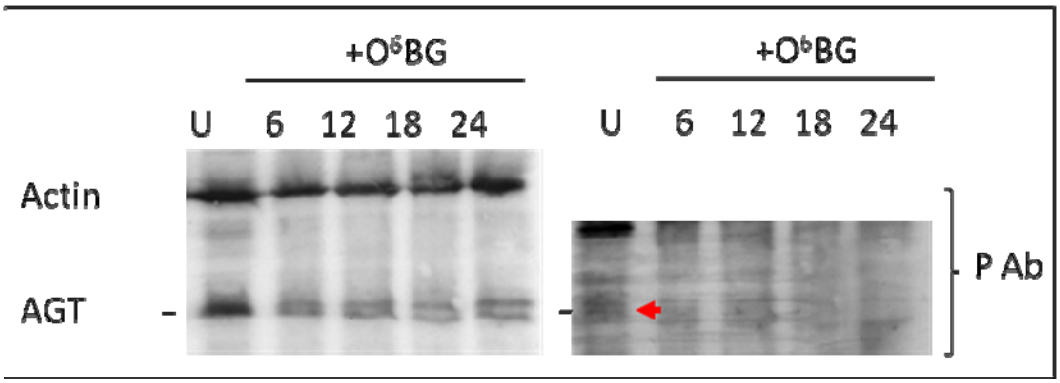

B) HeLa E11 cells

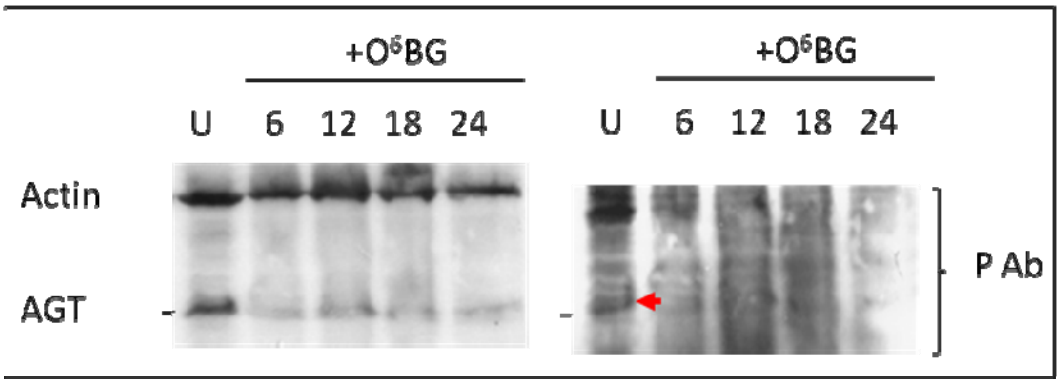

C) HeLa CT cells

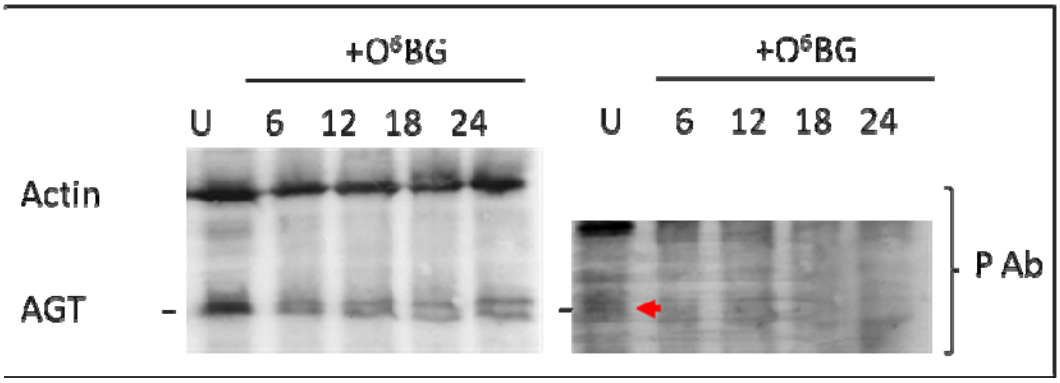

Figure 51, Western blot analysis of AGT in vitro degradation by O^6BG over 24 hrs in HeLa and HeLa transfected cells. The membrane was reprobed with anti-phosphoser/thr-pro and anti-phosphotyrosine antibodies.

To assess whether dephosphorylation occurs before alkyl lesion transfer or afterwards, we treated HeLa cells with 200 µM of BCNU. After 6 hours of BCNU treatment, lysates were prepared (0 time point) and were assessed by ATP driven *in vitro* degradation of alkyl AGT. AGT degradation would then be a measure of alkyl-AGT generation.

It was found that on BCNU treatment, AGT is dephosphorylated (0 time point; Fig, 52). Alkyl-AGT was generated within 6 hours of treatment as AGT degradation was supported on providing ATP and $MgCl_2$. We were not able to find any specific band that corresponded to the ubiquitin modified forms of AGT using this assay protocol. We were thus unable to assess possible phosphorylation modification post ubiquitination.

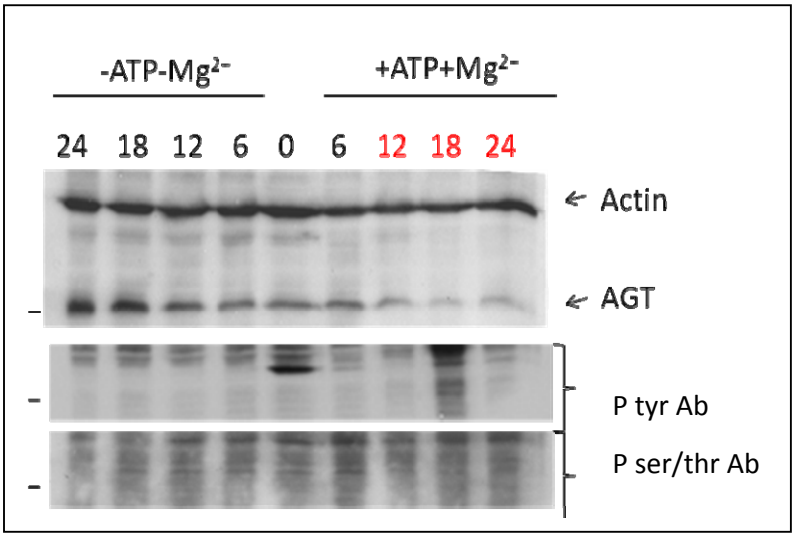

Figure 52, Western blot analysis of HeLa cell lysates treated with BCNU for 6 hours in vivo followed by AGT in vitro AGT degradation over 24 hrs. The membrane was reprobed with anti-phospohrylated ser/thr and tyrosine antibodies.

We then undertook the study of phosphorylation status of AGT in untreated and

BCNU exposed HeLa cells. 200µM of BCNU was added to live HeLa cells and incubated for 16 hours. Nuclear and cytoplasmic extraction was performed on untreated and treated lysates. Samples were resolved on SDS PAGE and probed for AGT protein and its phosphorylation, if any. AGT was predominantly nuclear in HeLa cells (Fig, 53). Nuclear AGT was poorly phosphorylated compared to cytoplasmic AGT. On BCNU treatment, AGT was dephosphorylated in the nucleus and AGT reduction was noted. Phosphorylation status did not change in the cytoplasmically expressed protein. This suggested that dephosphorylation was essential for protein activity and was an event specific to the nuclear protein. It must be noted that phosphorylation effects can be very transient, and our experimental set up allows for a snapshot understanding. We cannot rule out rapid phosphorylation and dephosphorylation events that may occur in between alkyl lesion repair and AGT degradation. Further detailing of phosphorylation is currently being pursued by our group using 2 dimensional separation followed by protein characterization.

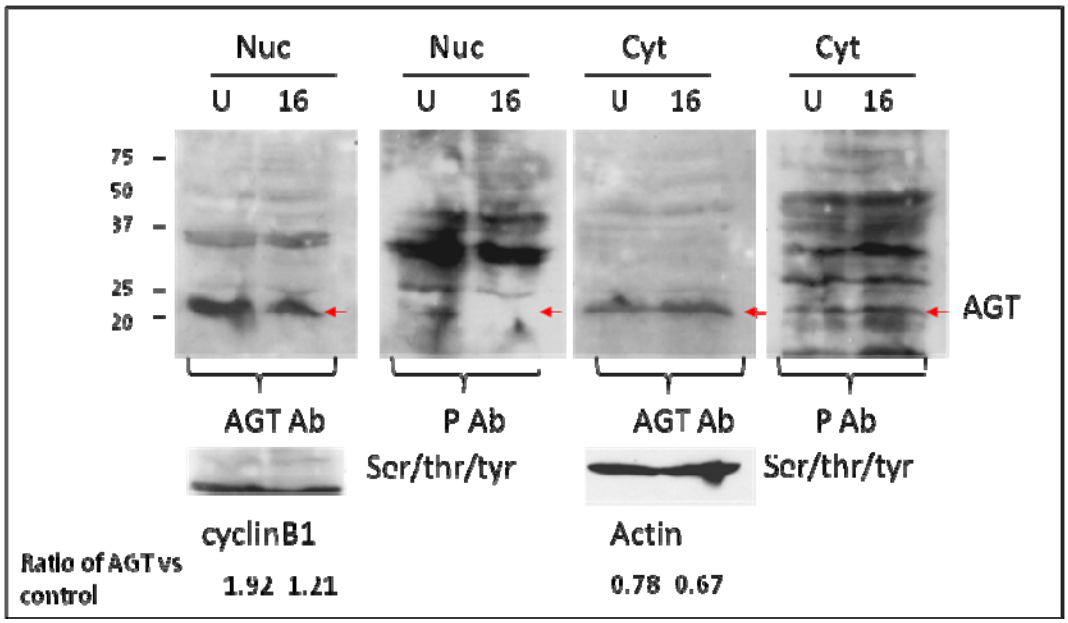

Figure 53, Western blot analysis of AGT in nuclear and cytoplamic fractions of

untreated (U) and BCNU treated cells (16) HeLa cells. The blots were reprobed with anti-phosphorylated ser/thr-pro and tyrosine antibodies. Cyclin B1 is the control for nuclear fraction and actin is the control for cytoplasmic fraction. Both nuclear and cytoplasmic AGT were phosphorylated.

3.10.2 Regulation of AGT in Capan-1 cells

Capan-1 cells express significant amounts of AGT, comparable to HeLa. To understand the processing ability of the protein expressed in Capan-1 cells, we undertook *in vivo* AGT degradation analysis. Cells were either exposed to CHX alone or co-exposed with to O^6BG and CHX and sampled at indicated time points. Total cell lysates were resolved by SDS PAGE, membrane blotted and probed for AGT and Actin. We were able to establish unaltered AGT expression in CHX exposed cultures (Fig, 54). In Capan-1 cells, we noted significant reduction in AGT expression (45%) after 18 hr exposure to O^6BG (Fig, 54). We have previously shown an AGT reduction of 64% in HeLa cells under identical conditions (Fig, 47A).

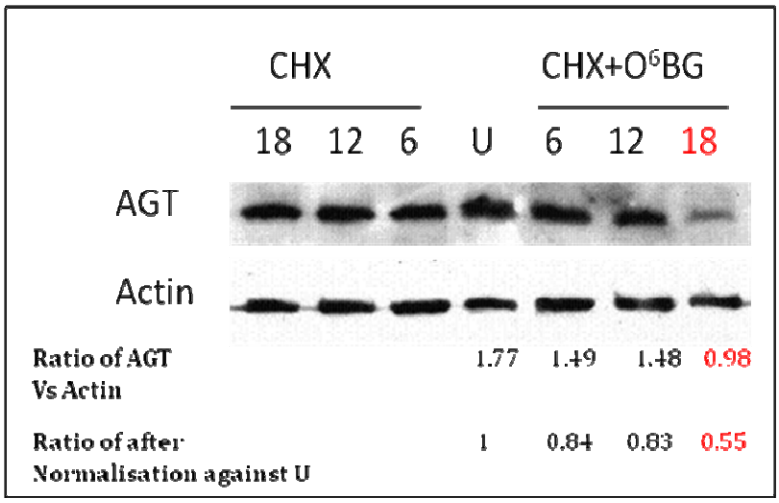

Figure 54, In vivo AGT degradation in Capan-1 cells.

Although the rate of AGT destruction in Capan-1 cells was slower than in HeLa cells, this data indicated that alkyl-AGT processing was supported in Capan-1 cells. However in our short term drug sensitivity assay, Capan-1 cells were found to be hypersensitive to alkyl lesions (Fig, 10A). Our premise at the onset of the study was that the absence of nuclear BRCA2 contributed to this hypersensitivity. To verify AGT related cellular blocks, we verify its localisation in cells by IF staining.

Immunofluorescence staining for AGT and BRCA2 proteins was undertaken in Capan-1 and HeLa cells. In HeLa cells, AGT was predominantly nuclear (Fig, 55a; left panel). AGT staining was diffusedly cellular in Capan-1 cells (Fig, 55b; left panel). BRCA2 protein also stained nuclear in HeLa cells and as predicted was identified as cytoplasmic in Capan-1 cells. Since both BRCA2 and AGT are DNA binding proteins, we undertook identification of chromatin bound fraction of each protein. In HeLa cells, a good part of BRCA2 and AGT were observed to be chromatin bound (Fig, 55a; right panel). In Capan-1 cells, chromatin bound BRCA2 and AGT were poorly detected (Fig, 55b; right panel). It seems possible that AGT in Capan-1 cells is predominantly cytoplasmic/or bound DNA poorly when in the nucleus by itself.

HeLa cells

Total cells Chromatin bound

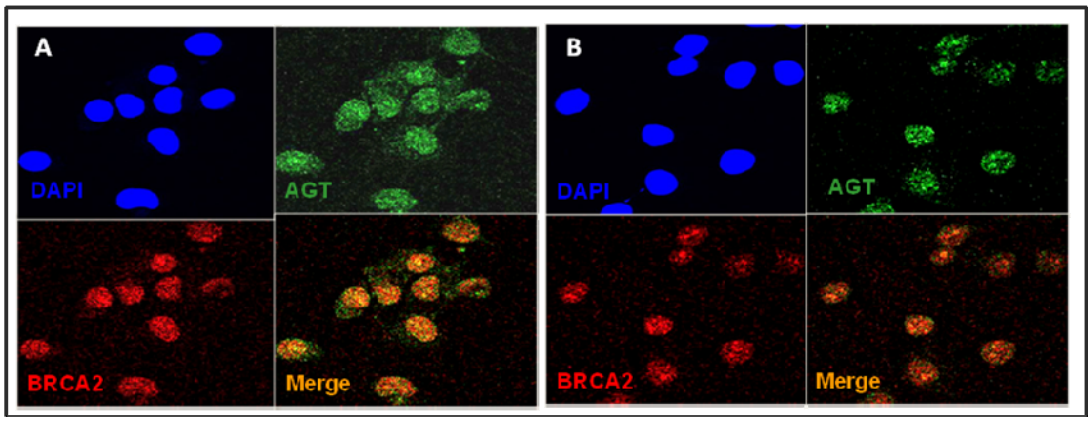

a) Capan-1 cells

Total cells Chromatin bound

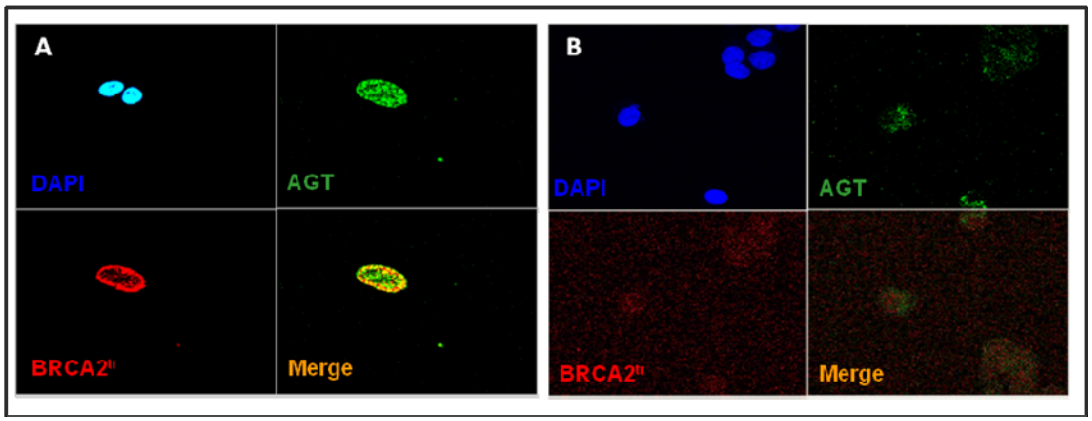

Figure 55, IF staining of BRCA2 and AGT in HeLa (a) and Capan-1 cells (b). Panel A represents BRCA2 and AGT staining. Panel B represents Chromatin bound BRCA2 and AGT. Majority of BRCA2 and AGT were chromatin bound in HeLa cells but not in Capan-1 cells (courtesy of Joyce Tan Jia Li).

To investigate this further, Capan-1 cells were treated with 200µM of BCNU for 16 and 20 hours and nuclear/cytoplasmic extractions were performed on untreated and treated cells. Western blot for AGT was undertaken using actin as a cytoplasmic

loading control and Cyclin-B1 as a nuclear control. Majority of AGT was observed to be localised in the cytoplasm of untreated Capan-1 cells (Fig, 56). After 16 to 20 hours of BCNU treatment, significant increase in AGT levels was detected in the nucleus. With increased nuclear AGT detection, we observed AGT decrease in the cytoplasmic compartment. It was also noted that the mobility of nuclear AGT and cytoplasmic AGT were different. To establish the contribution of post-translational modifications, we reprobed the blot with anti-phosphoserine/threonine and tyrosine antibodies. The retarded mobility of AGT observed in the cytoplasmic fraction corresponded to a phosphorylated protein. It is likely that the cytoplasmic AGT in Capan-1 cells is protected by phosphorylation, and dephosphorylation is required to activate it. It is possible that dephosphorylation occurs in the nucleus and requires a stimulus such as an alkyl-lesion to activate the recruitment of the cytoplasmic protein to nucleus.

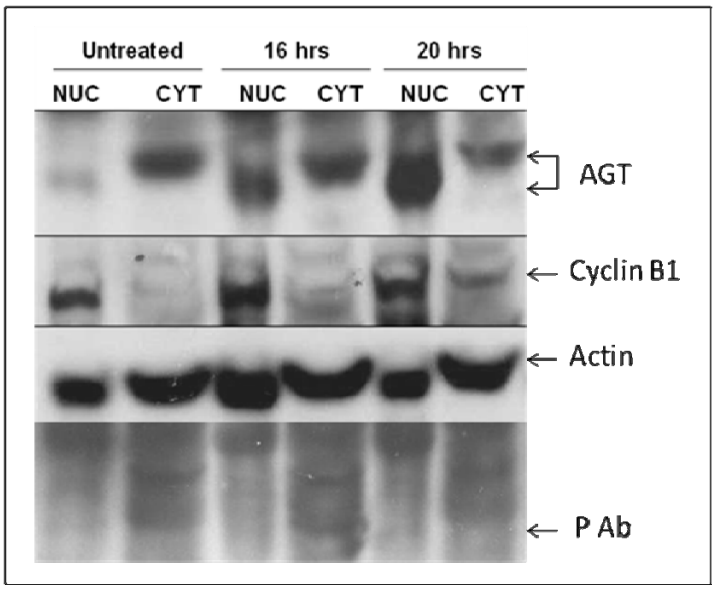

Figure 56, Western blot analysis of AGT in nuclear and cytoplamic fractions of untreated Capan-1 cells and those treated with 200µM of BCNU. 16 and 20 hours indicate the recovery times allowed. Actin and cyclin B1 were used as loading controls. Blot was reprobed with anti-phosphorylated ser/thr-pro and tyrosine antibodies (in collaboration with Ezhilarasan Rajaram).

From these observations, we noted that AGT is poorly represented in the nuclei of Capan-1 cells. The AGT protein in the cytoplasm exists in a phosphorylated form. AGT enters the nucleus in response to stimulus and needs to be dephosphorylated to become repair capable. Our data suggests that cellular regulation of AGT by phosphorylation is an important mode of maintaining the protein's endogenous levels and protecting it from processing and degradation. Alkyl-AGT processing requires BRCA2, specifically the E11 region that drives processing via interaction and recruitment of cytosolic factors.

3.10.3 Regulation of O^6-alkylgunine DNA alkyltransferase

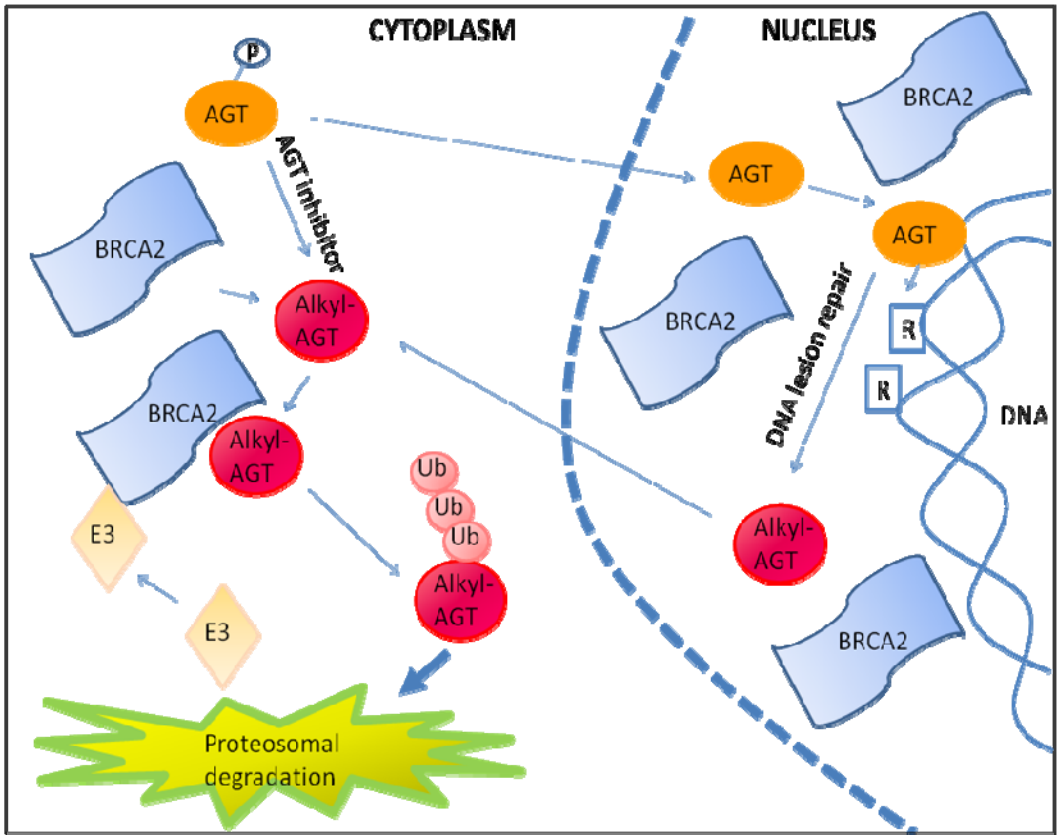

Figure 57, Cellular regulation of O^6-alkylgunine DNA alkyltransferase in a cell expressing full length BRCA2. R represents alkyl lesions.

There are two modes of alkyl-AGT generation in cells addressed through this study. AGT in cells can be inactivated by direct alkyl lesion transfer from an AGT inhibitor such as O^6BG or AGT is inactivated when it repairs alkyl lesions from DNA (Fig, 57). AGT is localised in the cytoplasm in an inactive phosphorylated state. This serves as a pool of reserve protein that is readily available for repair when dephosphorylated.

Direct activation of AGT is possible on alkyl DNA lesion generation. Phosphorylated AGT is translocated into the nucleus where it is rapidly dephosphorylated. We

suggest that dephosphorylation occurs soon after transport to the nucleus based on the motilities of AGT protein in the two cellular compartments and on our inability to detect any phosphorylated AGT in the nuclear compartment. Dephosphorylated AGT is activated and scans DNA for alkyl lesions. When it encounters an alkyl lesion, AGT flips out the alkylated guanine and transfers the alkyl lesion onto its active site thus modifying itself. Majority of alkylated AGT is transported out of the nucleus.

The interaction of alkyl-AGT with BRCA2 possibly allows for the recruitment of factors that allow ubiquitin mediated proteosomal processing. Alkyl-AGT gets polyubiquitinated and targeted for proteosomal degradation. Cytoplasmic alkyl-AGT is thus rapidly degraded. Alkylated AGT can be processed in the nucleus of cells; however the rate of such processing is greatly retarded and largely not favoured. While we can not rule out the interaction of full length BRCA2 and AGT in the nucleus, we believe that co-export into the cytoplasm is unlikely given the size of BRCA2. O^6BG can directly inactivate AGT in cells by transferring its benzyl group to the cysteine active site of AGT; dephosphorylation may not be necessary for this mode of alkyl-AGT generation. Subsequent modification and degradation of the alkyl-AGT in the cytoplasm requires the presence of cytoplasmic BRCA2.

3.10.4 AGT expression is downregulated in Capan-1 cells expressing full length BRCA2

The restoration of full length BRCA2 into Capan-1 cells has been performed previously by Wang *et al.*, 2002. They found that expression of wild-type BRCA2 inhibited cell proliferation in culture and suppressed tumor growth in animals. In a similar attempt by J. Holt, 2008 utilising different vectors, restoration did not improve survival responses of cells to irradiation. Both groups however achieved poor levels of full length BRCA2 expression. To assess whether the cellular response studies by these groups was affected by poor BRCA2 re-expression, we undertook overexpression of BRCA2 in Capan-1 cells. Full length BRCA2 was cloned into a p3XFLAG-CMV10 vector. This construct was introduced into Capan-1 cells and stable transformants were selected. The resulting cell line was designated Capan-1 pfl (Fig, 58; C-1 pfl) and expressed very high levels of full length BRCA2.

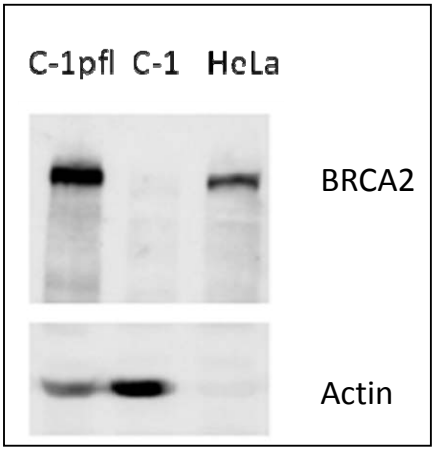

Figure 58, Western blot detection of full length BRCA2 in Capan-1 pfl cells using BRCA2 C-terminus specific antibody (courtesy of Saofiah).

We observed significantly changed morphologies in Capan-1 cells transfected with full length BRCA2 (Fig, 59). Capan-1 cells are highly irregular in shape and typically grow in clusters making it hard to obtain 100% confluency. Capan-1 pfl cells however were more epithelial like and non-clumpy. Cultures of Capan-1 cells routinely exhibit 5% to 10% floaters that fail to establish on re-culturing. No such losses were observed in Capan-1 pfl cultures. Capan-1 pfl cells also exhibited significantly improved proliferation rates as assessed by 3T3 assay (data not included).

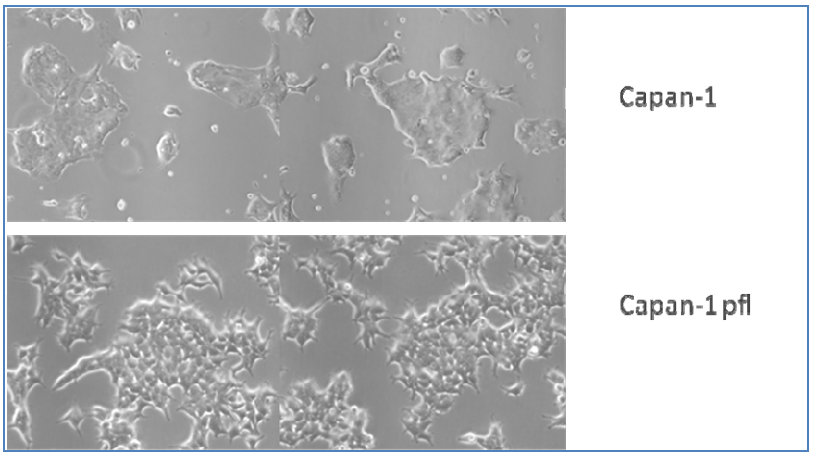

Figure 59, Capan-1 cells exhibited a more epithelial morphology after re-introduction of full length BRCA2.

While characterising the DNA repair capacity of our Capan-1 pfl cells, we realised that they exhibited distinct sensitivities towards certain genotoxins. Capan-1 cells showed dose dependent response to BCNU treatment with an IC_{50} of 50µM of BCNU (Fig, 60A). Interestingly, on full length BRCA2 transfection, Capan-1 pfl cells became hypersensitive to BCNU with an IC_{50} of about 16µM of BCNU. Capan-1 cells were resistant to MNU, showing a slight sensitivity of 5% at 256µM MNU and 20% at 512µM of MNU. Capan-1 pfl cells showed slight dose dependent response to MNU with 40% death at 256µM drug (Fig, 60B).

A)

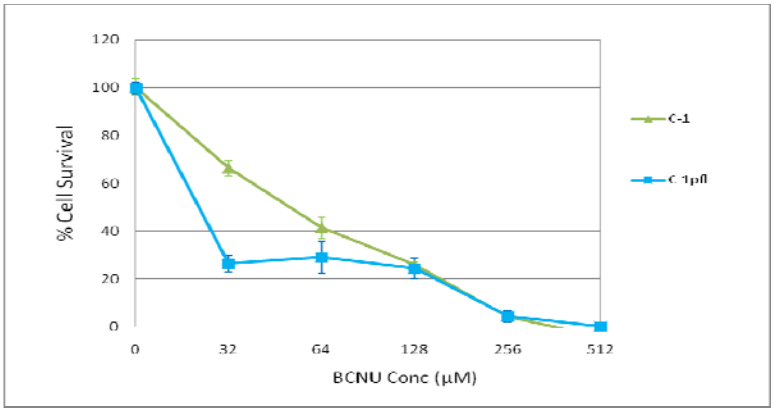

B)

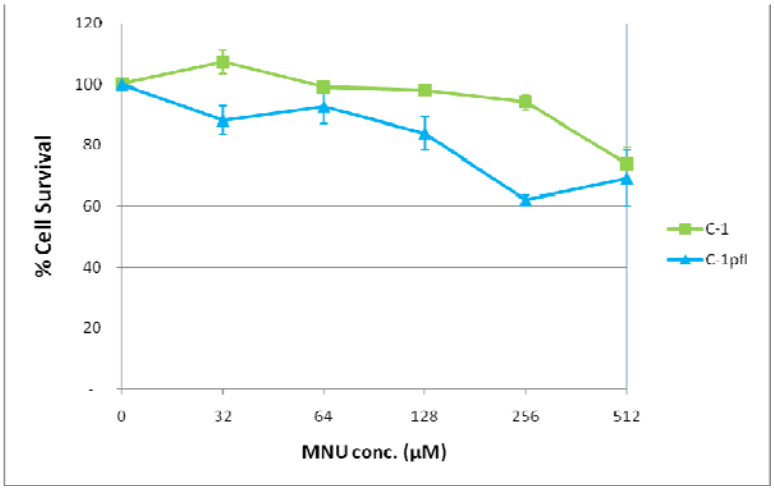

C)

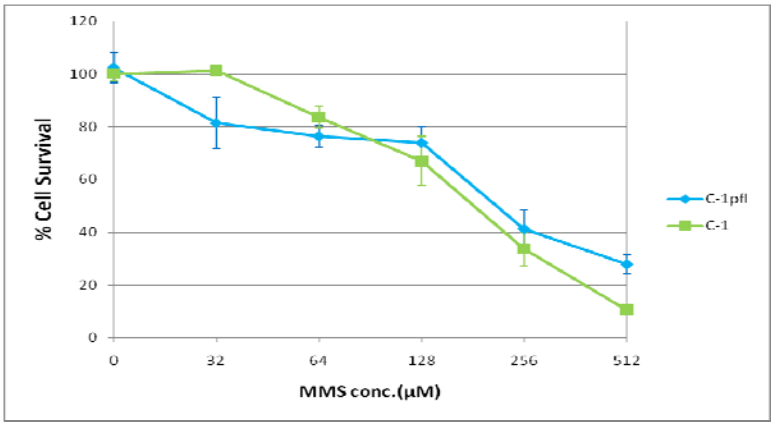

Figure 60, Short term drug sensitivities of Capan-1 and C-1 pfl cells. Data presented represent mean values and standard deviations of three independent assessments.

BCNU is a monofunctional alkylating agent that has some selectivity for chloroethylating guanine at the O^6 position. MNU is an S_N1 type alkylating agent generates N^3 lesions on guanines, N^1 and N^3 lesions on adenine, N^3 lesions on cytosine and O^4 lesions on thymine. While all other lesions are managed by the BER pathway, the O^4 thymine lesions can be repaired by AGT. Thus both drugs create damages that are repaired by AGT.

Analysis of the repair capabilities of Capan-1 and Capan-1 pfl cells by exposure to Methyl Methane Sulfonate (MMS) lesions was also undertaken. Capan-1 and Capan-1 pfl cells showed dose dependent response to MMS. Both cell lines showed dramatic sensitivity between 128 and 256 µM of MMS with an IC_{50} achieved at 192µM of MMS. Guanine modifications at the N^7 position is the predominant DNA lesion generated on MMS exposure. This drug can also cause 3-methyl purines that are routinely repaired by the BER pathway. Our data suggests similar capabilities of repair of all MMS lesions (thus pathways) in the untransfected and transfected Capan-1 cells.

The heightened sensitivity of Capan-1 pfl cells towards alkylating genotoxins prompted us that expression of repair factors may be altered on overexpression of BRCA2. We performed western analysis for AGT expression in Capan-1 pfl cells. Western blot data indicated that initially there was no change in AGT expression soon after transfection, levels of AGT protein expression was greatly reduced after 1 month in culture.

AGT is known to be inducible by BCNU stimulus in various cells lines. Thus we tested if AGT in C-1 pfl cells could be induced by exposure to 200 µM of BCNU for 16 hours. AGT expression in Capan-1 cells was unaltered on BCNU treatment (Fig, 61). We were unable to induce AGT in BCNU treated Capan-1 pfl cells. We observed the presence of AGT degradation product in Capan-1 pfl cells in both untreated and treated states. We ruled out loss of AGT genomic locus by PCR amplification of the coding region from Capan-1 pfl cells (data not shown).

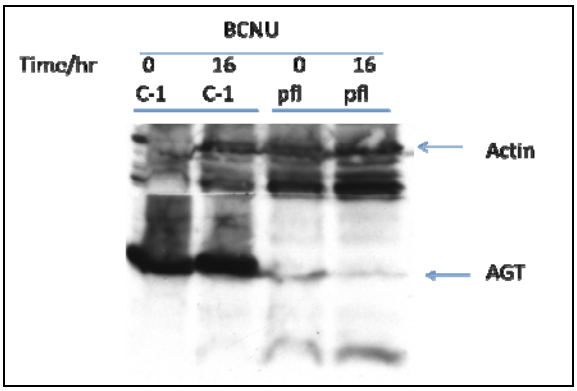

Figure 61, Western analysis of AGT in Capan-1 and C-1 pfl. AGT is poorly expressed in Capan-1 pfl cells and could not be induced on BCNU exposure.

We thus analysed possible silencing of expression through epigenetic mechanisms and assessed BRCA2's role as a transcriptional regulator. We thus cloned the NT of BRCA2 from exon 2 to 10 to assess its contribution to AGT expression regulation.

3.11 BRCA2 mediated regulation of AGT expression

3.11.1 AGT expression is reduced in HeLa cells expressing BRCA2 NT

The poor AGT expression observed in Capan-1 pfl cells prompted us to investigate the region of BRCA2 that could contribute to gene regulation. The NT of BRCA2 harbours a transactivation domain and repressor domains. It has transcriptional activation potential and the transactivation domain of NT is reported to bind to transcriptional co-activator protein, P/CAF and p300 (Milner *et. al*, 1997; Fuks F *et. al*., 1998). We thus cloned the NT of BRCA2 by engineering exon2 to 10 of BRCA2 into the NotI/ HindIII cloning sites of p3xFLAG-CMV-10. The vector p3xFLAG-CMV-10 harbours ampicillin resistance gene for bacterial selection, neomycin resistance gene for selection of stable mammalian cell lines, the cytomegalovirus immediate-early (CMV) promoter for high-level expression in a wide range of mammalian cells and 3xFlag epitope-tag for identification. HeLa cells were transfected with plasmids carrying NT of BRCA2 selected in culture and stable clones were analysed for expression.

Western blot showed positive protein expression for NT (77kDa) detected using BRCA2 specific antibodies (Fig, 62A). Initial detection utilising anti-Flag antibody was not successful possibly due to structural constraints of the tagged protein. NT protein was detected both in nuclear and cytoplasmic fractions. We cloned the NT of BRCA2 without a nuclear localisation signal based on reports of interaction of this region with a nuclear transport molecule. Interaction of PALB2 with BRCA2 N-terminus has been reported to allow for transport of BRCA2 into the nucleus (Xia B, 2006).

A)

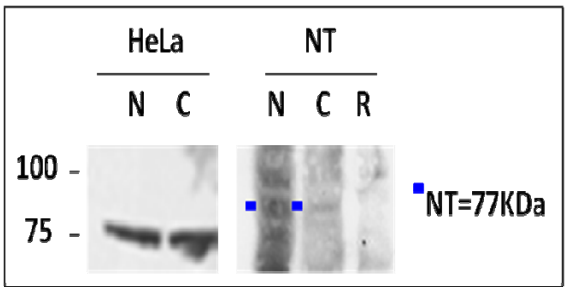

B)

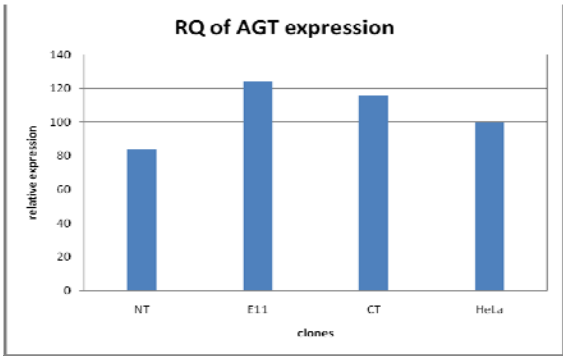

C)

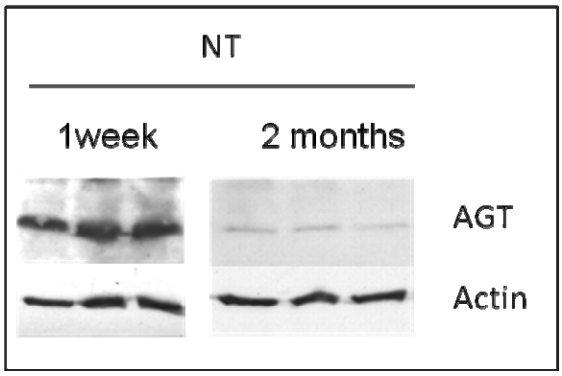

Figure 62, A) Detection of BRCA2 NT protein expression in HeLa background using HeLa lysates as control. N represents the nucleoplasmic extract; C is the cytoplasmic extract while R is the insoluble residue. B) AGT mRNA expression analysis using Real time PCR. The NT BRCA2 clone showed about 20% reduction in AGT message compared to HeLa cells. GADPH was used to normalise expression. C) Detection of AGT in HeLa cells after NT transfection; 1 week post selection and 2 months after the

end of selection.

Real time PCR was carried out on HeLa NT cells to study AGT gene expression at the end of the selection. HeLa E11 and CT cells showed higher AGT expression than HeLa cells control. HeLa NT BRCA2 cells however showed about 20% downregulation of AGT mRNA compared to HeLa and the other two HeLa transfected clones (Fig, 62B).

We assessed AGT protein expression by western blot. One week after selection, AGT expression was significantly high in these cells (Fig, 62C). But after two months in culture, AGT expression was poorly detected. Thus, long term stable expression of BRCA2 NT caused AGT expression downregulation in cultures. We speculate that AGT downregulation could not be due to mutations in AGT sequences (regulatory/coding) as AGT was still expressed 1 week after transfection.

To assess the effect of AGT protein downregulation in HeLa NT cells, we undertook sensitivity assays of HeLa and HeLa NT cells towards genotoxins. Bleomycin creates double strand breaks in DNA. Sensitivity to DBS in DNA would not be observable within 1-2 generations. Thus clonogenic survival assay was undertaken for this assessment. HeLa cells were sensitive to bleomycin with about 39 to 37% cells surviving after treatment with 10 to 40µunits of drug. NT cells were more compromised upon bleomycin treatment. They exhibited 25 to 14% cell survival after bleomycin exposure (Fig, 63). While we do not have an explanation for such enhanced DSB sensitivity, we suspect that the NT of BRCA2 possibly also regulates the expression of critical repair proteins important for DBS repair through indirect mechanisms. To specifically address effects of AGT loss, we undertook sensitivity

analysis to Streptozocin and BCNU.

A)

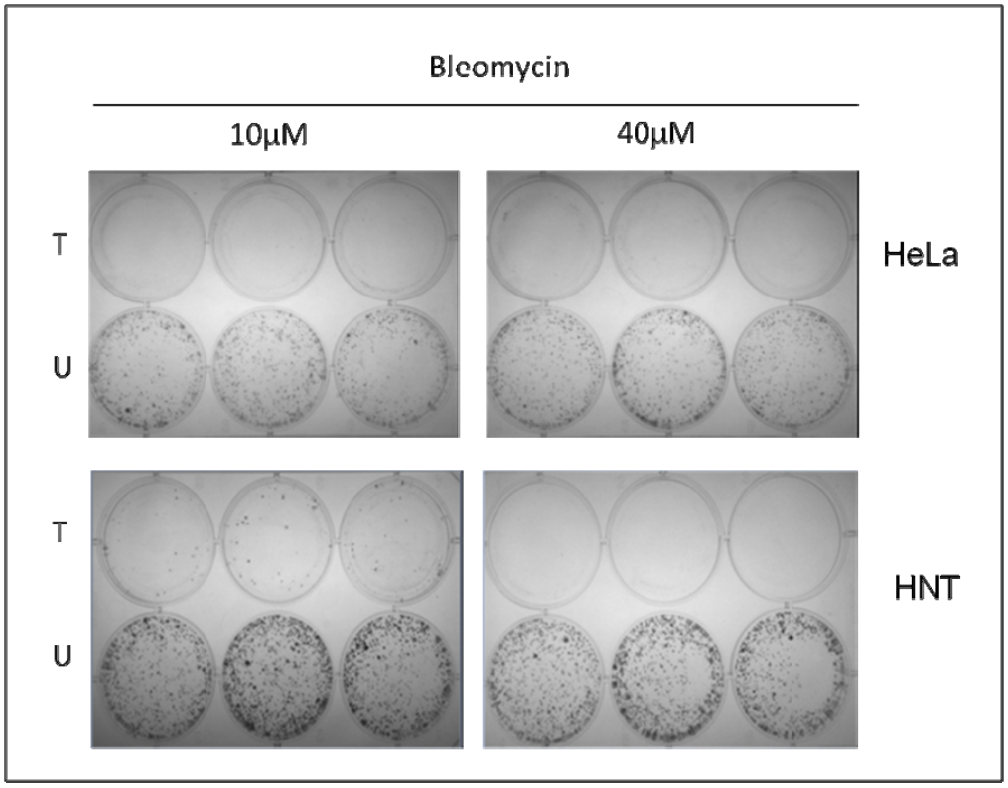

B)

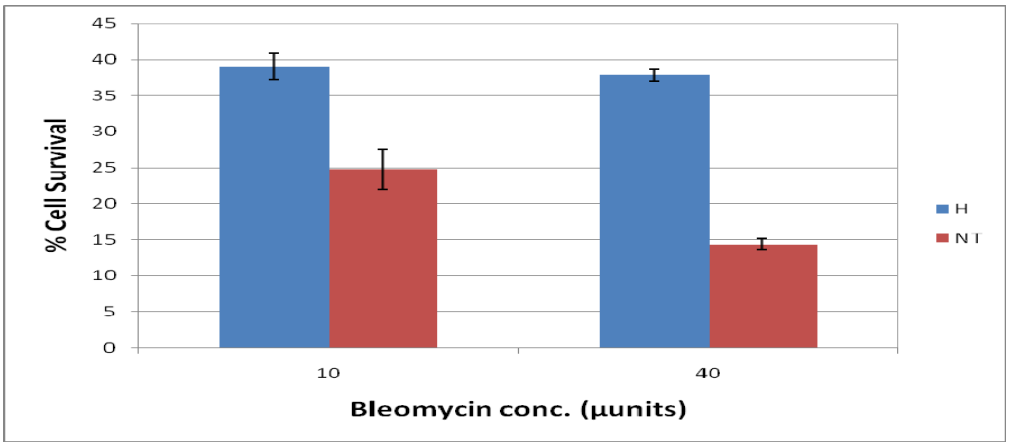

Figure 63, Long term survival response of HeLa and HeLa NT cells to bleomycin. A) Images of cologenic survival of HeLa NT cells after 10µM and 40µM of bleomycin

treatment. T represents treated cells and U represents untreated cells in triplicate. B) Percentage cell survival quantitated and expressed as histogram. Data presented represent mean values and standard deviations of three independent assessments.

HeLa cells were able to tolerate the Streptozocin well and did not exhibit any sensitivity to a 10µM dose. NT cells however were hypersensitive to streptozocin on long term culture. 21% of HeLa NT cells survived exposure to 10µM of streptozocin (Fig, 64A). Streptozocin causes intrastrand crosslinks by DNA alkylation principally repaired by AGT. If left unrepaired, these lesions may inhibit DNA replication and/or may generate DNA strand breaks that are routinely repaired by homologous recombination. The heightened sensitivity of HeLa NT cells towards streptozocin is possibly due to AGT downregulation.

In the long term survival assay for BCNU sensitivity, HeLa cells showed 40% cell survival with an initial 10µM of BCNU exposure. However, only 23% NT cells survived at the same dose (Fig, 64B). These suggested that AGT downregulation in cells is sensitising them to drugs that cause DNA lesions that are mainly repaired by AGT.

A)

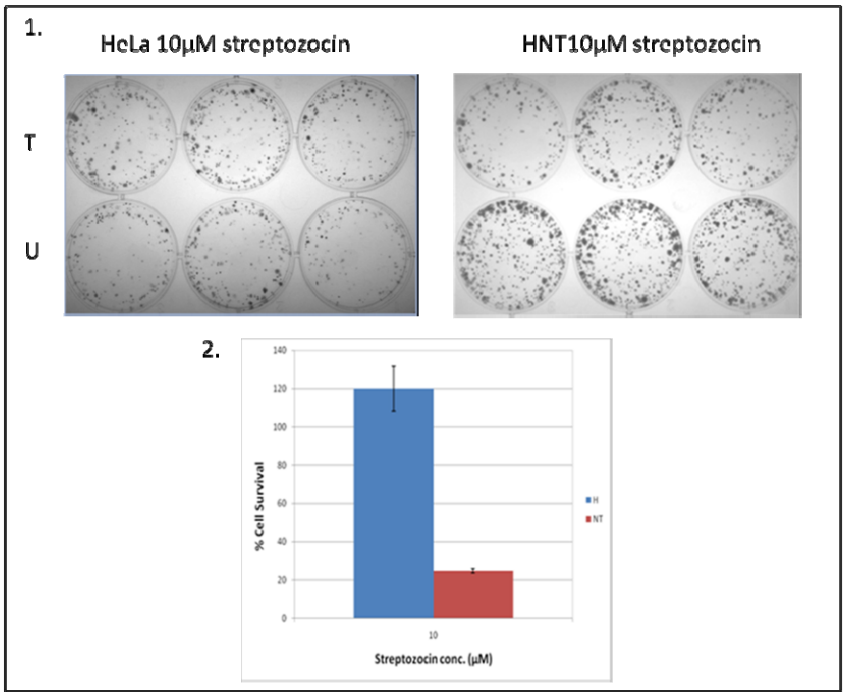

B)

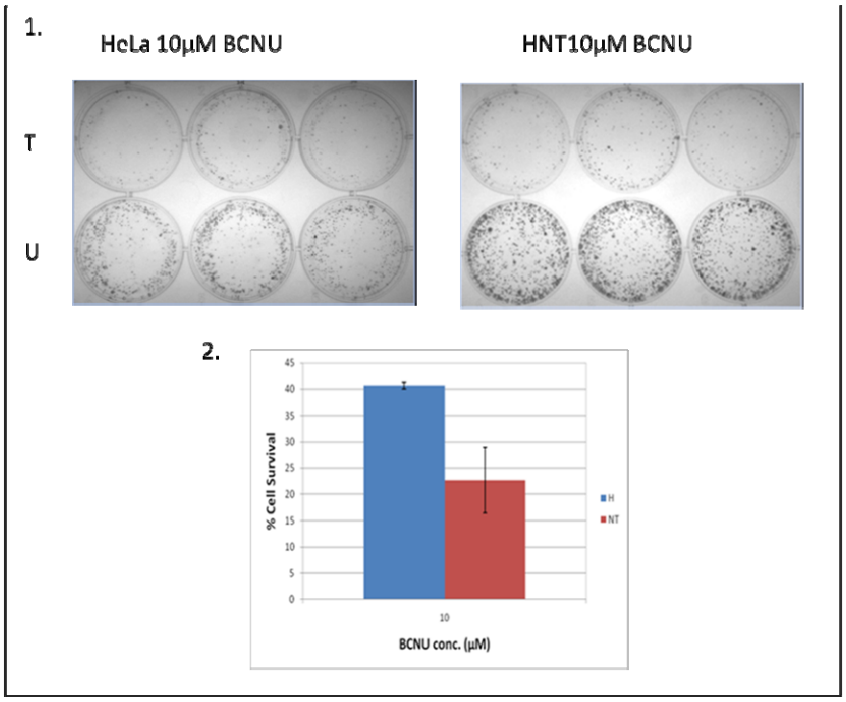

Figure 64, Clonogenic survival of HeLa NT cells to various genotoxins. 1) Images of long term survival of cells after 10µM of streptozocin (A) or BCNU treatment (B). T

represents treated cells and U represents untreated cells. 2) Percentage cell survival quantitated and expressed as histogram. Data presented represent mean values and standard deviations of three independent assessments.

Our data on enhanced losses to expression over time obviates loss of AGT coding region due to deletion or non-inclusion in genome. We thus undertook test for epigenetic silencing as a possible mechanism for alterations to AGT expression in these cells.

3.11.2 Methylation of AGT promoter region is the cause of AGT downregulation on BRCA2 NT/full length overexpression

In many cancers, AGT is found to be downregulated due to hypermethylation of its CpG islands in the promoter region. (Filipe V. Jacinto, 2007). Analysis of the AGT promoter region was undertaken to decipher whether the downregulation of AGT in Capan-1 pfl cells and HeLa NT cells could be attributed to promoter methylation. Genomic DNA was extracted from cells and the DNA was treated with sodium bisulfite. PCR was performed using AGT promoter region primers recognising unmethylated/methylated DNA sequences (Materials & Methods 2.16). PCR products were analysed by electrophoresis.

Our analysis indicated that HeLa cells have similar representation of methylated and unmethylated promoters in their genomic DNA (Fig, 65). But both HeLa NT and C-1pfl cells showed significantly more methylated AGT promoter region amplifications than unmethylated.

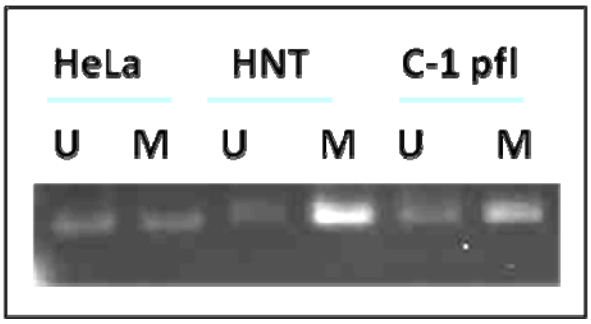

Figure 65, Analysis of AGT promoter methylation in 500ng genomic extracts of indicated samples. Primers recognising unmethylated (U) and methylated (M) promoter sequences were used. Increased Promoter region methylation was constantly observed in samples exhibiting poor AGT expression.

The role of BRCA2 in the methylation of AGT promoter region was studied by Chromatin immunoprecipitation (ChIP). ChIP is a method used to determine the location of DNA binding sites on the genome for a particular protein of interest. This technique gives a picture of the protein-DNA interactions *in vivo*. Firstly, HeLa, HeLa NT and Capan-1 pfl cells were crosslinked by formaldehyde and then lysed. The DNA was sheared into uniform pieces by sonication. Immunoprecipitation was performed on the sonicated lysates using anti-BRCA2 and anti-Flag antibodies. The purified protein-DNA complexes were reverse crosslinked at 65°C for 4 hours with high salt and DNA was purified and bisulfite treated. PCR using nested primers around the promoter region was employed in the first instance. Products of the nested PCR were divided equally for a second round of amplification utilising methyl/unmethylated specific primers. The fragments amplified were then visualised on agarose gel.

DNA has to be sheared by sonication to pieces of 300 to 800 bp ideally in order to carry out the ChIP assay. An initial optimisation protocol was performed and it

showed that sonication in pulses of 10 that last for 10 seconds each, with an off time of 30 seconds was the best protocol to consistently generate DNA fragments of 300 to 800 bp (Fig, 66). Thus subsequent ChIP assays were performed with this protocol.

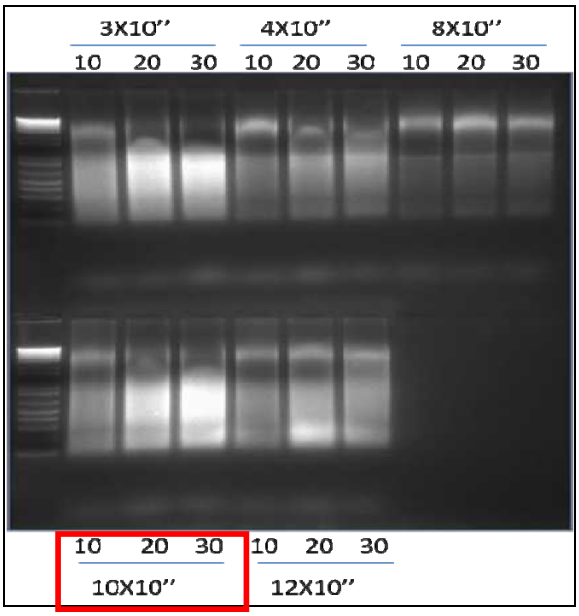

Figure 66, Agarose gel analysis of genomic DNA fragmentation association. 10 pulses/10seconds constantly give DNA fragments of 300 to 800bp.

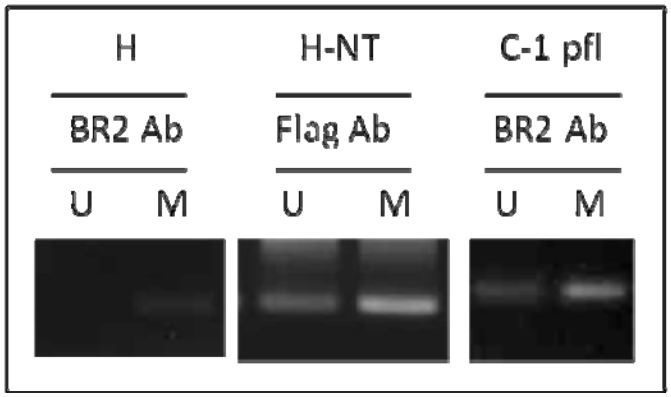

Figure 67, Agarose gel electrophoresis of DNA amplified from ChIP samples. A first round of nested PCR was performed initially on 100ng of ChIP DNA. PCR products of the nested run were equally divided and a second round of PCR to detect

unmethylated (U) and methylated (M) region was undertaken. Association of BRCA2 with AGT promoter region was suggested for HeLa NT and Capan-1 pfl samples.

In HeLa cells, a full length BRCA2 antibody could pull down weak amount of methylated promoter region of AGT (Fig, 67). From HeLa NT cells, anti-flag antibody could pull down both the methylated and unmethylated promoter region of AGT. However more methylated AGT promoter region was pulled down. In Capan-1 pfl cells, anti-BRCA2 CT antibody recognising full length BRCA2 could pull down both the methylated and unmethylated promoter region of AGT. However, more methylated promoter region was pulled down than unmethylated promoter region. This suggests a role for BRCA2 in chromatin remodelling and silencing of AGT protein expression via promoter region methylation. This finding could be of value for AGT expression regulation in cells.

4. Conclusion and Clinical implications

Repair enzyme AGT is unique among all known DNA repair proteins. It is believed to act alone in the repair of DNA alkyl lesions, affect repair in a single step damage reversal reaction and target itself for degradation. Hypersensitivity of Capan-1 cells towards alkylating agents has indicated the involvement of BRCA2 in this seemingly single step repair. Introduction of BR2d105 into COS7 cells rendered cells extremely sensitive to alkylating damage. These observations pointed consistently to an involvement for BRCA2 in the AGT mediated repair process.

This study details significant advancement in our understanding of AGT mediated repair function. We established that AGT exists in an inactive phosphorylated form in the cytoplasm. This pool of inactive AGT is readily activated by dephosphorylation when provided the right stimulus such as an alkyl-DNA lesion. Phosphorylated cytosolic AGT is translocated into the nucleus in response to such signals and is rapidly dephosphorylated on entry. While dephosphorylation is required for repair of alkyl-DNA lesions, it may not be essential for interaction of AGT with inhibitors such as O^6BG. We also noted that BRCA2 does not interfere with phosphorylation modification of AGT in cells. Nuclear AGT scans DNA for alkyl-lesions and upon encountering it, AGT accepts the alkyl residue onto its cysteine active site thus generating alkyl-AGT.

From the AGT-GFP and IF studies, AGT was observed to be able to form foci on treatment only when endogenous AGT was available. This suggested that AGT

normally binds DNA in a concerted fashion and multiple loading of repair protein is the norm even if repair is affected at a 1:1 alkyl lesion to alkyl-protein ratio. We noted that expression of bulky tags such as GFP along with AGT renders the protein unable to form foci by itself. However, repair is efficient and processing seems to be less hindered. This suggests that processing of alkyl-AGT in nuclei are regulated and greatly slowed due to multiple loadings or foci formations.

It is largely believed that after repair, alkyl-AGT dissociates from DNA and is targeted for proteosomal degradation. However, further details of such processing have not been available thus far. We established that processing of alkyl-AGT is supported in the cytoplasm within cells. Alkyl-AGT generated by DNA lesion repair in the nucleus is transported to the cytoplasm for processing. It was also found that alkyl-AGT processing requires BRCA2. Our co-IP experiments suggested that BRCA2 could bind to alkyl-AGT preferentially. Our data suggests that there are multiple AGT interaction sites in BRCA2 molecule. E11 region of BRCA2 could bind to both alkyl-AGT that is formed directly (AGT inhibitor) or indirectly through repair of a DNA lesion (alkylating drugs). E11 region of BRCA2 supports accelerated AGT processing.

We show that overexpression of full length BRCA2 and specifically the N-terminus of BRCA2 can regulate AGT expression. BRCA2's role in chromatin remodelling and hypermethylation of the promoter region of AGT is indicated. Overexpression of BRCA2 could serve as a transcriptional regulator of AGT expression.

This study is of significance as it demonstrates that BRCA2 can serve as a potential candidate for AGT regulation. Current management of cancers overexpressing AGT

involves co-administration of alkylating drugs with AGT inhibitors such as O^6BG. However, efficacy of treatment was limited due to combined myelosuppression and toxicity. With this study, we were able to ascertain increased cytotoxicity to cells using one drug but by targeting two pathways crucial for the maintenance of genomic fidelity viz the homologous recombination pathway and AGT mediated repair.

E11 region of BRCA2 could serve as a good candidate for peptidomimetic development. Such a molecule co-administered with potent AGT inhibitors could enhance responses of alkyl therapy resistant cancers. We also found by IP experiments that BRCA2 C-terminus has the potential to bind to alkyl-AGT created by AGT inhibitor. This CT region interestingly also increases AGT degradation rate like E11 but however to a lesser extent. Further analysis of this system is also warrented.

Ongoing experiments in the laboratory include further dissecting the Exon 11 and CT regions of BRCA2 protein to determine the minimal processing requirements. Understanding the smallest region of BRCA2 that is actively responsible for faster alkyl-AGT degradation could greatly aid AGT inhibitor development and therapy resistant cancer management. My laboratory is in the process of developing our own antibodies recognising AGT. We wish to perform IP coupled with mass spectrometry as a way to detect rapid or short post translational changes of AGT as a means of its regulation.

5. References

1. Abbott DW, Freeman ML. and Holt JT (1998). Double-strand break repair deficiency and radiation sensitivity in BRCA2 mutant cancer cells. *J. Natl. Cancer Inst*. (Bethesda); *90*, 978-985.

2. Ayi T-C, Oh H-K, Lee TK-Y., and Li BFL. (1994). A Method for Simultaneous Identification of Human Active and Active-site Alkylated 06-Methylguanine-DNA Methyltransferase and Its Possible Application for Monitoring Human Exposure to Alkylating Carcinogens. *Cancer Research;* 54: 3726-3731.

3. Baer JC *et al.* (1993). Depletion of O^6-alkylguanine-DNA alkyltransferase correlates with potentiation of temozolomide and CCNU toxicity in human tumour cells. *Br J Cancer*; 67(6):1299–302.

4. Beranek DT (1990). Distribution of methyl and ethyl adducts following alkylation with monofunctional alkylating agents. *Mutat Res; 231*, 11–30.

5. Bertwistle D, Swift S, Marston NJ, Jackson LE, Crossland S, Crompton MR, Marshall CJ and Ashworth A (1997). Nuclear location and cell cycle regulation of the BRCA2 protein. *Cancer Res;* 57, 5485-5489.

6. Bignell G, Micklem G, Stratton MR, Ashworth A and Wooster R (1997). The BRC repeats are conserved in mammalian BRCA2 proteins. *Hum Mol Genet*; 6, 53-58.

7. Blackshear PE, Goldsworthy SM, Foley JF, McAllister KA, Bennett LM, Collins NK,

Bunch DO, Brown P, Wiseman RW and Davis BJ (1998). Brca1 and BRCA2 expression patterns in mitotic and meiotic cells of mice. *Oncogene;* 16, 61-68.

8. Bolzan AD, Bianchi MS (2002). Genotoxicity of Streptozotocin. *Mutation Research*; 512; 121-134.

9. Bork P, Blomberg N and Nilges M (1996). Internal repeats in the BRCA2 protein sequence [letter]. *Nat Genet;* 13, 22-23.

10. Boulton SJ (2006). Cellular functions of the BRCA tumour-suppressor proteins. *Biochemical Society Transactions;* 34.

11. Brent TP, von Wronski M, Pegram CM and Bigner DD (1990). Immunoaffinity purification of human O^6-alkylguanine-DNA alkyltransferase using newly developed monoclonal antibodies. *Cancer Res;* 50: 58-61.

12. Burney S, Niles JC, Dedon PC, Tannenbaum SR (1999). DNA damage in deoxynucleosides and oligonucleotides treated with peroxynitrite. *Chem Res Toxicol.*;12:513–520.

13. Caporali S *et al.* (2004). DNA damage induced by temozolomide signals to both ATM and ATR: role of the mismatch repair system. *Mol Pharmacol*; 66(3):478–91.

14. Chang J-S, Swaminathan S (2006). Generation and analysis of *BRCA2* associated mutations, NUS honours submission.

15. Chen JJ, Silver D, Cantor S, Livingston DM and Scully R. (1999). BRCA1, BRCA2,

and Rad51 operate in a common DNA damage response pathway. *Cancer Re*, 59, 1752-1756.

16. Collins N, McManus R, Wooster R, Mangion J, Seal S, Lakhani S, Ormiston W and Daly PA (1995). Consistent loss of the wild-type allele in breast cancers from a family linked to the BRCA2 gene on chromosome 13q12-13. *Oncogene;* 10, 1673-1675.

17. Connor F, Smith A, Wooster R, Stratton M, Dixon A, Campbell E, Tait TM, Freeman T and Ashworth A (1997). Cloning, chromosomal mapping and expression pattern of the mouse BRCA2 gene. *Hum. Mol. Genet*. ;6: 291-300.

18. Cornelis RS, Neuhausen SL, Johansson O, Arason A, Kelsell D, Ponder BA, Tonin P, Hamann U, Lindblom A, Lalle P *et al*. (1995). High allele loss rates at 17q12-q21 in breast and ovarian tumors from BRCAl-linked families. The Breast Cancer Linkage Consortium. *Genes Chromosomes Cancer*; 13: 203-210.

19. Court DL, Swaminathan S, Yu D, Wilson H, Baker T, Bubunenko M, Sawitzke J, and Sharan S (2003). Mini-λ: a tractable chromosome and BAC engineering. *Gene*; 315: 63-69.

20. Daniels DS, Tainer JA. (2000). Conserved structural motifs governing the stoichiometric repair of alkylated DNA by O(6)-alkylguanine-DNA alkyltransferase. *Mutat Res* ;460(3-4):151-63.

21. Daniels DS, Woo TT, Luu KX, Noll DM, Clarke ND, Pegg AE, Tainer JA (2004). DNA binding and nucleotide flipping by the human DNA repair protein AGT. *Nat*

Struct Mol Biol. ;11(8):714-20.

22. Davies AA, Masson JY, McIlwraith MJ, Stasiak AZ, Stasiak A, Venkitaraman AR and West SC (2001). Role of BRCA2 in control of the RAD51 recombination and DNA repair protein. *Mol. Cell;* 7: 273-282.

23. Dolan ME, Oplinger M, Pegg AE (1988). Use of a dodecadeoxynucleotide to study repair of the O^4-methylthymine lesion. *Mutat Res*;193(2):131–7.

24. Dolan ME, Moschel RC and Pegg AE (1990). Depletion of mammalian O6-alkylguanine-DNA alkyltransferase activity by O6-benzylguanine provides a means to evaluate the role of this protein in protection against carcinogenic and therapeutic alkylating agents. *Proc. Natl. Acad. Sci. U.S.A.;* 87: 5368-5372.

25. Dolan ME, Mitchell RB, Mummert C, Moschel RC & Pegg AE (1991). Effect of O^6-benzylguanine analogues on sensitivity of human tumour cells to the cytotoxic effects of alkylating agents. *Cancer Res*; 51(13):3367–72.

26. Dolan ME, Pegg AE, Moschell RC & Grindey GB (1993a). Effect of O6-benzylguanine on the sensitivity of human colon tumor xenografts to 1,3-bis(2-chloroethyl)-1-nitrosourea (BCNU). *Biochem. Pharmacol; 46*: 285-290.

27. Dolan ME, Pegg AE, Biser ND, Moschel RC & English HF (1993b). Effect of O6-benzylguanine on the response to 1,3-bis(2-chloroethyl)-1-nitrosourea in the Dunning R3327G model of prostatic cancer. *Cancer Chemother. Pharmacol.;* 32: 221-225.

28. Chen F, Medhurst AL , Winter JP de, Waisfisz Q, Rooimans MA, Oostra AB, Meyer S, Zhang KJ, Xia B, Pals G, Arwert F, Zwaan CM and Joenje H (2004). Apparent absence of BRCA2 protein in a proportion of acute myeloid leukemia cell lines. *Leukemia* ; 18: 1918–1920.

29. Fisher JC, Hollomon JH (1951). A hypothesis for the origin of cancer foci. *Cancer.;* 4(5):916-8.

30. Fried MG *et al.* (1996). DNA binding mechanism of O^6-alkylguanine-DNA alkyltransferase: stoichiometry and effects of DNA base composition and secondary structure on complex stability. *Biochemistry*; 35(48): 15295–301.

31. Gale JM, Smerdon MJ (1988). UV-induced pyrimidine dimers and trimethylpsoralen cross-links do not alter chromatin folding *in vitro*. *Biochemistry* ; 27 (19): 7197–7205.

32. Major GN, Gardner EJ, Carne AF and Lawley PD (1990). Purification to homogeneity and partial amino acid sequence of a fragment which includes the methyl acceptor site of the human DNA repair protein for O^6-methylguanine. *Nucleic Acids. Res*.; 18: 1351-1359.

33. Gerson SL (2004). MGMT: its role in cancer aetiology and cancer therapeutics. *Nature Reviews Cancer;* 4: 296-307.

34. Gray SE, Kay E, Leader M, Mabruk M. (2008). Molecular genetic analysis of the *BRCA2* tumor suppressor gene region in cutaneous squamous cell carcinomas. *Journal of Cutaneous Pathology;* 35:1-9(9).

35. Haglund K, Di Fiore PP, and Dikic I (2003). Distinct monoubiquitin signals in receptor endocytosis. *Trends Biochem. Sci*.**;**28:598-603.

36. Hay RT (2005). SUMO: a history of modification. *Mol. Cell.;* 18:1–12.

37. Howlett NG, Taniguchi T, Olson S et al. (2002). Biallelic inactivation of BRCA2 in Fanconi anemia. *Science*; 297:606–9.

38. Holt J, Toole W, Patel V, Hwang H, Brown E (2008). Restoration of CAPAN-1 cells with functional BRCA2 provides insight into the DNA repair activity of individuals who are heterozygous for BRCA2 mutations. *Cancer Genetics and Cytogenetics*; 186: 85-94.

39. Ilyinskii PO, Meriin AB, Gabai VL, Usachev E, Prilipov AG., Thoidis G, Shneider AM (2009). The proteosomal degradation of fusion proteins cannot be predicted from the proteosome susceptibility of their individual components. *Protein Science.*

40. Jacinto FV, Esteller M (2007). MGMT hypermethylation: a prognostic foe, a predictive friend. *DNA repair;* 6: 1155–1160.

41. Kanugula S, Pegg AE (2003). Alkylation damage repair protein O^6-alkylguanine-DNA alkyltransferase from the hyperthermophiles Aquifex aeolicus and Archaeoglobus fulgidus*. BiochemJ*; 375(Pt. 2):449–55.

42. Lee SFA, Swaminathan S (2007). BRCA2-mediated regulation of O^6-alkylguanine-DNA alkyl-transferase (AGT) activity. NUS honours submission.

43. Lim IK, Park TJ, Paik WK (2000). Phosphorylation of methylated-DNA-protein-cysteine S-methyltransferase at serine-204 significantly increases its resistance to proteolytic digestion. *Biochem J*.;352 (3):801-8.

44. Liu L, Xu-Welliver M, Kanugula S, Pegg AE. (2002). Inactivation and degradation of O(6)-alkylguanine-DNA alkyltransferase after reaction with nitric oxide. *Cancer Res*.;62(11):3037-43.

45. Livinston DM (2004). EMSY, a BRCA-2 partner in crime. *Nature Medicine;* 10: 127 – 128.

46. Marathi UK, Kroes RA, Dolan ME & Erickson LC (1993). Prolonged depletion of O6-methylguanine DNA methyltransferase activity following exposure to O6-benzylguanine with or without streptozotocin enhances 1,3-bis(2-chloroethyl)-1-nitrosourea sensitivity in vitro. *Cancer Res.; 53*:4281-4286.

47. Margison GP, Povey AC, Kaina B and Koref MFS (2003). Variability and regulation of O6-alkylguanine–DNA alkyltransferase. *Carcinogenesis*; 24(4): 625-635.

48. Milner J, Ponder B (1997). Transcriptional activation functions in BRCA2. *Nature*; 386:772-3.

49. Mitra S, Kaina B (1993). Regulation of repair of alkylation damage in mammalian genomes. *Prog Nucl Acid Res Mol Biol* ;44:109–42.

50. Moore MH *et al.* (1994). Crystal structure of a suicidal DNA repair protein: the

Ada O6-methylguani ne-DNA methyltransferase from E. coli. *EMBO J*; 13(7):1495–501.

51. Mullapudi SR, Ali-Osman F, Shou J, Srivenugopal KS (2000). DNA repair protein O6-alkylguanine-DNA alkyltransferase is phosphorylated by two distinct and novel protein kinases in human brain tumour cells. *Biochem J*.; 351 (2):393-402.

52. Preobrazhenska O, Yakymovych M, Kanamoto T, Yakymovych I, Stoika R, Heldin C-H and Souchelnytskyi S (2002). BRCA2 and Smad3 synergize in regulation of gene transcription Oncogene; 21(36): 5660-5664.

53. Pauly GT, Hughes SH, Moschel RC (1994). Response of repair competent and repair-deficient Escherichia coli to three O6-substituted guanines and involvement of methyldirected mismatch repair in the processing of O6-methylguanine residues. *Biochemistry*; 33(31):9169–77.

54. Pegg AE *et al.* (1993). Mechanism of inactivation of human O6-alkylguanine-DNA alkyltransferase by O6-benzylguanine. *Biochemistry*; 32(45):11998–2006.

55. Pegg AE *et al.* (1995). Increased killing of prostate, breast, colon, and lung tumour cells by the combination of inactivators of O6-alkylguanine-DNA alkyltransferase and N, N'-bis(2-chloroethyl)-N-nitrosourea. *Biochem Pharmacol*; 50(8):1141–48.

56. Pegg AE. (2000). Repair of O(6)-alkylguanine by alkyltransferases. *Mutat Res;* 462:83–100.

57. Potter PM, Harris LC, Remack JS, Edwards CC, Brent TP.(1993). Ribozyme-mediated modulation of human O6-methylguanine-DNA methyltransferase expression. *Cancer Res.* ;53(8):1731-4.

58. Powell SN, and Kachnic LA (2003). Roles of BRCA1 and BRCA2 in homologous recombination, DNA replication fidelity and the cellular response to ionizing radiation. *Oncogene; 22*:5784-5791.

59. Rajan JV, Wang M, Marquis ST and Chodosh LA (1996). BRCA2 is co-ordinately regulated with Brca1 during proliferation and differentiation in mammary epithelial cells. Proc. Natl. Acad. Sci. USA; 93: 7131-7136.

60. Rasimas JJ, Pegg AE, Fried MG (2003). DNA-binding mechanism of O6-alkylguanine-DNA alkyltransferase. Effects of protein and DNA alkylation on complex stability. *J Biol Chem*; 278 (10):7973–80.

61. Rinne ML, He Y, Pachkowski BF, Nakamura J, and Kelley MR (2005). N-methylpurine DNA glycosylase overexpression increases alkylation sensitivity by rapidly removing non-toxic 7-methylguanine adducts. *Nucleic Acids Research;* 33(9): 2859-2867.

62. Sedgwick B, Robins P, Totty N, and Lindahl T (1988). Functional domains and methyl acceptor sites of the *E.coli* Ada protein. *J. Biol. Chem*.; 263: 4430-4433.

63. Sharan SK and Bradley A (1997). Murine BRCA2: sequence, map position, and expression pattern. *Genomics* ;40: 234-241.

64. Sharan SK, Morimatsu M, Albrecht U, Lim DS, Regel E, Dinh C, Sands A, Eichele G, Hasty P, and Bradley A (1997). Embryonic lethality and radiation hypersensitivity mediated by Rad51 in mice lacking Brca2. *Nature;* 24,386(6627): 804-10.

65. Sharan SK, Pyle A, Coppola V, Babus J, Swaminathan S, Benedict J, Swing D, Martin BK, Tessarollo L, Evans JP, Flaws JA, Handel MA. (2004). BRCA2 deficiency in mice leads to meiotic impairment and infertility. *Development* ; 131(1):131-42.

66. Srivenugopal KS, Yuan XH, Friedman HS, Ali-Osman F (1996). Ubiquitination-dependent proteolysis of O^6-methylguanine-DNA methyltransferase in human and murine tumour cells following inactivation with O6-benzylguanine or 1,3-bis (2-chloroethyl)-1-nitrosourea. *Biochemistry*; 35:1328–34.

67. Srivenugopal KS, Mullapudi SR, Shou J, Hazra TK, Ali-Osman F (2000). Protein phosphorylation is a regulatory mechanism for O6-alkylguanine-DNA alkyltransferase in human brain tumor cells. *Cancer Res;* 60(2):282-7.

68. Srivenugopal KS, Ali-Osman F (2002). The DNA repair protein, O(6)-methylguanine-DNA methyltransferase is a proteolytic target for the E6 human papillomavirus oncoprotein. Oncogene ;21(38):5940-5.

69. Subha P, Swaminathan S, Kuznetsov SG, Kanugula S, Biswas K, Chang S, Loktionova NA, Haines DC, Kaldis P, Pegg AE, and Sharan SK (2008). Degradation

of BRCA2 in Alkyltransferase-Mediated DNA Repair and Its Clinical Implications. *Cancer Re;* 68: (23).

70. Swaminathan S, Ellis HM, Waters LS, Yu D, Lee EC, Court DL, and Sharan SK (2001). Rapid engineering of bacterial artificial chromosomes using oligonucleotides. *Genesis;* 29:14-21.

71. Tian X-X, Rai D, Li J, Zou CZ, Bai Y, Wazer D, Band V and Gao QS (2005). BRCA2 Suppresses Cell Proliferation via Stabilizing MAGE-D1. *Cancer Research*; 65:4747-4753.

72. Tong WP, Kirk MC, Ludlum DB (1982). Formation of the cross-link 1-N3-deoxycytidyl,2-[N1-deoxyguanosinyl]ethane in DNA treated with N,N'-bis(2-chloroethyl)-N-nitrosourea. *Cancer Res*; 42 (8):3102–5.

73. Tubbs JL, Pegg AE and Tainer JA (2007). DNA binding, nucleotide flipping, and the helix-turn-helix motif in base repair by O6-alkylguanine-DNA alkyltransferase and its implications for cancer chemotherapy. *DNA Repair (Amst)*.;6(8):1100-15.

74. Vaughn J, Cirisano FD, Huper G, Berchuck P, Futreal A, Marks JR *et al* (1996). Cell cycle control of BRCA2. *Cancer Res*; 56:4590-4.

75. Verbeek B, Southgate TD, Gilham DE, Margison GP (2008). O6-Methylguanine-DNA methyltransferase inactivation and chemotherapy. *Br Med Bull*. ;85:17-33.

76. von Wronski M, Bigner DD, and Brent TP (1990). Amino acid sequence data from

immunoaffinity-purified human O^6-methylguanine-DNA methyltransferase. Proc. Am. Assoc. *Cancer Res*.; 31:446.

77. Wang S-C, Shao RP, Pao YA, Zhang S, Hung M-C, and Su L-K (2002). Inhibition of Cancer Cell Growth by BRCA2. *Cancer Research*; 62: 1311–1314.

78. Warren M, Smith A, Partridge N, Masabanda J, Griffin D, and Ashworth A (2002) Structural analysis of the chicken BRCA2 gene facilitates identification of functional domains and disease causing mutations. *Human Molecular Genetics;* 11: 841-851.

79. Wooster R, Bignell G, Lancaster J, Swift S, Seal S, Mangion J, Collins N, Gregory S, Gumbs C, Micklem G, Barfoot R, Hamoudi R, and 29 others (1995). Identification of the breast cancer susceptibility gene BRCA2. *Nature*; *378*: 789-792.

80. Xia B, Sheng Q, Nakanishi K, Ohashi A, Wu J, Christ N, Liu XG, Jasin M, Couch FJ, and Livingston DM (2006). Control of BRCA2 Cellular and Clinical Functions by a Nuclear Partner, PALB2. *Molecular Cell;* 22, 719–729.

81. Yang H, Jeffrey PD, Miller J, Kinnucan E, Sun Y, Thoma NH, Zheng N, Chen PL, Lee WH, Pavletich NP (2002). BRCA2 function in DNA binding and recombination from a BRCA2–DSS1–ssDNA structure. *Science;* 297: 1837–1848.

6. Appendix

Appendix 6.1, Sequence confirmation of engineered BAC showing the 105 bp deletion in BRCA2 gene. The sequence highlighted in black in the wild type shows the deleted sequence.

Wild Type

TTTCCAAGCA GGATTTTAAT TCAAAACCAT AATTTACAC
CTAGCCAAAA GGCAGAAATT ACAGAACTTT CTACTATATT
AGAAGAATCA GGAAGTCAGT TTGAATTTAC TCAGTTTAGA
AAACCAAGCT ACATATTGCA GAAGAGTACA TTTGAAGTGC
CTGAAAACCA GATG

105-bp deletion

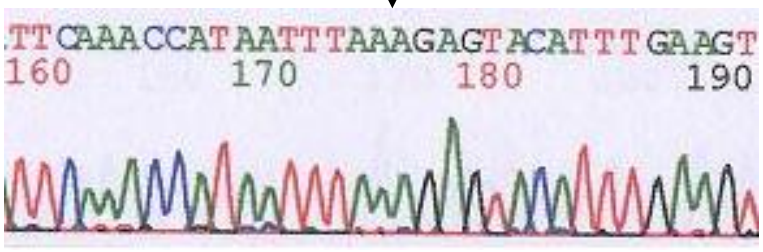

Appendix 6.2, Sequence of AGT-GFP with forward primer, AGT coding region was free of mutations.

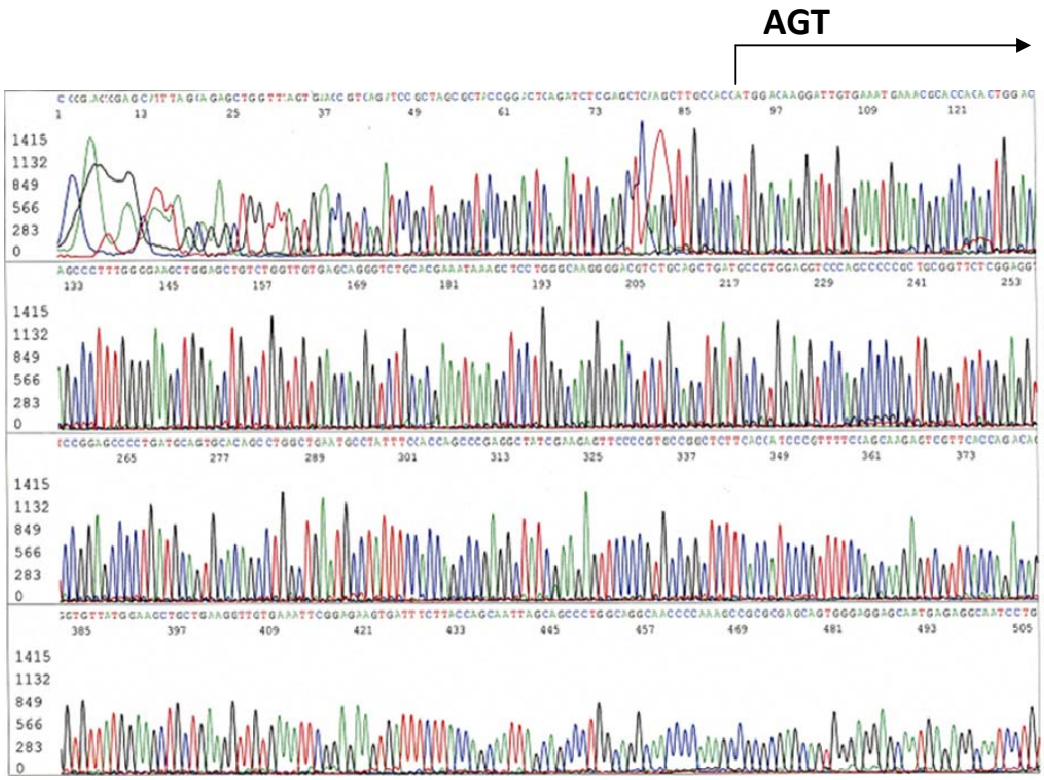

.

Appendix 6.3, Sequence of AGT-GFP with reverse primer. Cloned AGT was free of coding errors. GFP was expressed in frame with AGT protein.

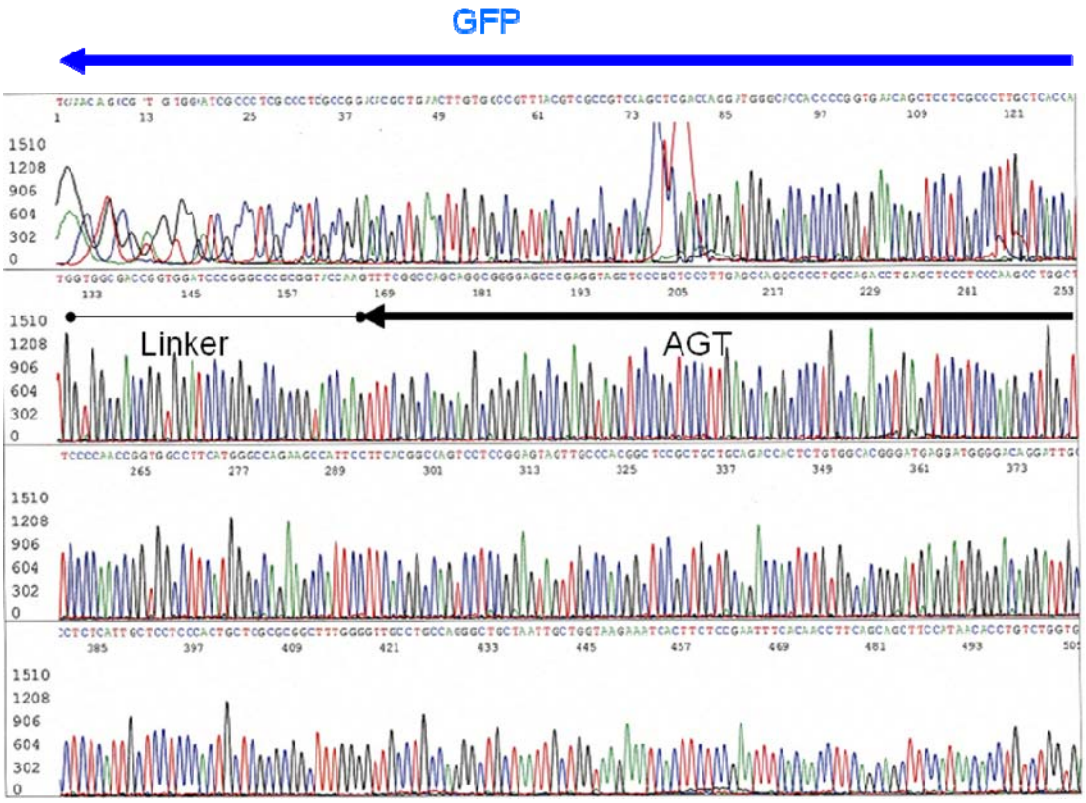

Appendix 6.4, Fluorescence activated cell sorting (FACS) data. Hela-GFPHi and 231-GFPhi cells fluoresce at higher intensities than Hela-GFPlow cells and 231-GFPlow cells.

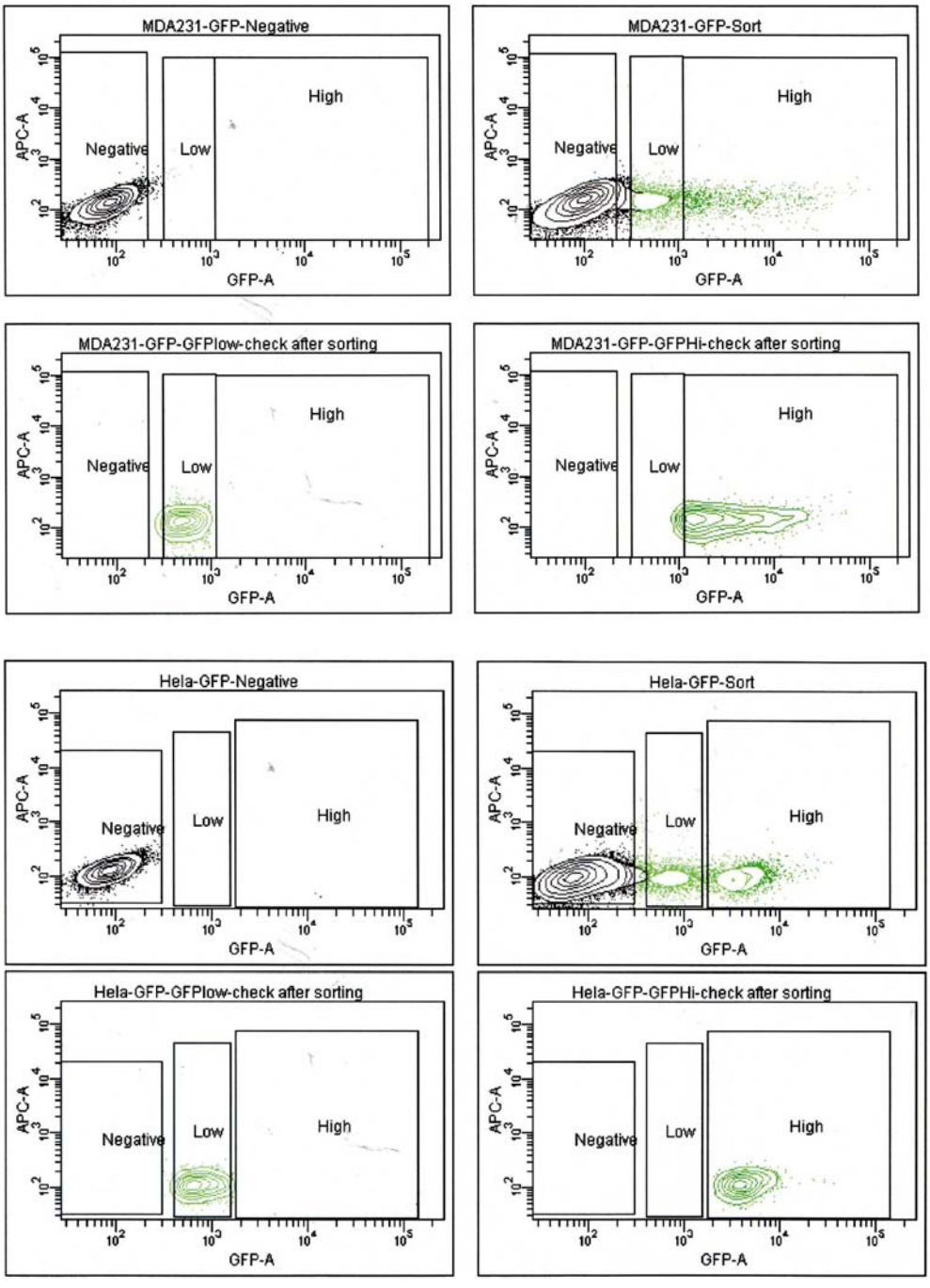

Appendix 6.5, Table of the expression of cell adhesion and ECM proteins

Genbank	Description	Fold changes to expression in comparison to HeLa	
		HCT	HE11
NM_000092	Homo sapiens collagen, type IV, alpha 4 (COL4A4), mRNA.	-2.03	-2.16
NM_000091	Homo sapiens collagen, type IV, alpha 3 (Goodpasture antigen) (COL4A3), transcript variant 1, mRNA.	-2.05	-2.31
NM_001855	Homo sapiens collagen, type XV, alpha 1 (COL15A1), mRNA.	-2.24	-2.34
NM_000088	Homo sapiens collagen, type I, alpha 1 (COL1A1), mRNA.	-2.23	-2.73
NM_001145	Homo sapiens angiogenin, ribonuclease, RNase A family, 5 (ANG), mRNA.	-2.95	-4.82
NM_003881	Homo sapiens WNT1 inducible signaling pathway protein 2 (WISP2), mRNA.	-5.61	-6.03
NM_014376	Homo sapiens cytoplasmic FMR1 interacting protein 2 (CYFIP2), mRNA.	-4.08	-2.48
NM_201253	Homo sapiens crumbs homolog 1 (Drosophila) (CRB1), mRNA.	-2.69	-2.56
NM_001034852	Homo sapiens SPARC related modular calcium binding 1 (SMOC1), transcript variant 1, mRNA.	-2.91	-2.68
NM_201253	Homo sapiens crumbs homolog 1 (Drosophila) (CRB1), mRNA.	-2.69	-2.56